Ore Petrography, Geochemistry, and Genesis of Epithermal Silver-Gold Veins on Florida Mountain, Silver City District, Idaho

by

Michael Stuart Mason

A thesis submitted to the Graduate Faculty of
Auburn University
in partial fulfillment of the
requirements for the Degree of
Master of Science

Auburn, Alabama
August 1st, 2015

Keywords: Epithermal, Silver-Gold, mid-Miocene, Silver City district, Florida Mountain, Owyhee County

Approved by

James A. Saunders, Chair, Professor of Geosciences
Willis E. Hames, Professor of Geosciences
Robert B. Cook, Professor Emeritus of Geosciences

Abstract

Geochemical and petrographic studies were conducted on the Black Jack-Trade Dollar vein, a high-grade, low-sulfidation epithermal Ag-Au deposit hosted in mid-Miocene volcanic rocks of the Owyhee Mountains in southwestern Idaho. Petrographic studies of high-grade ore samples were conducted in both reflected and transmitted light. These petrographic studies revealed ore textures that indicate boiling and colloidal transport as important ore deposition mechanisms. Geochemical analysis indicated high levels of Au, Ag, Se, S, and Cu in the ores. Further analysis of the ores with an electron microprobe showed the presence of a compositional continuum of silver sulfo-selenides ranging from naumannite (Ag_2Se) to acanthite (Ag_2S). Additionally, the microprobe analyses revealed an unidentified Ag-Au-Se-S phase with an estimated formula of Ag_3AuSeS. Stable isotope studies of ore-stage chalcopyrite grains showed that $\delta^{65}Cu$ measurements range from -2 to 1‰ and $\delta^{34}S$ measurements range from -1 to 1‰. Both Cu and S isotopes indicate a magmatic source for the metals. Textural, geochemical, and isotopic evidence suggests that the high-grade ores were formed when Au- and Ag-rich hydrothermal fluids were evolved from a magmatic source. These hydrothermal fluids apparently deposited their metals in the shallow vein through a combination of colloidal transport, cooling, and boiling.

Acknowledgments

I would like to thank my advisor Dr. James Saunders for his support and guidance. This thesis would never have been written without many long discussions and much patience on his part. I am grateful to my office mate, Erin Summerlin, for her help in both the field and in the office. Her talents at finding ore samples, keeping me on task, and making me laugh far exceeded my own abilities. I would like to thank the faculty, staff, and students of the Department of Geology for their support throughout my time at Auburn University. Discussions with many of my fellow graduate students, especially Josh Poole and Chris Smith, helped focus and strengthen this thesis, and to them I am grateful. I would especially like to thank my committee members, Dr. Robert Cook and Dr. Bill Hames, for their corrections, suggestions, and help in assembling this thesis. I would like to thank Dr. Ryan Mathur and Dr. George Kamenov for their help in interpretating my copper and lead isotope data. I would also like to thank Dr. Doug Crowe and Chris Fleisher at the University of Georgia for their help in performing sulfur isotope analyses and electron microprobe analyses on my samples. I would like to thank the National Science Foundation for providing support for this project through NSF grant #1004381370012000. I would like to thank Mary O'Malley for her hospitality and vast knowledge of local geography and mining history during my stay in Silver City. Finally, I would like to thank my family. I am forever indebted to them for the love, phone calls, cards, and care packages they sent to me during my time at Auburn University.

Style manual or journal used: Economic Geology

Computer software used: Microsoft Word, Microsoft Excel, Microsoft Powerpoint, Microsoft Paint, Geochemist Workbench

Table of Contents

List of Tables

List of Figures

1. INTRODUCTION

Epithermal Gold-Silver Deposits

Epithermal deposits are a class of hydrothermal ore deposits that have been the source of a significant portion of the world's historic gold (7%) and silver (16%) supply (Simmons et al., 2005). Epithermal deposits are formed at shallow depth (<1.5 km) and relatively low-temperature (150-300°C). These ores often occur in steep-dipping, sulfide-bearing quartz veins that are usually hosted in volcanic rocks of Tertiary age or younger. The lack of older epithermal deposits is likely caused by the erosion of the shallow epithermal veins (Simmons et al., 2005). Within the class of epithermal deposits, there is a wide range of gold to silver ratios (1:1 – 1:400), apparently caused by different ore-fluid compositions. Ore in an epithermal system can be hosted in a variety of different textures including stockwork veins, hydrothermal breccias, banded veins, and disseminated bodies.

Because of the large amount of deposit diversity, there have been several different classification systems for epithermal deposits. Current classification systems recognize two distinct styles of epithermal mineralization. The acid-sulfate or high-sulfidation style of mineralization is closely related to acidic magmatic fluids associated with an underlying magma chamber. The adularia-sericite or low-sulfidation style of mineralization is formed from less reactive neutral pH ore fluids with a low (<5 wt. % NaCl) total salt content (Heald et al., 1987; Hedenquist and Houghton, 1987). Between

these two end members, Hedenquist et al. (2000) defined a third style of epithermal deposit called "intermediate sulfidation" that contains less gold, more silver, and contains more base-metal sulfides as a result of higher NaCl content (10-20 wt. %).

History of Epithermal Deposit Models

Epithermal deposits were named and first described in detail by Lindgren (1933). His classification scheme separated shallow metal-bearing veins into nine deposit types based upon the elements present in the vein. In addition to his classification scheme, Lindgren made many observations that are still noted in modern descriptions of epithermal vein deposits. He noticed that most epithermal deposits were quartz-adularia veins that produced gold and silver and were associated with volcanic rocks, especially around the Pacific Ocean's "Ring of Fire". Lindgren also described the features of epithermal veins, including banded veins with open-fill textures and hydrothermal breccias. These textures led Lindgren to hypothesize that the silica and metals filling the veins were "deposited rapidly near the surface as colloids" which then recrystallized to coarser grained quartz (Lindgren, 1933).

The next advance in the history of epithermal deposits was the application of stable oxygen and hydrogen isotopes in the early 1970s. Taylor (1973; 1974) and O'Neil and Silberman (1974) conducted studies of several epithermal districts which showed that the main source of the waters in epithermal veins was meteoric in origin. White (1969, 1974) expanded upon this idea by showing that the hydrothermal fluids in epithermal systems resembled those of meteoric-dominated geothermal systems such as Yellowstone

National Park and Steamboat Springs, Nevada. This led to the idea that epithermal mineral deposition occurred as a result of hydrothermal convection of meteoric water in a geothermal system. Based upon this idea, Skinner (1979) said "any rock can serve as a source of geochemically scarce metals provided a hydrothermal solution undergoes the reaction that will extract them". This was the birth of the idea that ore components were leached from the country rocks surrounding an epithermal vein. This model for epithermal deposits was later popularized and widely circulated in Guilbert and Park's (1986) textbook on mineral deposits.

Buchanan (1981) developed a model for bonanza-style deposits that formalized important structural, mineral zonation, and depositional aspects of epithermal veins. He introduced the structural complexity of hanging wall splays into his model of vein formation. Buchanan also observed that ore minerals showed a consistent zonation, with base metal sulfides lower in the vein and precious metal deposition higher up. However, perhaps Buchanan's most important contribution to the epithermal deposit model was to recognize that bonanza ore textures were formed by boiling of the ore fluids. Similar to the experimental work of Drummond and Ohmoto (1985), Buchanan proposed that boiling causes the loss of H_2S and CO_2 volatiles into a vapor phase. The loss of H_2S destabilizes the chloride (Cl^-) and bisulfide (HS^-) aqueous complexes that transport the gold and silver, which causes them to come out of solution and deposit in the veins. The loss of H_2S and CO_2 also causes the pH to rise, reducing the solubility of any metals remaining in the ore fluids. Essentially, this boiling process leads to the exceptionally high grades and chaotic textures present in bonanza-style epithermal ores.

In the mid-1990s, a radical shift in ideas about epithermal deposits occurred. Hedenquist and Lowenstern (1994) postulated that the metals and ligands that make epithermal deposits come from a magmatic source. Using gas fluxes in volcanoes with associated active geothermal systems, they showed that degassing magmas could provide enough metal to create an ore deposit over a reasonable time frame. Hedenquist and Lowenstern stated that both the significant distance and the mixing with heated groundwater between a magmatic source and a low-sulfidation epithermal deposit likely leads to water-rock interactions that could hide the magmatic signatures in ore-forming solutions that deposited an ore.

In their report on the Sleeper Mine, Nash et al. (1995) struggled to adequately explain how such a rich bonanza deposit formed using the traditional model for epithermal deposits. Because there is no evidence of igneous intrusions nearby, it was assumed that faults provided the pathway for ore fluids to reach the deposition site. Based upon previous estimates for low-sulfidation epithermal deposits (Henley and Ellis, 1983; Hedenquist, 1992), less than 10 percent of the water that was present at Sleeper was thought to be of magmatic origin. The authors admitted that there was no known source for the amount of gold present in the Sleeper deposit. One possible solution came from the idea, advanced by Saunders (1990; 1994), that gold was transported as colloids from some gold source at depth. Nash et al. (1995) labelled this hypothesis "unorthodox" and based on "circumstantial fragments of evidence".

The next change to models of epithermal deposit genesis resulted from the documentation and development of the idea of vapor transport of metals. Heinrich et al. (1999; 2004) discovered the existence of two distinct phases within fluid inclusions found

in porphyry copper deposits. One phase was a dense brine that contained copper, lead, and tin; the second phase was vapor-rich, low-density supercritical fluid that contained elevated levels of silver, gold, copper, and sulfur. Further work by Heinrich (2005) and Williams-Jones and Heinrich (2005) showed that gold and copper followed different paths through the hydrothermal system based on their volatile complexing associations. Gold is more likely to form aqueous complexes with HS^- whereas copper forms aqueous complexes with Cl^-. Heinrich (2005) argued that if gold formed a bisulfide complex in a vapor phase, it would be relatively easy to transport it the long distances needed to create epithermal deposits. This strengthened the idea of a porphyry-epithermal connection by implying that epithermal deposits have a magmatic source for their gold.

By the early 2000s, the idea that epithermal deposits had some connection to magmas was accepted by many researchers. However, some researchers then began to question how significant the magmatic connection was. John (2001) proposed a tectonic genetic model for two epithermal deposit types in the Northern Great Basin. He described a bimodal volcanic assemblage, which includes most of the bonanza gold deposits of northern Nevada, as having an uncertain connection to magmatism. This led John to state that magmas may have only been a heat source to drive the primarily meteoric geothermal systems that created the low-sulfidation epithermal deposits. As part of his model, he noted that there was a lack of stable isotope analyses of the ore stage minerals themselves. The John et al. (2003) study of the Mule Canyon deposit included several $\delta^{34}S$ measurements on ore stage pyrites, but the wide range (-3 to 8‰) could reflect possible inputs from nearby evaporite beds.

The most recent description and classification of epithermal deposits is Simmons et al. (2005). In their paper, Simmons et al. summarized the physical, chemical, and mineralogical differences between high-sulfidation and low-sulfidation epithermal deposits. High-sulfidation deposits were described as having a strong connection to magmatism as evidenced by their more acidic mineral assemblage. Low-sulfidation deposits, however, were interpreted to have formed by mixing meteoric and magmatic waters. Simmons et al. (2005) stated that boiling within a narrow vertical range leads to gold and silver being deposited when the bisulfide (HS^-) complexes transporting them are lost as hydrogen sulfide gas (H_2S). They stated that due to the diversity of mineralization styles, epithermal deposits were difficult to force into one unified model. It was also noted that, due to the nature of the deposits, no chemical measurements had been taken directly from the ore-bearing fluids. To that end, Simmons et al. acknowledged that new research in epithermal deposit genesis should focus on determining the original ore fluid composition using new analytical techniques becoming available.

Problems with the Current Epithermal Deposit Model

Even though Simmons et al. (2005) gave a thorough, state-of-the-art treatment to our modern understanding of epithermal mineral systems, there are apparent inconsistencies with their genetic model, especially for low-sulfidation systems. First, none of the current models (i.e., John, 2001; Simmons et al., 2005) agree on the extent of the magmatic connection to low-sulfidation epithermal systems. Ever since the magmatic connection was described by Hedenquist and Lowenstern (1994), no models have given

any estimates on the magnitude of the magmatic input. The second problem with the current model is that most of the fluid inclusion measurements from vein minerals are taken from quartz crystal inclusions that may not be similar to ore-bearing fluids. These fluid inclusion measurements may have been taken simply because suitable inclusions could only be found in the barren portions of the vein where no ore minerals were present. Kouzmanov et al. (2010) showed that fluid inclusions in ore minerals, at least locally, are different from those in closely associated quartz crystals. Similarly, almost all $\delta^{34}S$ measurements made in epithermal veins have been taken on sulfides, especially pyrite, that may not have been part of the ore-stage mineralization. John et al. (2003) is a notable exception because sulfide paragenesis was rigorously established. Lastly, the most important problem is that none of the models previously discussed gave any satisfactory explanation for the source of the metals and ligands, such as sulfur, that make an ore deposit. Previous models invoked the leaching of silver and gold from the surrounding country rocks, but that seems highly unlikely based on at least two observations: 1) the low abundance of gold and silver in Earth's crust, and 2) it has never been documented that metals have been depleted in the country rocks surrounding an ore deposit.

Objective of Study

The purpose of this study is to help improve the current understanding of the genesis of low-sulfidation epithermal deposits. This involves a study of various chemical and physical attributes of the Trade Dollar-Blackjack vein in the Owyhee Mountains of

Idaho, which is a typical Northern Great Basin epithermal deposit. These ores have the potential to shed light on the source of the metals in the deposit because the gold- and silver-bearing minerals are relatively coarse-grained and abundant and can constrain the timing of mineralization based upon the high-grade textures present in the mineralization. The hypothesis that the metals contained in the vein (Au, Ag, Cu, and Pb) come from a magmatic source is tested by studying the stable isotopes of sulfide minerals. One specific aspect of this involves determining if the lead present in the ores has the same isotopic signature as the lead in the gangue minerals. An investigation of the ore textures present is conducted in order to determine if nanoparticle/colloid transport had any impact on ore genesis. The final hypothesis tested is whether or not the host lithology for the ore has any control on the physical or chemical characteristics of the vein.

2. PREVIOUS WORKS AND GEOLOGIC SETTING

Northern Great Basin Au-Ag Deposits

Although mined sporadically for over 150 years, Northern Great Basin (NGB) epithermal ores have received very little modern research during the last four decades. Vikre (1985, 1987) provided a modern geologic description of the gold and silver veins of the historic National mining district in northern Nevada. In the National district, gold and silver mineralization occurs in bonanza-grade veins containing large amounts of silver selenide minerals. These veins are hosted in volcanic domes of rhyolitic composition erupted between 18 and 15 Ma. The mineralization of the National district is very similar to that of the Silver City district because they both occur in mid-Miocene volcanic rocks and contain abundant silver selenide minerals. In addition to describing the mineralization, Vikre (1987) used oxygen and hydrogen stable isotope analyses to characterize the paleohydrology of the National district and found it to be analogous to the geothermal and ecosystem that currently exists at Yellowstone National Park.

Saunders (1990, 1994) studied the textures present in the silica gels and electrum bands of the Sleeper deposit in northern Nevada, which was discovered in the mid-1980s. The interpreted former electrum colloids, silica gels, and opal bands at Sleeper showed fine banding and ripple textures on the tops of those bands. Based upon these apparently hydraulically-shaped textures, Saunders was the first person to describe a possible ore genesis mechanism for epithermal deposits using physical transport of ore components.

He later expanded upon the physical transport hypothesis by studying other districts in the Northern Great Basin, including the Silver City, Idaho district.

Bussey (1996) provides a summary of the geology of the Hog Ranch deposit in northwestern Nevada. Hog Ranch was a relatively small gold deposit (300,000 oz. Au) developed in a hot spring environment hosted by mid-Miocene tuffs. Mineralization styles were primarily low-grade disseminated gold with some high-grade veins present. These minor high-grade veins were found to be similar in character to those of the Sleeper deposit, with bands of electrum separated by chalcedony and adularia. Fluid inclusion homogenization studies showed that mineralization occurred at temperatures of 180-220 °C with salinities less than 2 weight percent NaCl. Like other NGB epithermal deposits, ores at Hog Ranch are essentially contemporaneous with their mid-Miocene (14.8-15.2 Ma) host rocks.

In a 1996 paper, Saunders et al. proposed for the first time that the emergence of the Yellowstone hotspot was a driving force behind the formation of many epithermal mineral deposits of the Northern Great Basin. Many of the low-sulfidation epithermal deposits in the Northern Great Basin (Fig. Figure **1**) are hosted by mid-Miocene (14-17 Ma) volcanic rocks and contain a majority of gold and silver minerals with very little base metals present in the veins. Saunders et al. (1996) argue that the large number of similar-aged epithermal deposits is related to the regional volcanism associated with the initial eruption of the Yellowstone hotspot near McDermitt, Nevada at ~16 Ma.

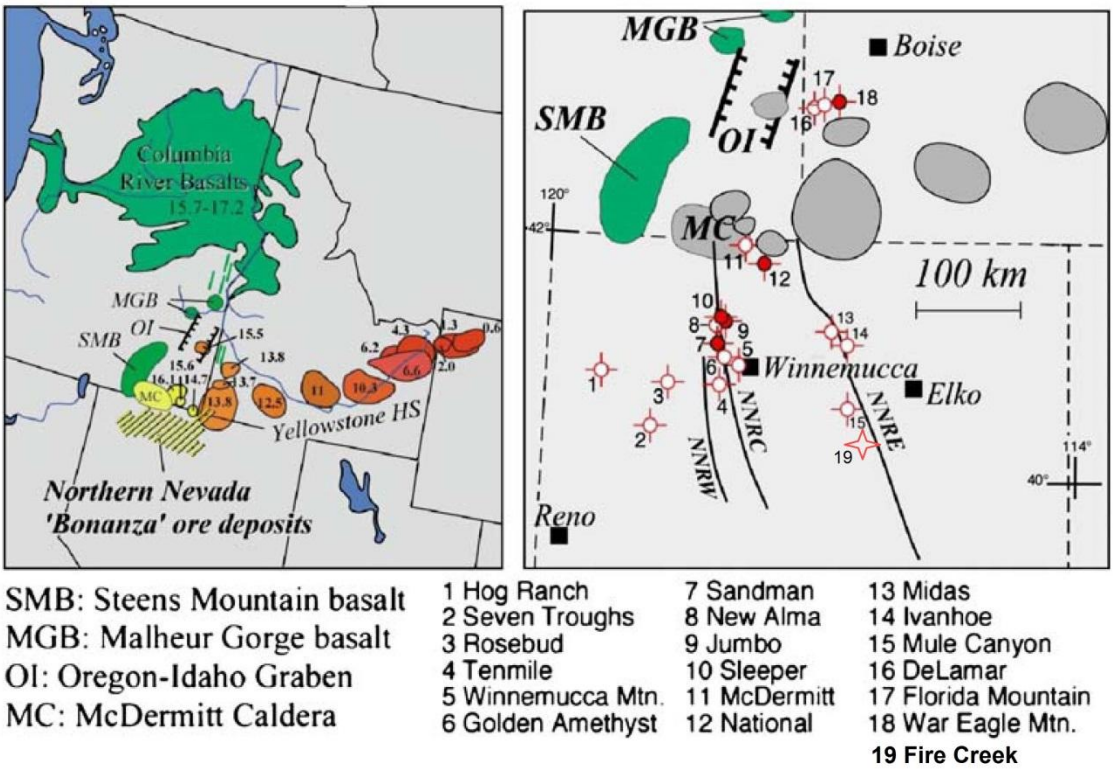

Figure 1- *Left*: Ages of calderas in the Yellowstone hotspot track with related flood basalts and field showing location of the majority of NGB bonanza epithermal deposits. *Right*: Locations of many of the mid-Miocene low-sulfidation epithermal deposits in NGB and important regional structures, such as the Northern Nevada Rift (NNRE, NNRC, NNRW). Modified from Saunders et al. (2008).

John (2001) defined two distinct Miocene-age metallogenic provinces in Nevada based on the associated rock types and mineral deposit of each area. The Western Andesite province is found near the California-Nevada border and contains Miocene to early Pliocene (22-4 Ma) subduction-related andesitic rocks that host both high sulfidation and low sulfidation epithermal deposits. The Bimodal Basalt-Rhyolite province is found in northern Nevada and is associated with mid-Miocene (16-14 Ma) rift-related bimodal assemblages of basalt and rhyolite which host only low sulfidation epithermal deposits.

John et al. (2003) described the geology of the Mule Canyon deposit in northern Nevada. This deposit is formed in the middle of the Northern Nevada Rift, which is composed of mafic lava flows contained within northwest trending normal faults. Unlike most of the other epithermal deposits in the region, the veins at Mule Canyon are hosted in basaltic rocks. This lead to the relatively narrow width of mineralized veins present at the mine. $^{40}Ar/^{39}Ar$ age dating of vein material yielded an age of 15.6 Ma for the mineralization at Mule Canyon. Stable isotope studies were performed and show that the quartz in the veins was made from geothermally circulating meteoric water. Additionally, John (2003) measured the sulfur isotope values in ore-stage pyrites and found that the $\delta^{34}S$ values range from -3 to +8‰.

Wallace (2003) described the Hg-Au mineralization in the Ivanhoe district, which is located approximately 15 km southeast of the Midas district. Mineralization at Ivanhoe was found to be coeval with rhyolite volcanism that occurred at 14.9-15.2 Ma, which is close in age to mineralization at Midas. At Ivanhoe, mineralization was primarily hosted by low-grade hot spring deposits, but there are some banded veins with electrum, silver selenides, quartz, and adularia present in the deeper levels of the system. To help with the interpretation of geochemical data, a factor analysis of trace elements was performed and showed that ores and host rocks are enriched in Au, Ag, As, Sb, Tl, and Hg. Overall, Wallace (2003) characterized the Ivanhoe district as an analog to the paleosurface and shallow subsurface that was once present at Midas because they formed under similar conditions in relatively close proximity.

Leavitt et al. (2004) detailed the geochronology of the Midas deposit, which is the largest known Au-Ag deposit related to the Northern Nevada Rift. The rocks in the

district show ages for mafic volcanism that range from 15.9 to 15.6 Ma and was replaced by felsic volcanism that was active until 15.2 Ma. The high-grade ore veins have ages of approximately 15.4 Ma. Thus, precious metal mineralization occurs at approximately the same time as the eruption of rhyolites within the district. This pattern may be repeated at other locations within the Northern Great Basin including the Silver City district (Aseto, 2012).

Leavitt and Arehart (2005) provide a detailed report on the alteration and geochemistry of the Midas deposit. There were several distinct alteration assemblages described for both felsic and mafic country rocks, including argillic, potassic, propylitic, and silicic assemblages. Alteration was principally potassic or silicic within a short distance (~10 m) of the mineralized veins and gradually transitioned to varying degrees of propylitic alteration at greater distances from the veins. The geochemistry of the Midas deposit was described as enriched in typical epithermal deposit elements, such as Au, Ag, Se, S, Cu, Sb, F, and Te. A correlation matrix was calculated for the geochemical data, and the strongest correlation was found between Ag and Se. These geochemical characteristics were found to be similar to other NGB low-sulfidation epithermal deposits.

Using laser ablation ICP-MS, Vikre (2007) detailed the geochemical similarities between the Hg-rich silica sinter formed at the paleosurface and the naumannite-rich veins on Buckskin Mountain in the National district and concluded they were connected hydrologically. The silica sinter, which is found on the mountain top, represents the paleosurface and is between 270 and 440 meters above the highest mineralization in the veins. Based on their similar geochemistries, both the sinter and the veins were formed

from the same hydrothermal solutions. Because both the sinter and veins are preserved, Buckskin Mountain presents the unique opportunity to observe and measure an entire ore-producing hydrothermal system.

Kamenov et al. (2007) measured the isotopic composition of lead (Pb) alloyed with gold, electrum (Au-Ag alloy), and naumannite (Ag_2Se) found in Middle Miocene epithermal deposits from the northern Great Basin. The isotopic composition of the metals was then compared to the surrounding granites, basalts, rhyolites, and metasedimentary units in order to determine if the lead came from the country rocks. Kamenov et al. found that the lead had a distinctly different and more primitive isotopic signature than that of the rocks hosting the ore deposits. This result supported the physical transport hypothesis and serves as the model for the isotope work performed in this study.

Saunders et al. (2008) provided a detailed description of the Yellowstone hotspot model for the development of Northern Great Basin epithermal ores. This model states that the bimodal basalt-rhyolite assemblage that hosts many of the low sulfidation epithermal ores was formed during the emergence of the Yellowstone hotspot during the mid-Miocene (~15-16 Ma). Saunders et al. (2008) observed that although the Yellowstone-related volcanics continue across the Snake River Plain to their current location, the associated mid-Miocene epithermal ores are found only in northern Nevada and southern Idaho. The model states that the hotspot-related mafic magmas were the source of the metals, metalloids, and sulfur that form the ores. Several lines of evidence are presented, including the age, mineralogy, and geochemistry of the deposits. This paper also characterizes the Pb isotopes of the region by measuring the Pb included in

electrum from the deposits. The Pb isotopes show a mantle signature for the gold in the Northern Great Basin ores.

Saunders and Brueseke (2012) described how the flat-slab subduction of the Farallon Plate during the Laramide Orogeny apparently enriched the mantle underlying the western United States in ore components. As the Farallon Plate was subducted, the increasing heat and pressure caused the metals and metalloids contained in the plate to be driven into the overlying lithospheric mantle (Fig. Figure **2**). As part of this study, a measure of the volatility of various epithermal elements (Au, Ag, Te, Se, Sb, As, Tl) showed that Se is more volatile than Te. This could explain the broad zonation of Se-rich deposits closer to the trench (the deposits in Nevada and Idaho) and Te-rich deposits further inboard (deposits in Colorado and Montana).

Over the last 30 years, knowledge of the epithermal deposits of the Northern Great Basin has advanced greatly. Several new deposits (Hog Ranch, Midas, Mule Canyon, and Sleeper) have been discovered, mined, and reclaimed. Several other deposits (Buckskin National, Ivanhoe, and Silver City) have been rediscovered and studied by geologists for the first time in many years. Many of these deposits have been found to occur in mid-Miocene volcanic rocks and have mid-Miocene mineralization ages. Almost all of these epithermal deposits fall into the low-sulfidation epithermal model. Along with this renewed research interest, new ideas concerning the genesis of these deposits have been hypothesized. The most promising of these ideas is that the preparation of the lithospheric mantle of the western United States by flat-slab subduction, together with the later emergence of the Yellowstone hotspot, created a world-class metallogenic province

in the Northern Great Basin highlighted by the abundance of bonanza-style, low-sulfidation epithermal deposits.

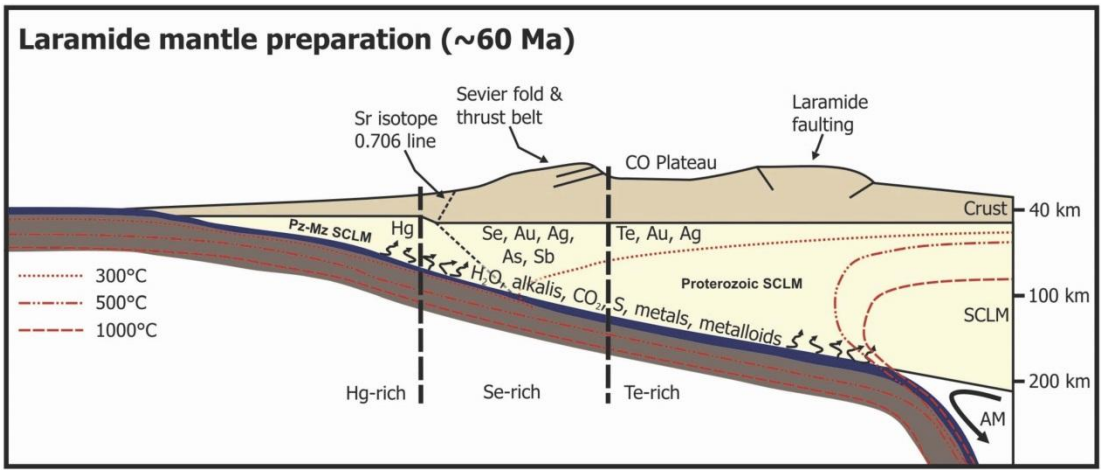

Figure 2: Diagrammatic cross section based upon concepts from Saunders and Brueseke (2012) showing Laramide flat-slab subduction and lithospheric mantle devolatilization underneath the western United States. The Silver City district is located in the Se-rich zone near the Sr isotope line.

Silver City Area

Lindgren (1898) was the first person to describe the geology, ore mineralogy, and structures of the Silver City district. This report is the first description of adularia, which is alkali feldspar that has been formed by hydrothermal fluids. It, along with quartz, is a major gangue mineral in the Silver City district and especially on War Eagle and Florida Mountains.

In his geological report on the district, Lindgren (1900) described the Silver City area as having “simple geology” with Cretaceous granite unconformably overlain by Miocene basalts, which are then covered by Miocene rhyolites (Fig.

Figure **3**, Fig. Figure **4**). Because his report was written while many of the mines in the district were still active, Lindgren was able to see and give detailed descriptions of the veins and their alteration patterns in the underground mines.

Piper and Laney (1926) described the general geology of the Silver City district. Their study was conducted after all of the mines in the area had ceased production. This allowed them to report the total production of silver (15,421,700 oz.) and gold (132,580 oz.) for the early history of the mines exploiting the Black Jack-Trade Dollar vein (Table 1). Piper and Laney did basic petrography of the ore veins. In their report, they list 16 different silver minerals present in the veins, including acanthite (Ag_2S), cerargyrite (AgCl), electrum (Au,Ag), native silver (Ag), naumannite (Ag_2Se), proustite (Ag_3AsS_3), and pyrargyrite (Ag_3SbS_3). The most important part of Piper and Laney's report is the geologic map, which shows all of the different mines present in the district. This map is the most thorough compilation of mines, shafts, tunnels, and prospects from the Silver City district.

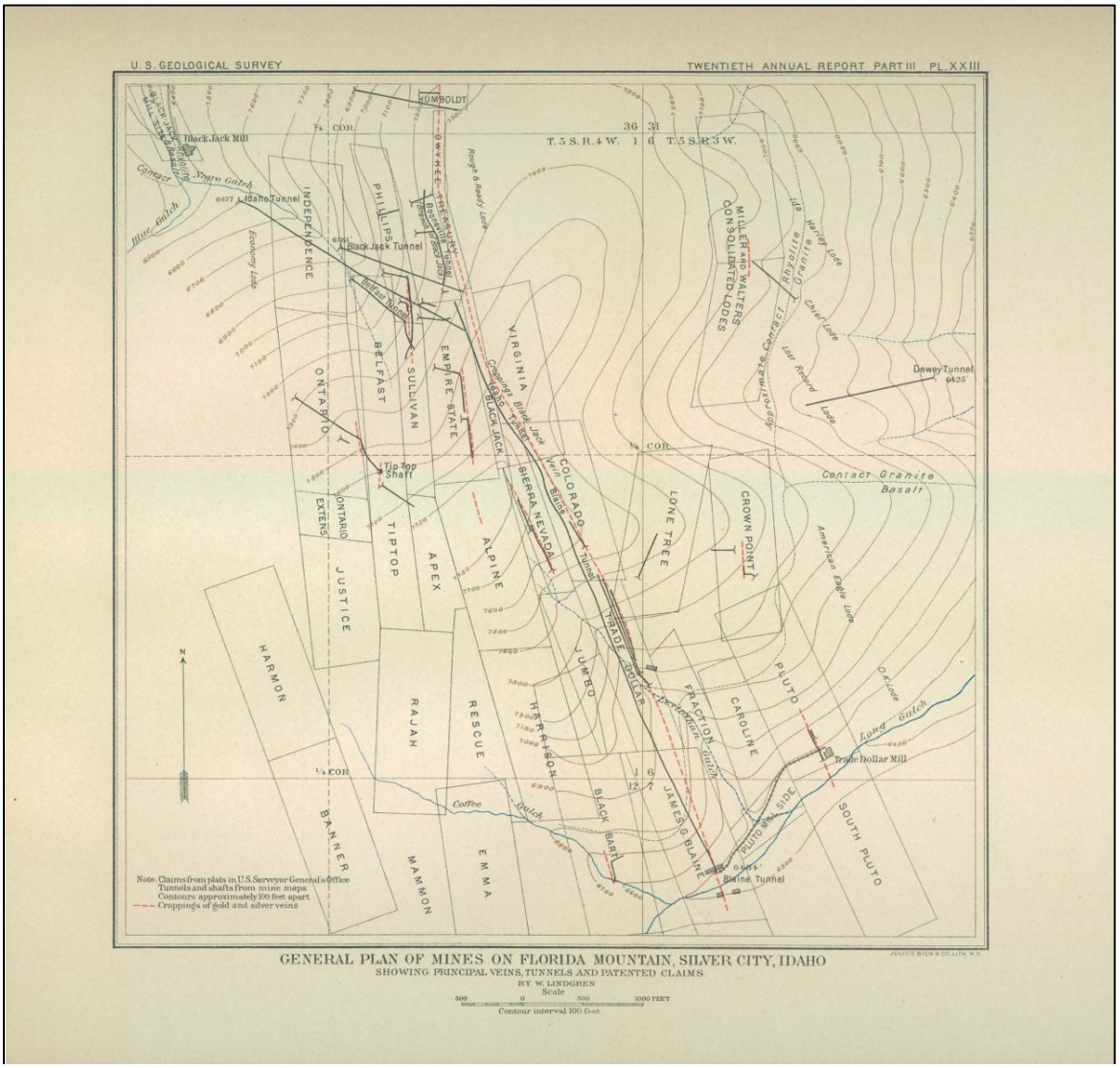

Figure 3: Topographic map of Florida Mountain showing the various mining claims and trace of the Ag-Au bearing veins as red dashed lines. The Black Jack-Trade Dollar vein is the longest vein present and strikes approximately N20W through the center of the map [from Lindgren (1900)].

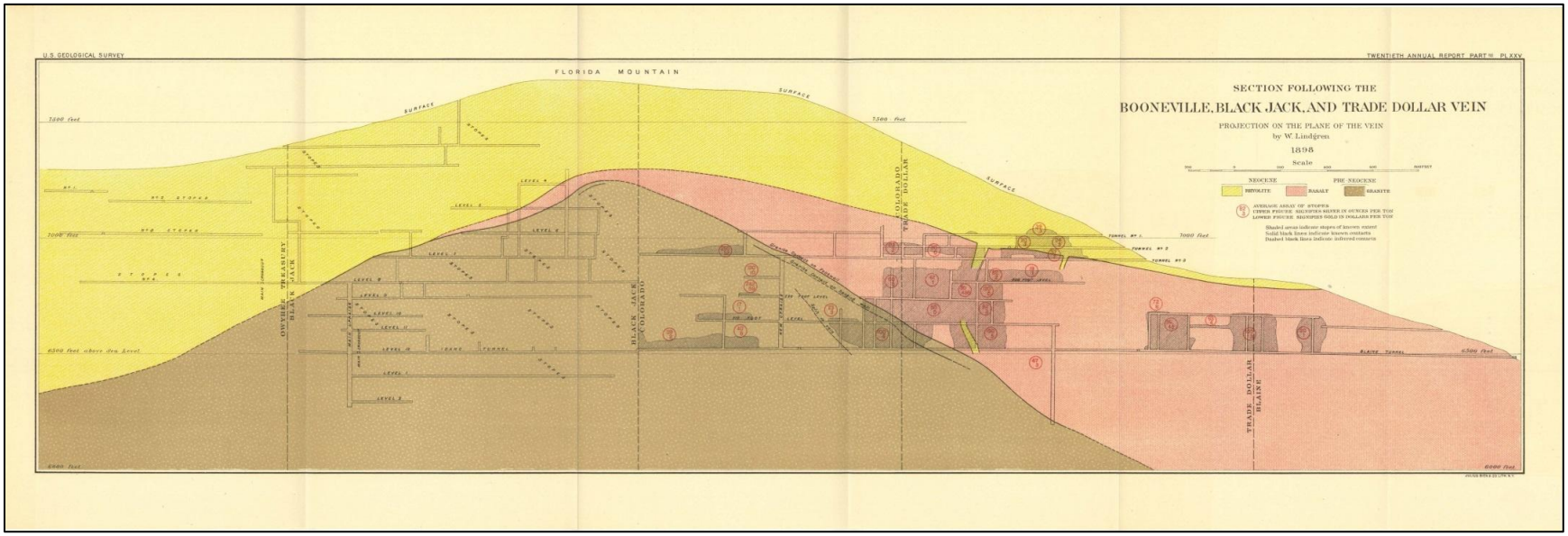

Figure 4: Cross section of Florida Mountain showing the simple geology of the district and the underground workings along the Trade Dollar-Black Jack vein. The gray areas are stopes with assays of Ag in ounces per ton (upper number) and Au in dollars per ton (lower number). From Lindgren (1900).

Table 1. Production of gold and silver from the Black Jack-Trade Dollar Mine. Data are from Piper and Laney (1926). Modified from Mitchell (2010).

Year	Weight in Fine Ounces		Value			Value of silver per fine ounce	Ratio of Au to Ag by wt.
	Gold	Silver	Gold	Silver	Total		
1865-91	19,300	1,335,000	$400,000	$1,500,000	$1,900,000	$1.156	—
1892	2,000	200,000	$41,500	$174,000	$215,500	$0.87	—
1893	2,000	200,000	$41,500	$156,000	$197,500	$0.78	—
1894	5,100	720,000	$105,500	$454,000	$559,500	$0.63	—
1895	4,900	695,000	$101,000	$442,000	$543,000	$0.65	1 to 166.7
1896	6,100	635,000	$126,000	$432,000	$558,000	$0.68	107.5
1897	6,000	625,000	$124,000	$375,000	$499,000	$0.60	121.5
1898	7,100	805,000	$147,000	$475,000	$622,000	$0.59	126.2
1899	11,750	1,075,000	$243,000	$645,000	$888,000	$0.60	108.3
1900	11,300	1,163,000	$233,500	$722,000	$955,501	$0.62	93.7
1901	10,500	1,210,000	$217,000	$726,000	$943,000	$0.60	116.7
1902	6,150	781,000	$127,000	$414,000	$541,000	$0.53	125.2
1903	5,600	690,000	$116,000	$372,500	$488,700	$0.54	123.0
1904	7,050	738,500	$145,500	$428,000	$573,500	$0.58	103.4
1905	8,500	1,422,000	$175,500	$867,000	$1,042,500	$0.61	178.5
1906	8,250	1,242,000	$170,500	$845,000	$1,015,500	$0.68	168.2
1907	4,650	653,000	$96,000	$431,000	$527,000	$0.66	139.1
1908	3,050	642,000	$63,000	$340,000	$403,000	$0.53	212.0
1909	2,900	519,000	$60,000	$269,000	$329,000	$0.52	189.4
1910	380	71,200	$7,900	$38,400	$46,325	$0.54	—
Totals	**132,580**	**15,421,700**	**$2,741,400**	**$10,105,900**	**$12,847,525**	—	**138.6**

Asher (1968) mapped the geology and evaluated gold-silver mineralization potential in the Silver City region. He recognized the mining potential of the disseminated mineralization in the rhyolites on top of Delamar Mountain and Florida Mountain. In his list of ore minerals present in the district, Asher noted that chalcopyrite, galena, and sphalerite were primarily found in the lower levels of the mines on Florida Mountain and War Eagle Mountain. In his report, Asher included a cross section (Fig. Figure **5**) of Florida Mountain showing the underground workings of the Black Jack-Trade Dollar vein similar to Lindgren's cross section from 1900 (Fig.Figure **4**).

Pansze (1975) did detailed field mapping of the volcanic sequence in the district. This mapping showed a bimodal distribution of alkali olivine basalts and rhyolites. Pansze attributed this bimodal distribution to the rifting of the Snake River Plain. He correlated the Silver City granite to the Idaho Batholith but stated that the basalts do not correlate with the Columbia River Basalts even though they are similar in appearance. Based on regional structures, Pansze states that the Owhyee Mountains show regional stresses from the rifting of both the Snake River Plain and the Basin and Range Province.

Bonnichsen (1983) compiled a summary paper of the general geology of both the entire district and the ore veins. He reported total production of silver (32.5 million ounces) and gold (1.1 million ounces) for the entire Silver City district. Using these production numbers, he calculated Au:Ag ratios that ranged from 1:1 to 1:1000 on individual veins. Bonnichsen stated that the ore was formed at 16 Ma by one mineralization event with multiple episodes of ore deposition, which accounts for the

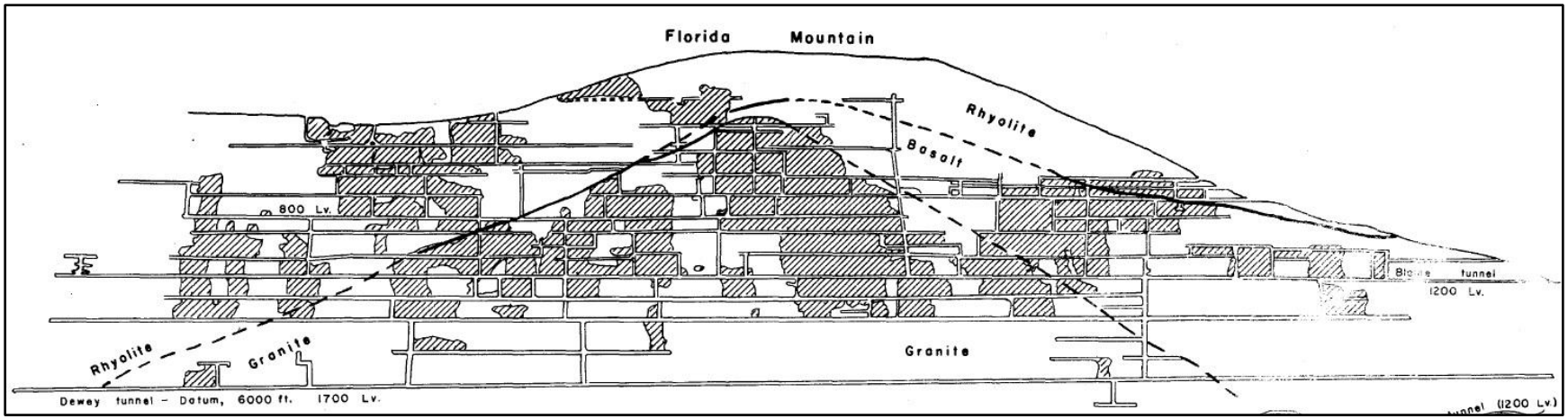

Figure 5: Cross section of Florida Mountain showing the simple geology of the district and the underground workings along the Trade Dollar-Black Jack vein. The gray areas are stopes that were mined from 1895 to 1915. Compare this cross section to Lindgren's 1900 cross section (Fig. Figure 4). From Asher (1968).

banded appearance of the veins. The mineralization age of 16 Ma is coeval with the eruption of the rhyolites in the district.

Barrett (1985) conducted a detailed study of the Milestone deposit. The Milestone deposit is located in the northwestern corner of the Silver City District about 1 mile northwest of the De Lamar silver mine. It is a silica sinter deposit formed by an ancient hot spring system. The mineralization is disseminated and hosted within both the silica sinter and the underlying rhyolite unit. The ore mineralogy matches much of the rest of the district and principally consists of naumannite (Ag_2Se), aguilarite (Ag_4SeS), acanthite (Ag_2S), and electrum (Ag,Au).

Halsor et al. (1988) represents the most recent published work in the Silver City district. This study was performed on the now closed modern mines present at the top of Delamar Mountain and, to a lesser extent, Florida Mountain. Like previous studies, Halsor et al. (1988) details the ore mineralogy of the veins. In this report, the primary silver minerals were naumannite (Ag_2Se), aguilarite (Ag_4SeS), and acanthite (Ag_2S). Additional silver-bearing phases were pyrargyrite (Ag_3SbS_3), argentopyrite ($AgFe_2S_3$), polybasite ($(Ag,Cu)_{16}Sb_2S_{11}$), cerargyrite (AgCl), and stephanite (Ag_5SbS_4). Fluid inclusions showed a homogenization temperature of 200-240 °C. K-Ar age dates measured on adularia from the veins were found to be 15.2 Ma.

Unger (2008) measured $^{40}Ar/^{39}Ar$ ages for adularia crystals found in Au-Ag veins from several low sulfidation epithermal deposits in the Northern Great Basin. These ages ranged from 16.53 to 15.61 Ma. Two of these ages came from ore material on War Eagle Mountain in the Silver City district and produced ages of 16.31 Ma and 15.61 Ma.

Steiner et al. (2012) reported on the fluid inclusions and silver mineralogy present in ore samples from the Black Jack mine dump on the Trade Dollar-Black Jack vein on Florida Mountain. In his fluid inclusions, Steiner et al. (2012) found homogenization temperatures of 230-310 °C with salinities between 0.18 and 0.7 wt. % NaCl. Both of these results fall within normal ranges for epithermal deposits. The silver minerals at Black Jack were analyzed with an SEM-EDAX and were found to form a solid solution between aguilarite (Ag_4SeS) and acanthite (Ag_2S).

Aseto (2012) described the geology, geochemistry, and geochronology of War Eagle Mountain, which is the mountain to the east of Florida Mountain. His systematic description of the mineralogy and silica textures present in the ores provides a framework for the current study. He reports the age of ore mineralization at 15.58 Ma using the $^{40}Ar/^{39}Ar$ method on adularia crystals present in the veins. He reported several adularia-based $^{40}Ar/^{39}Ar$ age dates on Florida Mountain that ranged from 15.367 Ma to 16.076 Ma. In addition to his geochronologic work, Aseto (2012) collected Pb isotope data from the electrum and naumannite ores on War Eagle Mountain.

Geologic Setting

The Silver City district is located in the Owyhee Mountains of Idaho approximately 80 kilometers southwest of Boise. The Owyhee Mountains are located within the Owyhee volcanic field and mark the northernmost extent of the Great Basin province (Pansze, 1975; Aseto, 2012). Within the Silver City district, there are three sub-districts with significant gold and silver production. From west to east, they are Delamar

Mountain, Florida Mountain, and War Eagle Mountain (Fig. Figure **6**). This research is focused on the epithermal ores found on Florida Mountain (Fig. Figure **7**).

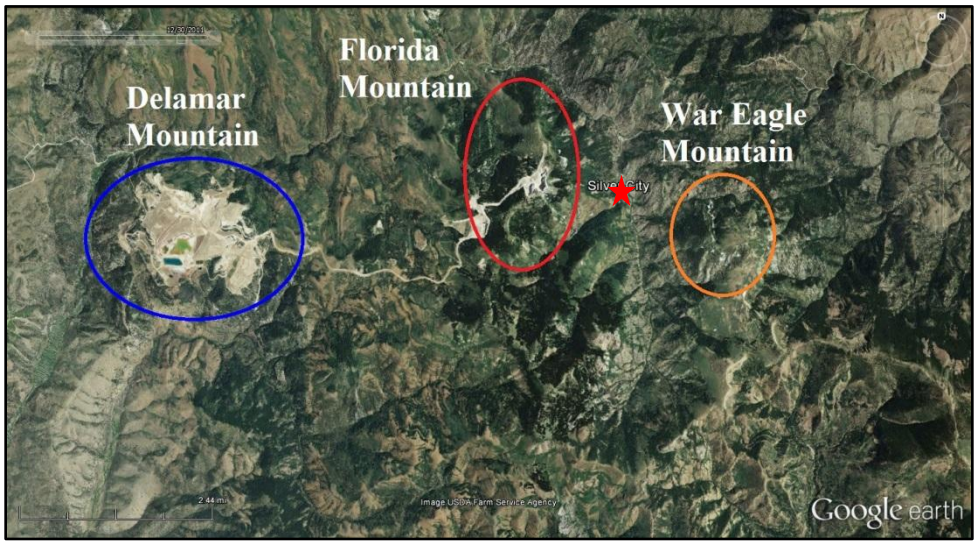

Figure 6: Google Earth image showing the location of the three main Ag-Au producing mountains in the Silver City District. Florida Mountain, which is located in the center of the district, is the focus of this study. The town of Silver City is marked by the red star.

Figure 7: Google Earth image showing the topographic relief of Florida Mountain, including the modern open pit mines on the mountaintop and the historic mine dumps on the mountain side. The town of Silver City is marked by the red star.

In the Silver City district, the general geologic framework (Fig. Figure **8**) is comprised of a Cretaceous granitoid overlain by Miocene volcanic rocks. Lindgren (1900) described the basement rock as Cretaceous granite in his geologic map (Fig. Figure **9**Figure **9**). This granitoid has been correlated with the Idaho Batholith (Lindgren, 1900; Pansze, 1975; Halsor et al., 1988). Miocene basalts lie unconformably on top of the granite and in turn, they are overlain by Miocene rhyolites (Aseto, 2012). The epithermal veins containing the gold-silver mineralization are hosted in all three units at various points in the district. At Florida Mountain, the ore-bearing veins are mostly hosted in the granite with some ore found in the basalts and rhyolites on top of the mountain.

Age (Ma)	Major Lithologies. Representative Epithermal Deposits in Parenthesis
Coeval to Steens Basalt eruption	Rhyolite/tuff and felsic flows/domes/breccias/tuffs (DeLamar Mine, Florida Mountain ores)
Inception of eruption 16.7Ma for ≥2Ma	Locally erupted Steens Basalt ("Lower" Basalt) (Black Jack Mine)
Unconformity	
Cretaceous granitoid stocks and plutons (Silver City batholith) and Triassic-Jurassic metasedimentary strata (War Eagle Mountain, Orofino and Poorman Veins)	

Figure 8: General stratigraphy and description of the rock units present in the Silver City District (Aseto, 2012).

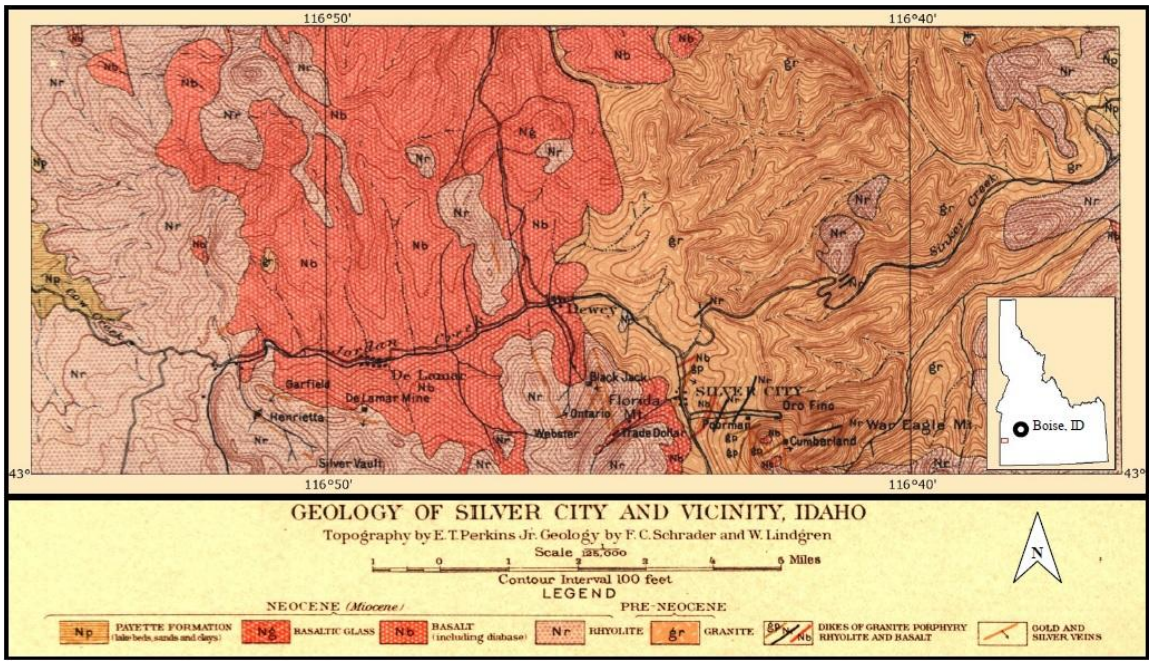

Figure 9: Lindgren's (1900) geologic map of the Silver City district. This was the first geologic map of the district, and is remarkably close to modern interpretations of the regional geology.

3. METHODOLOGY

Field Methods

Field work for this study was conducted during the summers of 2013 and 2014. In July 2013, high-grade ore samples were collected from the Trade Dollar, Dewey, and Idaho Tunnel historic mine dumps on Florida Mountain. In July 2014, additional samples were collected from the Blackjack and Dewey dumps. All sample locations are on mine dumps of material from the Black Jack-Trade Dollar vein. Sample locations were recorded using GPS and are shown on Figure 10. Promising high-grade ore samples were identified in the field based on the presence of dark banding in quartz vein material like that shown in Figure 11. At each sample location, an effort was made to collect ore samples in vein material surrounded by the various country rock units. Samples of country rocks, both hydrothermally altered and fresh, were also collected to compare their trace element geochemistry with that of the ore samples. Field work was completed by a team of three people from Auburn University: the author, Dr. James Saunders, and fellow graduate student Erin Summerlin. At the end of each field season, the collected samples were shipped back to Auburn University. Between both field seasons, a total of about 200 pounds of samples was collected.

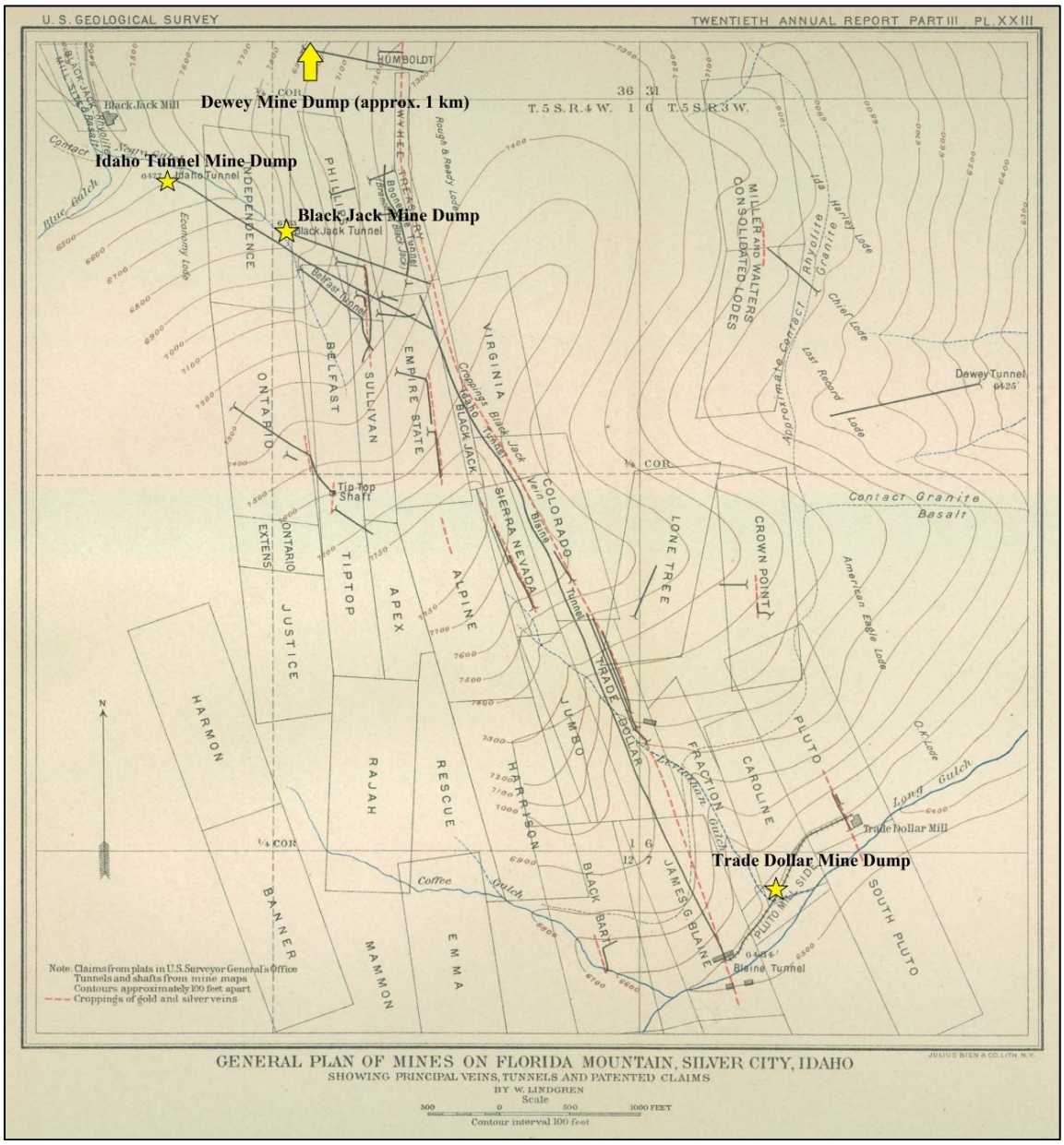

Figure 10: Map of Florida Mountain showing sampling locations for this study [modified from Lindgren (1900)].

Figure 11: Field photograph showing a finger pointing to the dark ore minerals marking the typical banding present in highest-grade ore samples collected for this study.

Sample Preparation

Samples were selected for further petrographic and geochemical analysis based on the quality and quantity of ore mineralization observed. All samples were cut into slabs using the diamond-coated trim saw in the Auburn University rock preparation lab. Samples with very high-grade mineralization were then labeled and cut into blanks to be used for petrographic study and geochemical analysis. Because the samples were chosen based upon their high-grade nature, they do not reflect the typical ore grades or textures present in the mineralized veins. The prepared samples were made into several splits so

that each sample would have geochemical, petrographic, and isotopic analyses performed. Samples of the country rocks were also cut into slabs to allow for geochemical and petrographic analyses.

Ore Petrography

In this study, samples were studied using three different microscope techniques. Transmitted light was used to identify and characterize minerals and textures present in the gangue portion of the ore samples. Transmitted light microscopy was performed on polished thin sections that were made by Quality Thin Sections in Tucson, Arizona. After they were returned to Auburn University, the billets of the thin section blanks were used to create polished sections for reflected light microscopy. This allowed for the same sample to be viewed in both transmitted and reflected light.

Reflected light microscopy was used to identify metallic minerals and look at the different textures present. In order to use reflected light, samples were set into Buehler EpoKwick Epoxy Resin and allowed to harden. Polishing was then performed by grinding the sample on a combination of glass plates and polishing wheels using seven different grit sizes. Grit sizes ranged from Buehler 120 µm silicon carbide powder down to Buehler 1 µm Metadi II diamond polishing compound. After the samples were polished, imaging was done using a Nikon Eclipse E400 POL light microscope. Identification of metallic, silver-bearing minerals using reflected light was aided by geochemical analysis and confirmed using the scanning electron microscope.

Electron Microprobe Analysis

One major problem with reflected light microscopy was that it could not resolve the different silver minerals present in the samples due to their similar optical characteristics. Mineral grains were qualitatively identified using a Bruker 5010 Silicon Drift Detector (SDD) energy dispersive x-ray (EDS) detector controlled by a Bruker Quantax energy dispersive analysis system. Backscattered electron (BEI) and x-ray maps were acquired using imaging software of the Quantax analysis system. In order to measure the chemical composition of the different silver phases, samples were analyzed using the University of Georgia Department of Geology JEOL 8600 electron microprobe. The microprobe used a 15 kV accelerating voltage, a 10 nA beam current, and 10 second counting times. Quantitative analyses were performed with wavelength dispersive spectrometers (WDS) automated with Advanced Microbeam, Inc. electronics and Probe for EPMA software, using 10 second counting times, and natural, synthetic, and elemental standards. Analyses were calculated using Armstrong's (1988) Phi-Rho-Z matrix correction model. Quantitative spot analyses of 117 silver grains and 32 electrum analyses produced atomic percent and weight percent values that are reported in Appendices 3 and 4.

Geochemical Analysis

For this study, geochemical analyses were performed on high grade ore samples and country rocks from Florida Mountain. Several additional Northern Great Basin

epithermal ore samples from the collection of Dr. James Saunders were also analyzed to provide a comparison for the Florida Mountain samples. A total of 36 samples, listed in Appendix 1, were sent for whole rock geochemical analysis using the 1EX package at Acme Analytical Laboratories Ltd. in Vancouver, Canada.

Isotope Analysis

Sulfur, copper, and lead isotope analyses were completed on samples from this study selected from remnants of blanks used for thin sections, polished sections, or geochemical analyses. Using a single sample for the petrography, geochemistry, and isotope studies allowed for each sample to be completely described.

Sulfur isotope analyses were performed at the University of Georgia's Stable Isotope laboratory. Chalcopyrite was drilled out of samples from the Trade Dollar, Idaho Tunnel, and Dewey mines under a binocular scope using a dental drill. Approximately 6 to 8 mg of powdered chalcopyrite were collected for each analysis. The mass was multiplied by the theoretical yield of SO_2 for chalcopyrite. This result was then divided by two, which gave the mass needed for each of the three reagents, vanadium pentoxide (V_2O_5), copper metal powder, and quartz powder. The mineral sample and the reagents were combined with an agate mortar and pestle under a fume hood until the mineral sample began to bond with the reagents (approximately 5-10 minutes). The sample was then loaded into a 6 mm quartz tube which was packed with silica fibers on each end. After sample preparation was complete, each sample was loaded into a 1050 °C furnace and combusted for 10 minutes. The resultant SO_2 gas was then cryogenically isolated

from the other gases produced (non-condensable gases, CO_2, and H_2O) on a cryogenic purification line. The amount of SO_2 produced was measured using a calibrated mercury manometer and reported as the actual SO_2 yield. Percent yield was calculated by comparing the actual yield to the theoretical yield. The SO_2 gas was collected in a Pyrex breakseal tube and was analyzed using a Finnigan MAT 252 mass spectrometer. An error of $\pm 0.03\sigma$ was calculated on replicate analyses of standards. Results are presented relative to Vienna Canyon Diablo Troilite (VCDT).

Dr. Ryan Mathur of Juniata College, using the laboratory facilities at the University of Arizona, conducted copper isotope analyses on samples of chalcopyrite for this study. Chalcopyrite-rich samples were dissolved using HF and the residuals were separated under a binocular microscope. The chalcopyrite samples were sequentially passed through two sets of exchange columns to separate the Cu from any Fe present. Cu-rich aliquots were collected. These samples were injected into a multicollector inductively-coupled-plasma mass spectrometer (MC-ICP-MS), the Micromass Isoprobe at the University of Arizona in low-resolution mode using a microconcentric nebulizer to increase sensitivity. The nebulizer flow was adjusted so that the intensity of the ^{63}Cu beam remained constant at 2 volts. Both on- and off-peak blank corrections were applied to the data and yielded the same result. The standard used was the NIST 976 Cu standard. Two blocks of 25 ratios are reported as an average for each run. Within each run the measurement error was less than $\delta^{65}Cu = 0.01‰$ for all analyses. This protocol was adapted from Mathur et al. (2009).

Lead isotope analyses for this study were performed in collaboration with Dr. George Kamenov at the Department of Geological Sciences at the University of Florida.

Samples were dissolved in HF and the residual sulfide or silicate mineral was picked for Pb isotopic analysis. Analyses were conducted using a Nu Plasma multi-collector ICP-MS (Nu Instruments, UK). Fresh Pb-Tl mixtures were prepared following the Tl normalization technique developed by Kamenov et al. (2004). Both sample and standard solutions were aspirated into the plasma source using a Micromist nebulizer with a GE spray chamber. Preamplifier gain calibrations were determined before each analysis. Analyses were conducted in static mode simultaneously acquiring ^{202}Hg on low-1, ^{203}Tl on low-2, ^{204}Pb on Axial, ^{205}Tl on high-1, ^{206}Pb on high-2, ^{207}Pb on high-3 and ^{208}Pb on high-4 Faraday detectors. All standard and sample results were normalized with ^{205}Tl/^{203}Tl = 2.38750 and age corrected using an approximate age for the Cretaceous Silver City granitoid (70 Ma). Results are reported as ratios of ^{206}Pb/^{204}Pb, ^{207}Pb/^{204}Pb, and ^{208}Pb/^{204}Pb.

4. RESULTS

Geochemical Analysis

The geochemical analyses performed on the Florida Mountain ores and host rocks showed several interesting geochemical characteristics. The results for Au, Ag, Cu, Pb, Zn, Sb, As, Se, Te, S, and Tl are shown in Table 2. The full geochemical dataset (40 elements) is shown in Appendix 2.

In order to describe how the mineralizing fluids affected them, both a fresh and an altered sample of the granite, basalt, and rhyolite were analyzed. Across all three rock types, the mineralized samples contain between 3 and 140 times more silver than their fresher counterparts. None of the country rocks contain any gold levels higher than the detection limit of 0.1 ppm. However, it is interesting to note that ore sample TD03 was collected less than 5 cm from the altered granite sample (shown in Figure 12) and has an assay of 57.6 ppm Au. This difference between the amount of gold and silver in the ores versus the country rocks shows exactly how localized the ore mineralization events are in these ore samples.

The ore samples have a gold grade ranging from 6 to >200 ppm and a silver grade of 58 ppm (in hot spring silica sinter) up to 30,227 ppm. Furthermore, the ore samples from the Silver City District contain significant amounts of copper (50 - 10,000 ppm). Copper is abundant in even the lowest grade samples analyzed. Some ore samples hosted by the Silver City Granite contain high concentrations of rubidium (200 - 450 ppm). Most

of these Rb-rich samples also contain fairly abundant adularia. Due to the geochemically similar nature of K and Rb, it is possible that the presence of rubidium is directly related to adularia in the mineralized veins.

In order to clarify geochemical relationships, several statistical methods were applied to the dataset. A Pearson correlation matrix (Table 3) was calculated in Microsoft Excel using the geochemical data from the Florida Mountain samples and NGB ores collected for this study. Linear correlations were determined for each pair of elements calculated from Au, Ag, Cu, Pb, Zn, As, Sb, Se, Te, Mo, Co, Ni, Cr, Fe, Mn, Sr, Ba, and Rb. There do not appear to be any strong correlations between Ag and Au, Ag and Se, or Ag and S. Based upon the silver selenide-rich nature of the ores, this lack of correlations with silver is surprising.

There are several problems with the geochemical data set in this study. The samples chosen for the geochemical study are highly biased towards high-grade ore. Even though studying the geochemistry of these ore samples was one of the goals of this research, without a larger suite of unmineralized rocks or large numbers of other deposits' ore samples to compare them against, these Black Jack-Trade Dollar vein ore sample geochemistries are not representative of the vein as a whole and only give a biased view of the geochemistry present in the vein.

The high-grade nature of the dataset also exposed a problem with the analytical method used. In the dataset, there was a problem with certain elements having values below detection (such as As) or above the upper detection limits (such as Ag) for many of the samples. For cases where the raw data were either above or below a detection limit, the issue was corrected by stating that the value was equal to the detection limit. For

example, there were only 14 samples that had arsenic contents above the detection limit of 1 ppm. For the other 22 samples, the value of arsenic was changed to 1 ppm.

The one exception to this rule was silver. After the initial multi-acid digestion analysis was performed, an additional gravimetric separation was performed to determine an accurate measure of the gold and silver for each sample. Unfortunately, there were only 12 ore samples with enough material left to perform this gravimetric analysis. This gives the values for silver a very bimodal character, with 14 ore samples showing 200 ppm and the other 12 ore samples exhibiting silver grades of approximately 3000 ppm up to 30,809 ppm.

Table 2: Geochemical Dataset for the Silver City and NGB Epithermal Ore Samples

	Location	Au ppm	Ag ppm	Cu ppm	Pb ppm	Zn ppm	Sb ppm	As ppm	Se ppm	Te ppm	S ppm	Tl ppm
	Lower Detection Limit	**0.1**	**0.1**	**0.1**	**0.1**	**1**	**0.1**	**1**	**1**	**0.5**	**1000**	**0.5**
AUMSM01	Sinter - Milestone?	1.3	75.1	18.6	1.8	6	11.2	43	47	0.5	1000	1.6
AUMSM02	Vertical Sinter - Milestone?	0.2	22.3	39.9	1.9	59	7.6	5	16	0.5	1000	0.5
AUMSM03	Mineralized Rhyolite	0.1	4.2	41.2	12.6	105	6.7	42	1	0.5	2000	0.9
AUMSM04	Unmineralized Rhyolite	0.1	1.3	8.5	21.6	47	0.6	3	1	0.5	1000	0.9
AUMSM05	Mineralized Basalt	0.1	43.1	1059	13.3	168	5.3	8	4	0.5	1000	2
AUMSM06	Unmineralized Basalt	0.1	0.3	48.2	2	90	0.9	2	1	0.7	1000	0.5
AUMSM07	Altered Granite	0.1	2.7	25.3	17.8	58	1.1	3	1	0.5	1000	2
AUMSM08	Fresh Granite	0.1	0.1	4	16.2	53	0.3	2	1	0.5	1000	0.5
AUMSM09	TD Petrie-made slide	58.3	10202	2497.3	730.5	224	9.1	1	919	0.5	12000	2.9
AUMSM10	TD Adit sample	102.8	200	5961.4	88.5	13	3.8	1	1000	9.5	7000	2
AUMSM11	TD03 - same as altered granite	57.6	11231	614.9	1299.5	610	2.4	1	1000	4.1	2000	3.8
AUMSM12	TD04 - high grade in basalt	87.4	20464	10000	4289.7	1480	4.2	1	1000	3	30000	3.2
AUMSM13	TD05 - high grade vein	36.6	8413	1362.4	475.5	163	46.4	1	589	3	2000	4
AUMSM14	TD06 - qtz-adularia vein	25.8	4833	951.6	218.3	59	2.5	1	551	0.6	1000	4.1
AUMSM15	IT01 - basalt country rock + vein wall	13.8	3853	588.2	374.8	343	3.3	1	363	1.9	2000	2.5
AUMSM16	IT02 - breccia	6	200	37.4	136.7	11	2.8	1	275	0.5	4000	5.1
AUMSM17	IT03 - same rock as IT1	200	200	1018.8	142.3	210	11.2	1	411	0.5	2000	2.4
AUMSM18	IT04	109.5	200	1581.9	10000	9124	7.7	1	1000	289.3	9000	4
AUMSM19	IT05	200	200	3156	629.4	567	13.6	1	1000	0.9	5000	3.1
AUMSM20	DEW1 - high grade puck	200	200	10000	10000	10000	22.4	1	1000	12.2	100000	1.8
AUMSM21	DEW2 - same as DEW2 slide	40.9	200	3582.5	3136.2	823	5	1	1000	21.8	5000	5.2
AUMSM22	DEW3 - high grade	86.8	200	588	1628.1	1423	3	1	1000	16.4	7000	3.4
AUMSM23	DEW4 - run of the mill high grade	26.8	3050	1043	650.3	358	2.2	1	242	4.7	1000	3.7
AUMSM24	DEW5 - high grade puck	96.3	200	10000	1630.3	1764	1.3	1	1000	5.4	9000	4.2
AUMSM25	Midas - Colorado Grande Vein	155.6	3482	1082.1	173.7	137	11.3	1	969	0.5	2000	0.9
AUMSM26	Buckskin	158.1	4060	54.3	84.7	33	145.3	1	955	0.5	1000	0.6
AUMSM27	DeLamar	9.6	30809	21.2	104.7	200	24.3	1	1000	0.5	2000	0.5
AUMSM28	Republic	200	200	10000	385.7	298	1983.8	1	1000	2.3	39000	0.8
AUMSM29	Pauper	21.2	200	548	320	353	742.5	826	306	0.5	4000	0.6
AUMSM30	Pauper	86.8	3370	1752.8	621.5	252	572.2	404	255	0.6	3000	0.5
AUMSM31	Blackjack 1 - really high grade	66.6	30227	22.8	236.9	133	5.1	1	1000	0.5	2000	1
AUMSM32	Blackjack 2		200	5.4	6.1	6	7.5	1	57	0.5	1000	2.5
AUMSM33	Henrietta 1 - mineralized breccia		200	2.2	19.5	12	75.3	196	130	0.5	10000	2.6
AUMSM34	Henrietta 2 - low grade		200	5.1	1.8	2	13.4	3	619	0.5	1000	0.5
AUMSM35	Milestone 1 - The Castle		141.6	4.4	18.7	5	37.3	27	64	0.5	1000	1.6
AUMSM36	Milestone 2 - Vertical Sinter		58.3	8.4	6.5	4	15.8	37	28	0.5	1000	1.5

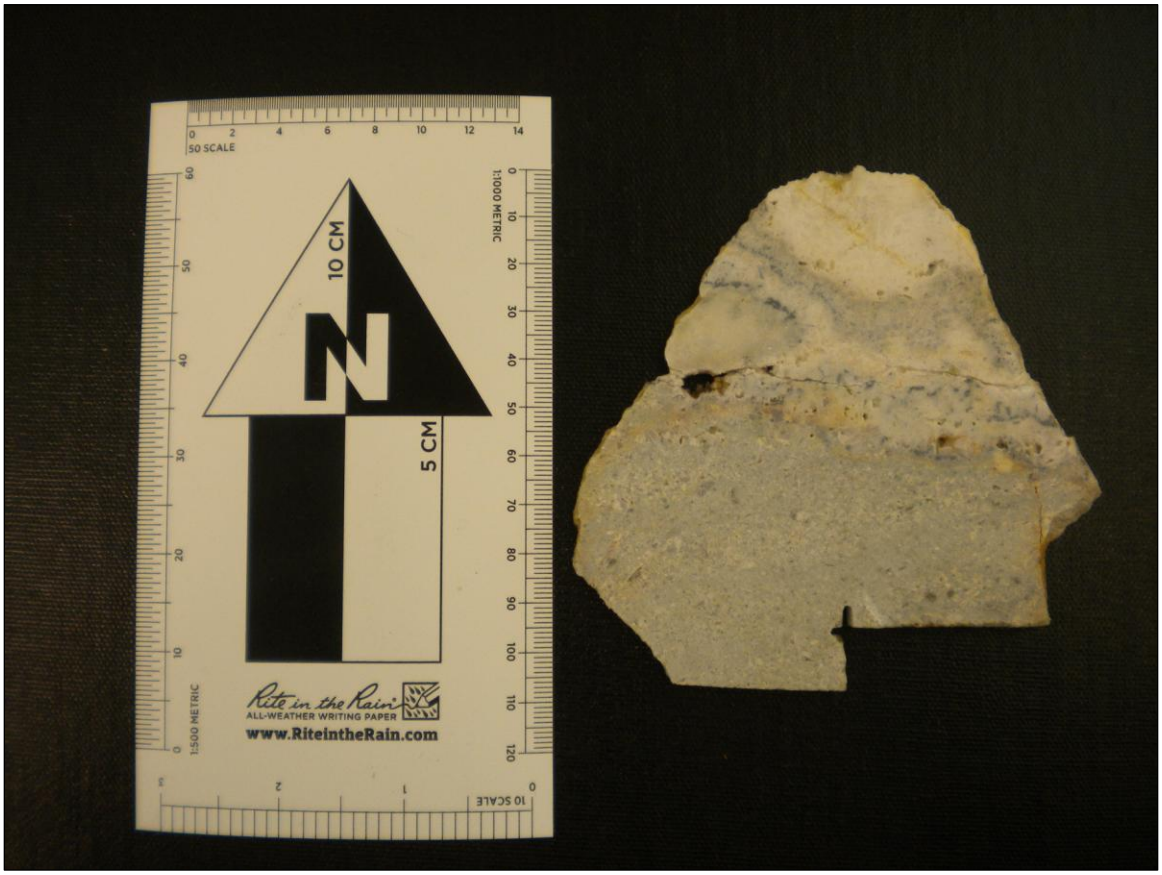

Figure 12: Photograph of an ore sample from the Trade Dollar Mine showing the gold-poor altered granite sample (chip was cut off the bottom of the sample) and the gold-rich mineralized vein less than 5 cm away.

Table 3: Correlation Matrix of Geochemical Data

	Au	Ag	Cu	Pb	Zn	As	Sb	Se	Te	Mo	Co	Ni	Cr	Fe	Mn	Sr	Ba	Rb
Au	1																	
Ag	-0.0982	1																
Cu	**0.5557**	0.0581	1															
Pb	0.3694	-0.0027	0.4627	1														
Zn	0.3856	-0.0978	0.4014	**0.9662**	1													
As	-0.1043	-0.0961	-0.1140	-0.0921	-0.0778	1												
Sb	0.3260	-0.1082	0.3570	-0.0954	-0.0814	0.3667	1											
Se	**0.6656**	0.3671	**0.5617**	0.4406	0.3656	-0.1894	0.1189	1										
Te	0.1337	-0.1048	-0.0027	**0.6826**	**0.6766**	-0.0648	-0.0648	0.2362	1									
Mo	0.1411	-0.0759	0.1729	0.2132	0.1658	0.4054	0.1709	0.0577	-0.0270	1								
Co	-0.1212	-0.0778	0.1186	0.1596	0.1877	-0.0951	-0.1327	-0.2249	-0.0851	-0.0624	1							
Ni	-0.2300	-0.0393	-0.1016	-0.1214	-0.1114	-0.0864	-0.1109	-0.2473	-0.0786	-0.1690	**0.8346**	1						
Cr	-0.1047	-0.0138	-0.2174	-0.1997	-0.1836	0.0618	-0.1111	-0.2215	-0.1423	-0.0805	0.0380	0.0876	1					
Fe	-0.0333	-0.0626	0.3271	0.1672	0.1671	-0.1170	0.0815	-0.1513	-0.0884	-0.1049	**0.9043**	**0.6811**	0.0124	1				
Mn	-0.3104	-0.1096	-0.1092	-0.1425	-0.1196	-0.0992	-0.1293	-0.3676	-0.0679	-0.1967	**0.8499**	**0.7958**	0.1139	**0.7798**	1			
Sr	-0.3876	-0.1347	-0.1036	-0.1502	-0.1480	-0.2314	-0.1841	-0.3163	-0.0734	-0.2238	**0.5644**	**0.7305**	-0.1280	0.4395	**0.6734**	1		
Ba	-0.4208	-0.1639	-0.2810	-0.2855	-0.2519	0.0170	-0.1531	-0.4228	-0.1765	-0.1394	-0.1771	-0.1513	-0.1526	-0.1474	0.0008	0.2133	1	
Rb	0.0934	-0.0916	0.1686	0.3500	0.2642	-0.2675	-0.3471	0.3647	0.3207	-0.0055	-0.2800	-0.2930	-0.2115	-0.2880	-0.2994	-0.0781	-0.0657	1

Note: Statistically significant correlations (greater than 0.5) are in bold.

In addition to the correlation matrix, a principal component analysis was performed on the geochemical data. A principal component analysis is a multivariable statistical method used to reduce the number of dimensions in a dataset based upon several underlying factors (Reyment and Jöreskog, 1993). In the past, this method has been used to identify groups of elements that have similar geochemical behavior in epithermal ore samples (Wallace, 2003; Smith et al., 2014). The graphical representation of the principal component analysis is shown in Figure 13.

In the figure, the values on the axes are merely remnants of the statistical method and do not have any spatial context for the deposit; however, it is possible to label the axes with a general character. The horizontal axis (PC1) likely represents the susceptibility to hydrothermal enrichment of an element, with more enrichment represented by the negative values. The vertical axis (PC2) appears to show some measurement of ion charge and field strength of the elements present, with highly charged elements having negative values and lower charged elements having positive values.

Based upon this analysis, it is possible to collapse the 40 elements present in the entire dataset down into three distinct groups. Group 1 consists of Au, Ag, Se, S, Te, Sb, Cu, Pb, Zn, Cd, Bi, Tl, Rb, K, and Mo. This group likely represents the elements that were initially present in the ore-forming fluids and are now concentrated in the mineralization. Group 2 consists of Fe, Ni, Co, Cr, Mg, Ca, Mn, V, Ti, P, Al, and Sr. The elements grouped into this group represent the whole-rock geochemistry and are a representation of the host rock composition. Group 3 contains Li, As, Zr, Y, Nb, Na, W,

Ce, Sn, La, U, Th, and Ba. These elements are usually found as highly-charged trace elements in granitic magmas, and the case is probably the same here.

One of the goals of a principal component analysis is to reduce the total variance of a dataset by defining the variance caused by intercorrelation between factors (Reyment and Jöreskog, 1993). The three factors in this analysis account for 80% of the total variance within the dataset.

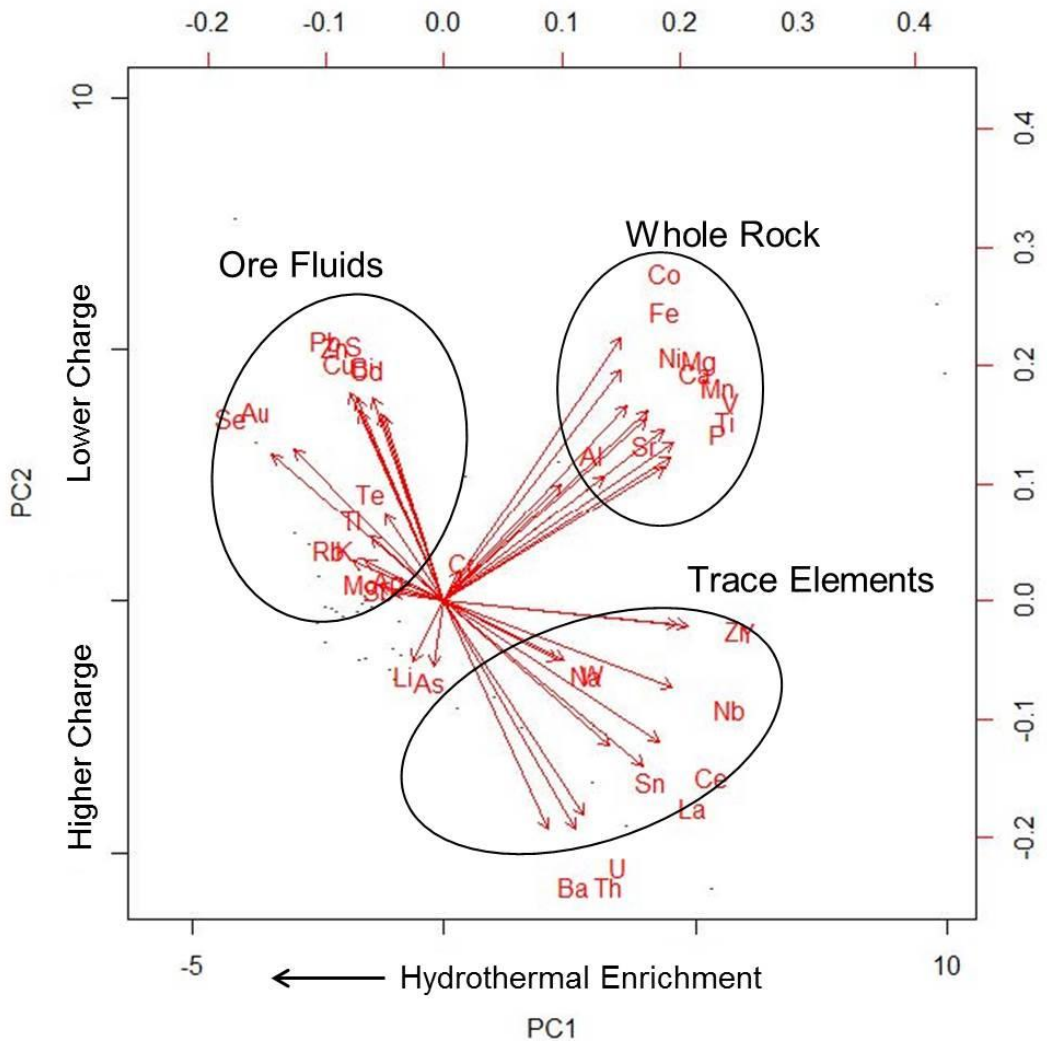

Figure 13: Graphical representation of the Principal Component Analysis showing three distinct clusters of elements.

Reflected Light Microscopy

There are several classes of textures that were observed in 18 polished sections of high grade ore from the four sampling locations [Trade Dollar (TD), Dewey (DEW), Idaho Tunnel (IT), and Black Jack (BJ)] along the Black Jack-Trade Dollar vein. For the purposes of mineral identification, almost all silver phases of varying compositions are referred to as naumannite in these reflected light photomicrographs.

Fractal Dendrites

Fractal dendrites are three-dimensional structures formed by random, diffusion-limited processes that occur in boiling hydrothermal solutions (Saunders et al., 1996). This ore texture is present in the highest grade ore samples from Trade Dollar and Dewey. Because the three-dimensional nature of this texture is difficult to see in polished section, dendritic growth of ore minerals is recognized by the dense clumps of intergrown sulfides and selenides (Fig. Figure **14**). In these dendrites, there is a chaotic, disorganized mixture of chalcopyrite (cp), naumannite (nm), electrum (el), sphalerite (sp), galena (gl), opalline silica (op), and quartz (qtz) (Fig. Figure **15** and Fig. Figure **16**). Individual grains of sulfides are small (<0.2 mm) and show each phase replacing and being replaced by its neighbors. Due to the intricate nature of the grain boundaries, all of the phases present appear to have been deposited at around the same time. Generally, the dendrites from Trade Dollar contain equal amounts of naumannite and chalcopyrite whereas Dewey has more chalcopyrite than naumannite.

Figure 14: Photograph of a hand sample from Trade Dollar showing several high-grade dendrites.

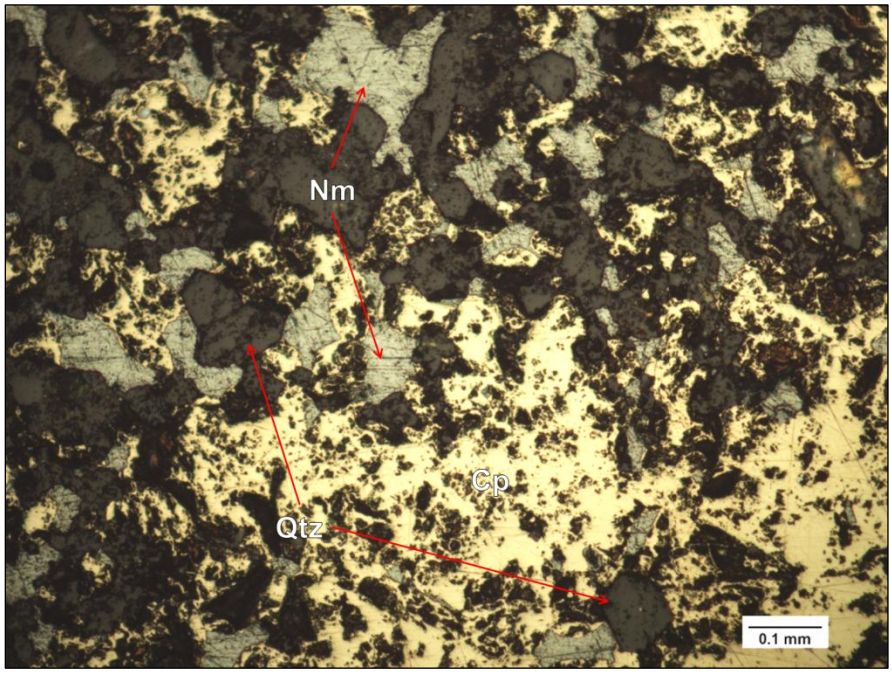

Figure 15: Photomicrograph of a portion of a dendrite from Dewey showing cp>nm with qtz.

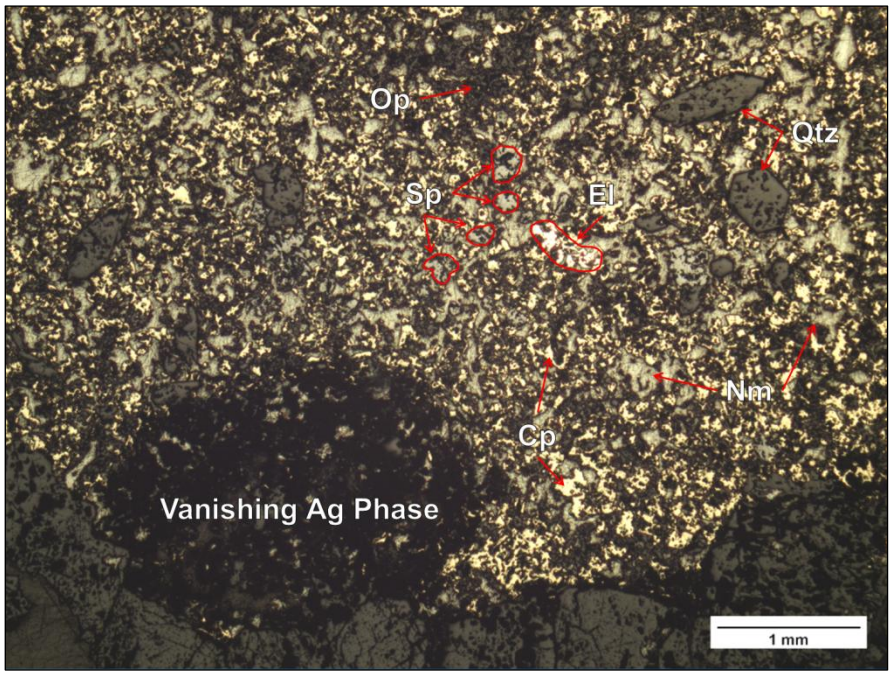

Figure 16: Photomicrograph of a portion of a dendrite from Trade Dollar showing cp ≈ nm with el, sp, op, and qtz.

Quartz Euhedra

Doubly terminated, euhedral quartz crystals have been observed within the highest-grade portions of the mineralization in the Black Jack-Trade Dollar vein. These crystals range in length from 0.1 mm to 0.7 mm and do not appear to be attached to any vein wall. Observing the double terminations ensures that the c-axis of the quartz crystal lies in the field of view and reduces the likelihood that it is attached to a vein wall. The euhedra are found within the high-grade dendrites co-deposited with sulfides, selenides, and opalline quartz (Fig. Figure **17**). Unlike other well-formed quartz crystals in the gangue, these quartz euhedra commonly contain inclusions of sulfide minerals. It is highly likely that these inclusions were captured as the quartz euhedra grew, free of the vein walls, while floating in metal-rich ore fluids. These quartz euhedra are co-deposited with opalline silica, which forms under very different thermodynamic conditions than those that typically form euhedral quartz crystals. This shows that the quartz euhedra were likely transported from some lower level of the vein system and were deposited amongst the high-grade dendrites. It is possible and maybe even likely that well-formed quartz euhedra exist within other portions of the mineralization. To date, they have only been identified within the high-grade dendrites due to the ease of distinguishing the doubly-terminated habit of the crystals when they are completely surrounded by metals and opalline silica.

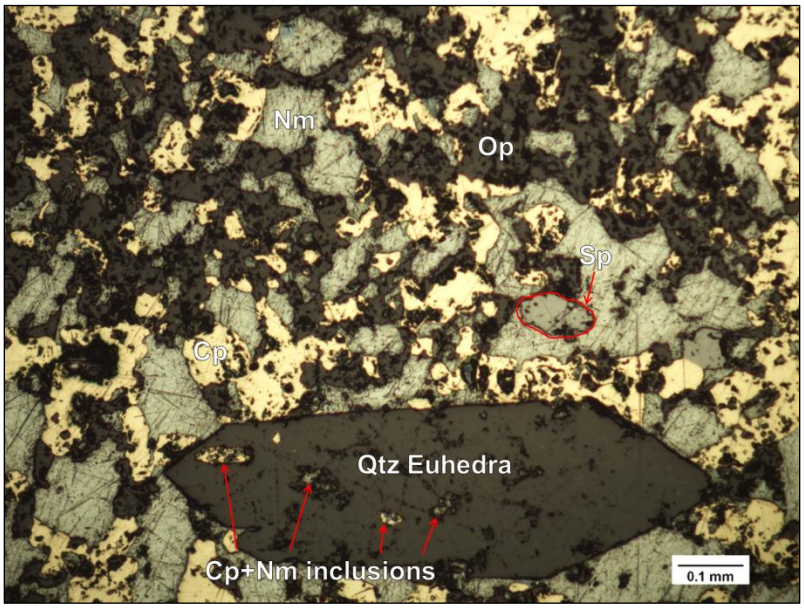

Figure 17: Photomicrograph of a doubly-terminated quartz euhedra (with inclusions of naumannite and chalcopyrite) shown “floating” in a dendrite with nm, cp, sp, and op.

"Vanishing" Silver Phase

This is a silver phase that was present when the ore sample was freshly cut that does not appear on the polished sections. Sometime before the ore sample was studied, this silver phase oxidized, crumbled away, and left visible holes in the polished sections. It is identified by its conspicuous absence with occasional relict pieces left in an otherwise empty space (Fig. Figure **18**). Because this phase disappears before it can be documented, its composition is unknown. It is typically observed in high-grade samples with dendrites or large clusters of sulfides and selenides, such as TD High Grade, TD5, and DEW2. Like the quartz euhedra, this phase may exist in other modes of mineralization, but it is, by its nature, easiest to recognize when it is entirely surrounded by other metallic phases.

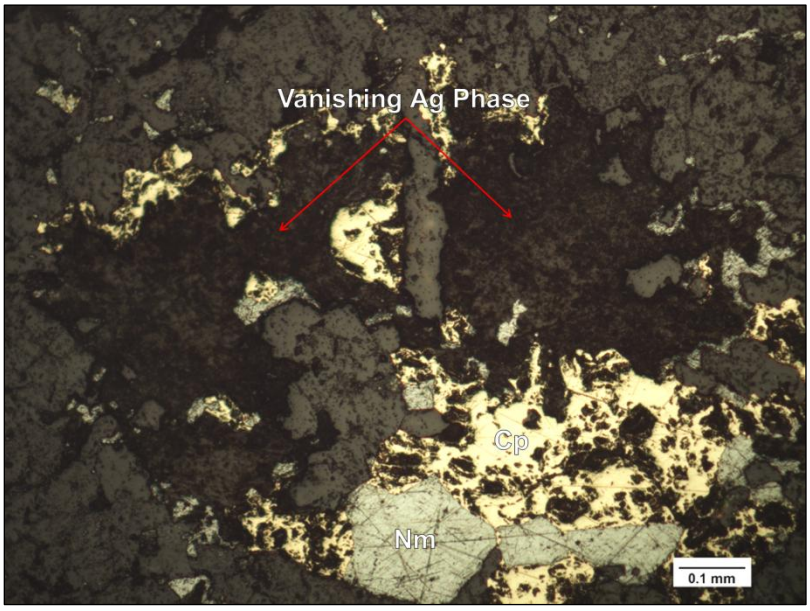

Figure 18: Photomicrograph showing the holes in this section where the "vanishing" silver phase was once found. Sample is DEW2 with nm, cp, and qtz also present.

Intergrown Silver Phases

Normally, the ore samples from the Black Jack-Trade Dollar vein contain different silver minerals that are so similar that they cannot be distinguished under the microscope and are simply identified as "naumannite". Because of the difficulty in distinguishing different silver phases in reflected light, this texture was only observed locally in the ore samples (Fig. Figure **19**). In sample DEW4, one grain contained chalcopyrite, galena, native silver, and at least three other distinct silver phases. These silver phases contained intricate intergrowths at the micro-scale and were only distinguished because of slight variations in polishing hardness and bireflectance. The presence of and differences between these phases was confirmed on similar grains from other samples by backscatter imaging on the electron microprobe. Native silver was identified based upon the disappearance of tarnish covering a distinct grain and the subsequent dramatic increase in reflectance after the sample was polished with a buffing pad.

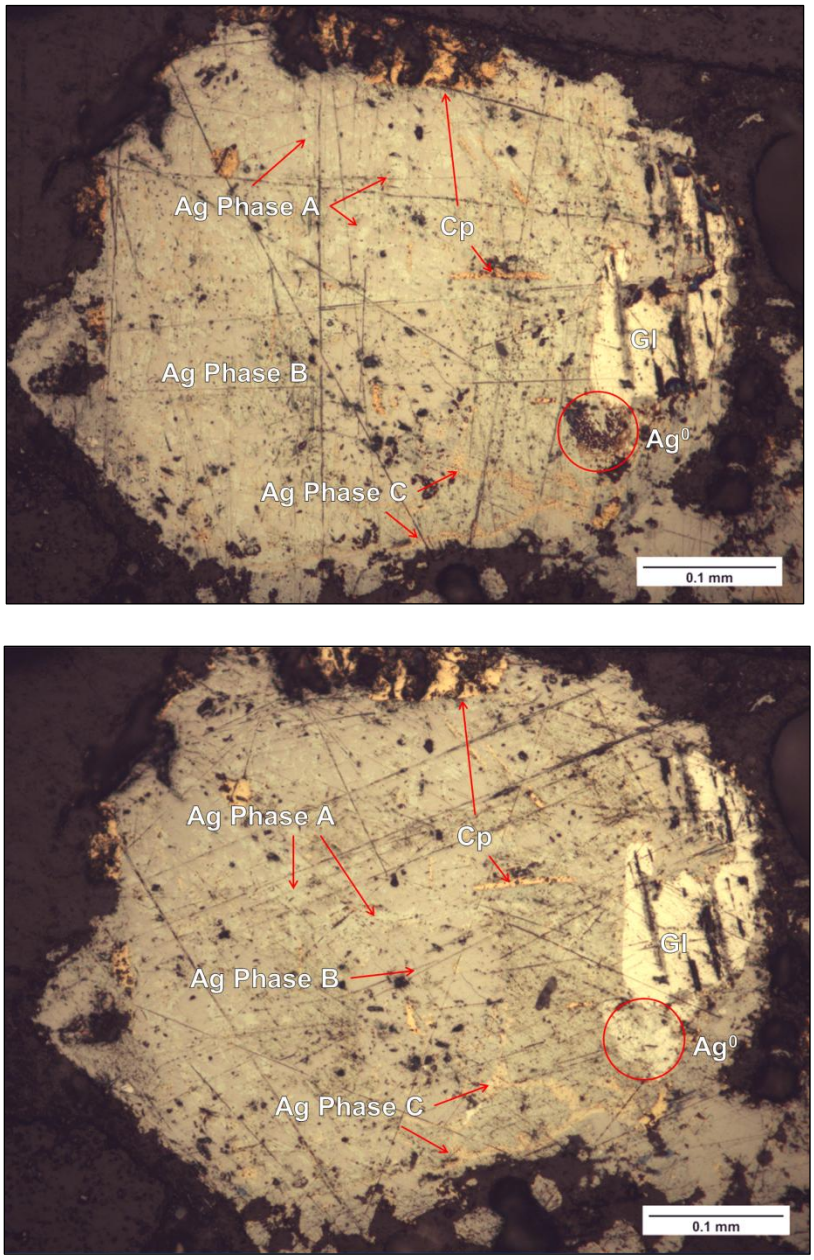

Figure 19: Photomicrographs of a grain from DEW4 showing galena (gl), chalcopyrite (cp), and four silver phases. Silver phases A, B, and C are identified based upon slight changes in color and polishing hardness. In the upper picture, there is a tarnished region (Ag^o), shown in the red circle, that becomes very bright when buffed, as shown by the lower picture.

Mineralized Veinlets/Fracture Zone Fill/Disseminated Naumannite

These three textures are classified together because they generally occur in the same portions of the mineralization. The few fracture zones that occur within the host rocks are typically mineralized (Fig. Figure **20**), resulting in thin veinlets filled primarily with naumannite±electrum, galena, and chalcopyrite. In some cases, these thin naumannite veinlets occur next to high concentrations of disseminated naumannite grains that may only be 10-100 µm wide (Fig. Figure **21**). In one ore sample, BJ2, there does not appear to be any visible sulfide/selenide mineralization except for some relict pyrite grains, but the sample contains more than 200 ppm Ag. This shows that disseminated naumannite grains likely account for a large portion of the massive amount of Ag mineralization in the Black Jack-Trade Dollar vein.

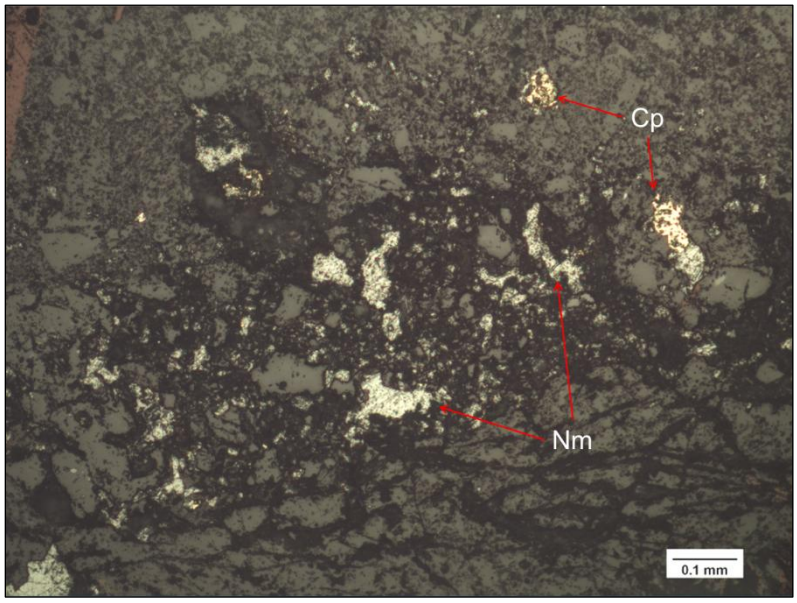

Figure 20: Photomicrograph of DEW1 sample showing cp and nm blebs in a mineralized fracture zone.

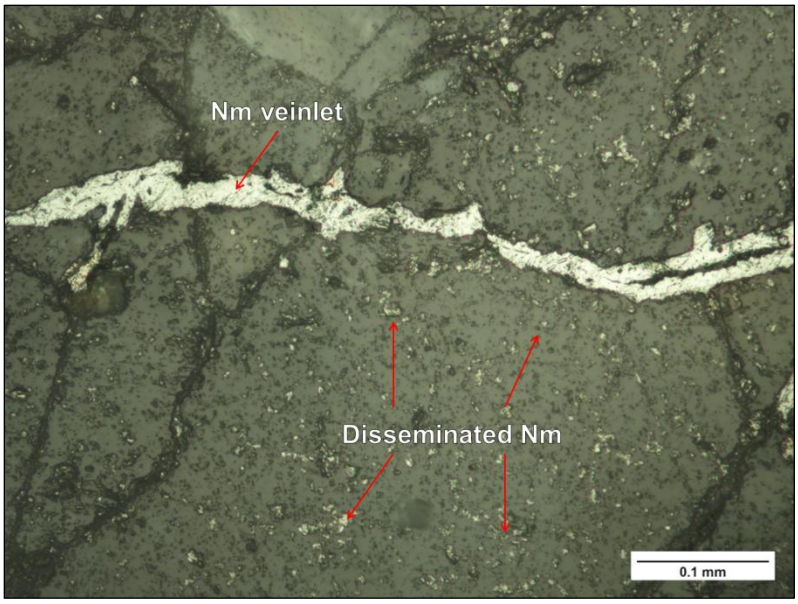

Figure 21: Photomicrograph of a thin nm veinlet with smaller grains of disseminated nm around it.

Relict Grains

There are many instances within isolated blobs of sulfides and selenides in which one phase exists as an "island" in a larger grain of another mineral. Based upon convex-concave grain boundary relationships, earlier-formed phases typically exhibit concave edges as they are replaced by later minerals. These relict grains typically belong to phases that formed earlier in the paragenetic sequence, such as pyrite (Fig. Figure **22**), chalcopyrite (Fig. Figure **23**), galena, or sphalerite. In instances where multiple sulfides are left as relict grains, it is possible to determine the entire paragenesis (described in a later section) of the Black Jack-Trade Dollar vein.

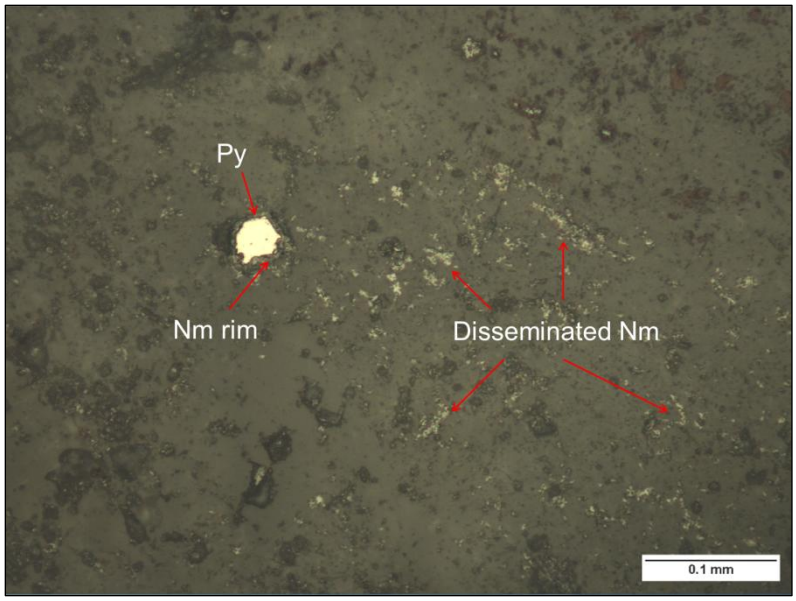

Figure 22: Photomicrograph from sample BJ2 showing a relict pyrite grain being replaced by later naumannite, as well as an area of small, disseminated naumannite grains.

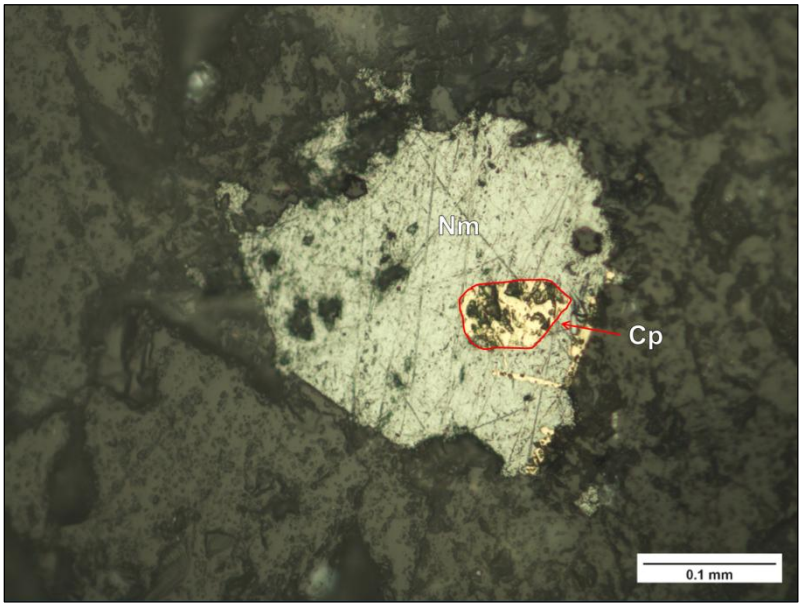

Figure 23: Photomicrograph of naumannite from Sample TD4 showing relict chalcopyrite grains in the center and rim of the grain.

Isolated Aggregates of Sulfides and Selenides

This is the most common ore texture present in the ores from the Black Jack-Trade Dollar vein. Small aggregates of sulfide-selenide minerals, typically less than 0.5 mm in diameter, occur in loosely defined bands of mineralization. These aggregates of sulfides and selenides appear to show many of the same textural relationships that appear in the high-grade dendrites, but on a much smaller scale. It is common within these groups of ore minerals to have islands of earlier phases intruded by later phases (Fig. Figure **24**). Based upon these relationships, it is possible to interpret the paragenesis of the ore minerals.

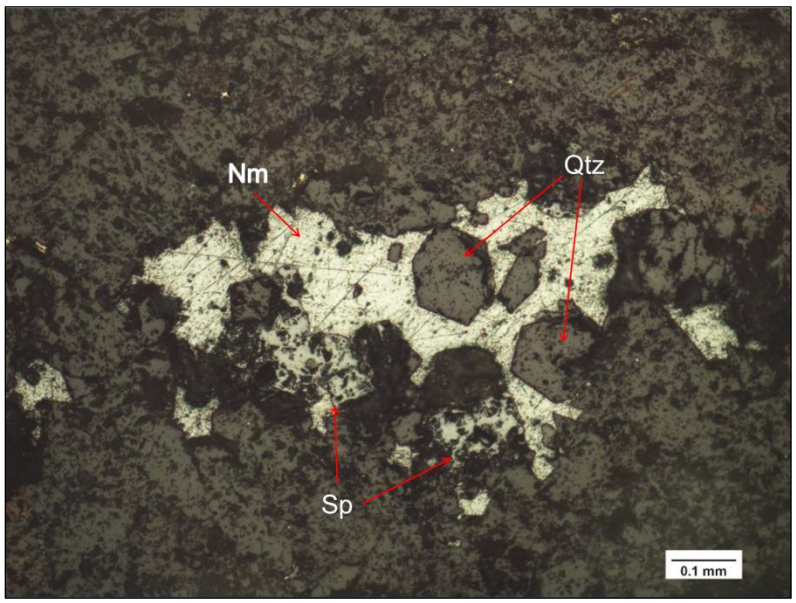

Figure 24: Photomicrograph of an isolated aggregate of sphalerite, naumannite, and quartz in sample DEW1.

Paragenesis of the Black Jack-Trade Dollar Vein

Based upon textural relationships (embayment, replacement, overgrowths, crustification, cross-cutting, etc.) between different mineral species, it is possible to interpret the general paragenesis of the Black Jack-Trade Dollar vein. The first mineral species to appear is pyrite, but it is rarely found associated with other ore minerals. When pyrite is found in the ore assemblage, it is typically being replaced by later sulfides and selenides. This is seen in Figure 25, where naumannite shows cusp and carries texture with the pyrite grain at multiple locations (Stanton, 1972). The next stage of the paragenesis involves the appearance of base metal sulfides such as chalcopyrite, galena, and sphalerite. Figure 26 shows several isolated aggregates of sulfides where galena is encrusted by sphalerite. At another location within the same aggregate of sulfides, chalcopyrite intrudes into sphalerite. Similar grain relationships can be found in all ore samples with isolated sulfide aggregates, but there is enough variation to make it impossible to distinguish which of the sulfides was deposited first, suggesting that deposition of chalcopyrite, galena, and sphalerite was contemporaneous. The last stage in the paragenesis is the deposition of electrum, naumannite, and other silver phases. Electrum and the silver minerals create embayments in, or surround islands, of all earlier sulfides. This is shown in Figure 27, where both electrum and naumannite are in contact with chalcopyrite and demonstrate cusp and carry texture grain boundaries that suggest replacement of the sulfide.

This paragenetic sequence generally applies in the lower-grade ore samples, but it is apparent that, based upon the textural relationships within the high-grade dendrites, the paragenesis does not apply to the high-grade ores. Within high-grade dendrites, all of the

ore minerals (sulfides, selenides, and electrum), except for pyrite, were deposited at approximately the same time. It is therefore appropriate that each stage in the paragenesis is more accurately described as a sub-stage of the mineralization.

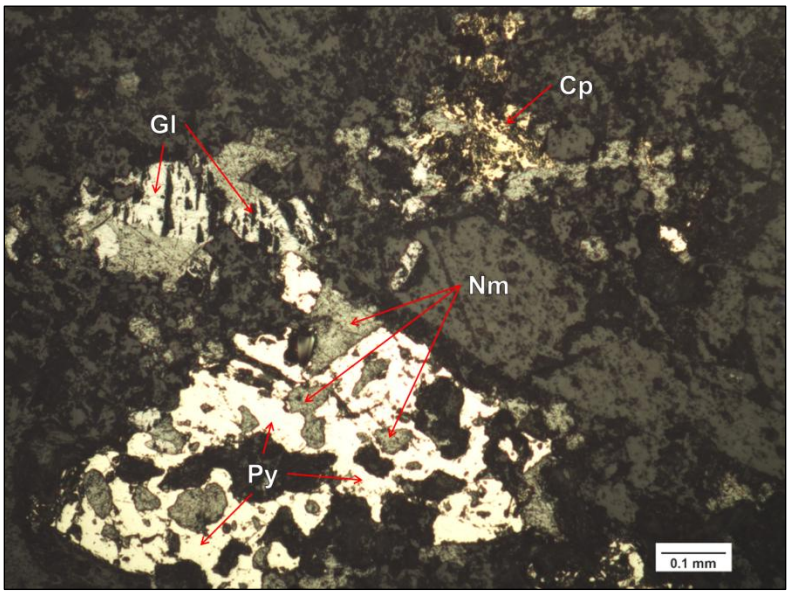

Figure 25: Photomicrograph of an isolated aggregate of ore minerals showing an early pyrite grain being replaced by naumannite with other sulfides (gl and cp) present.

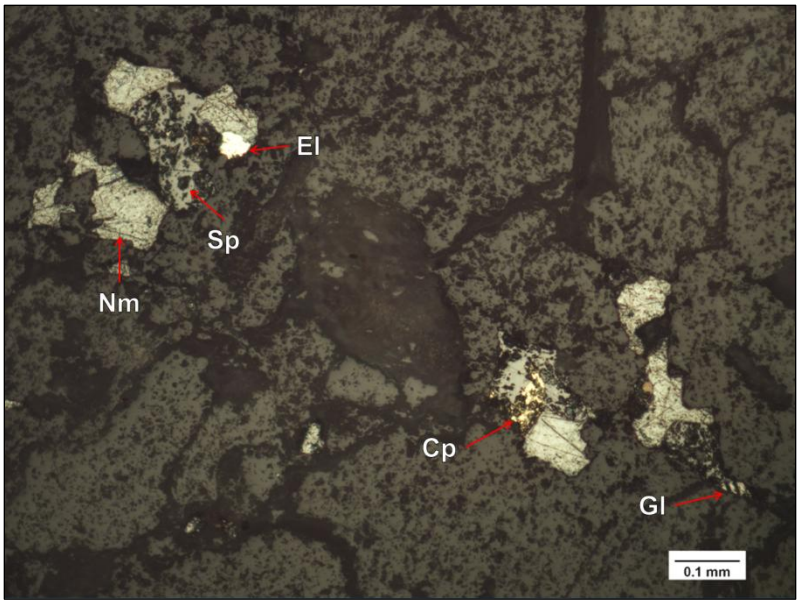

Figure 26: Photomicrograph of grains of galena, sphalerite, and chalcopyrite being encrusted by later naumannite and electrum.

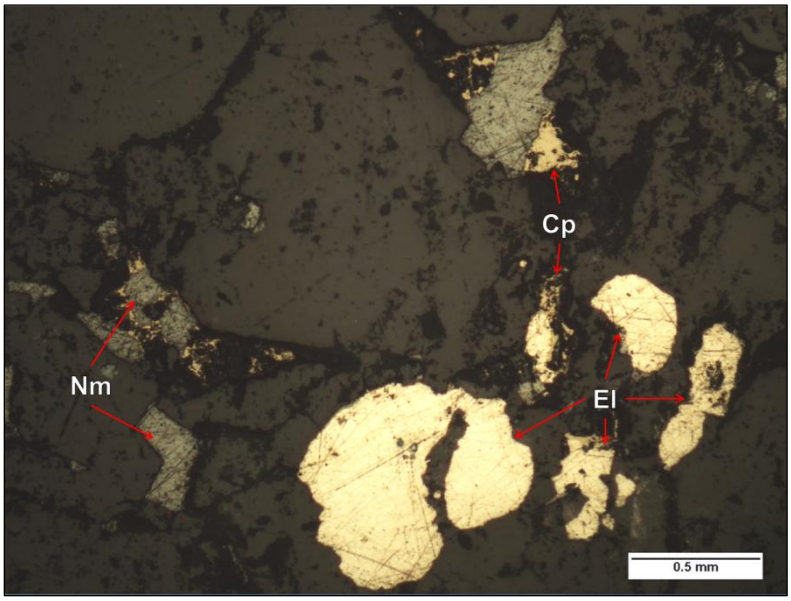

Figure 27: Photomicrograph of chalcopyrite grains being embayed by both electrum and naumannite, representing the latest stage of mineralization.

Transmitted Light Microscopy

In order to fully describe the ore samples found in the Black Jack-Trade Dollar vein, thin sections were made of the same ore samples and used to characterize the gangue mineral textures. Terminology used here to describe the gangue textures in the Black Jack-Trade Dollar vein follows that of the classification schemes of Sander and Black (1988), Dong et al. (1995), Morrison et al. (1995), Moncada et al. (2012), and Shimizu (2014).

Massive Quartz and Adularia

This texture represents the most common occurrence of gangue minerals in the vein and is composed of randomly oriented quartz and adularia grains. In thin section, massive quartz and adularia texture contains subhedral to euhedral grains of both quartz and adularia crystals of varying sizes. In hand sample, it is often difficult to distinguish between quartz and adularia unless you are looking at an open space in the vein.

In the Black Jack-Trade Dollar vein, quartz and adularia are found in approximately equal abundance, but the adularia grains tend to be much larger (2-5 mm) than the quartz grains (<1 mm). Larger crystals of adularia have been observed in hand sample (Fig. Figure **28**); the typical size and crystal habit of adularia is shown in Figure 29.

Figure 28: Photograph of a hand sample showing several large crystals of adularia with much smaller quartz grains surrounding them.

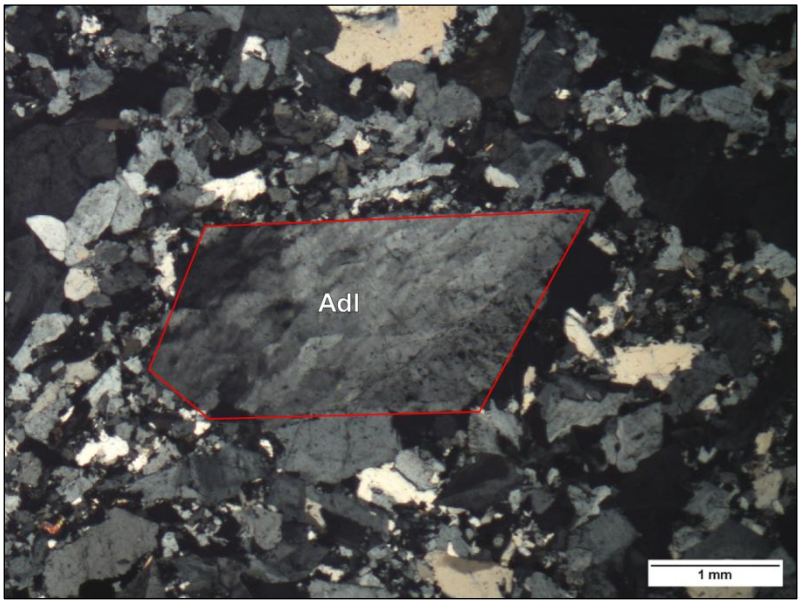

Figure 29: Photomicrograph (transmitted light with crossed polarizer) of the typical habit of adularia in the center of the image, surrounded by randomly oriented subhedral to euhedral quartz crystals of the massive quartz+adularia texture.

Comb Quartz

Comb quartz texture occurs when quartz crystals grow in subparallel, subhedral rows of crystals perpendicular to the vein wall. This results in a texture where rows of quartz prisms are growing inwards from a substrate and meeting in the center of a vein (Fig. Figure **30**). These comb quartz crystals grow into the free space present at the center of the vein and have been interpreted by earlier workers as forming from quiescient, slightly silica-supersaturated fluids (Fournier, 1985; Shimizu, 2014).

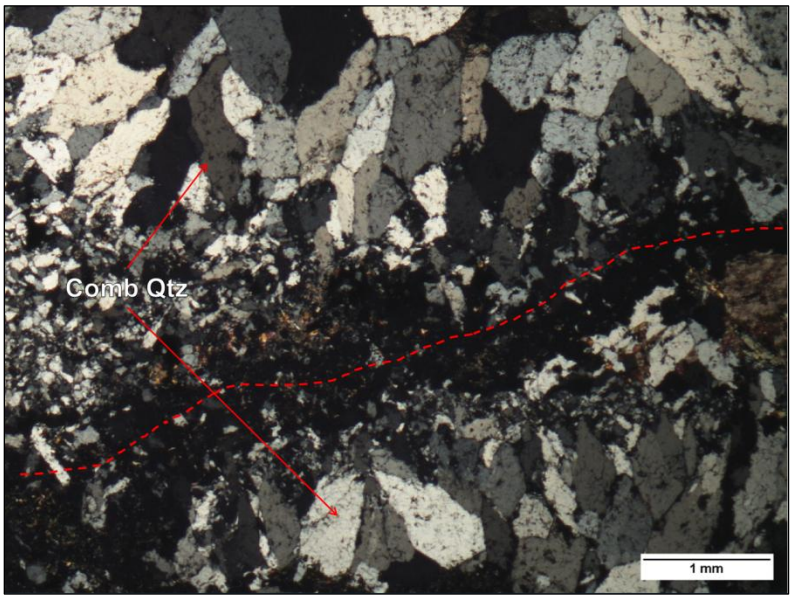

Figure 30: Photomicrograph (transmitted light with crossed polarizer) showing two generations of comb quartz (stacked on top of each other in the top and bottom of the image) growing towards the center of the vein (marked by the dashed line).

Crustiform/Cockade Quartz

Crustiform quartz texture is formed when multiple generations of quartz, formed into narrow bands, grow upon a substrate. This leads to a banded appearance of the

gangue minerals. The individual bands in crustiform habit can often be identified by differences in size and style of crystallization as shown by the layers of adularia and quartz in Figure 31. This same crustiform habit is called cockade quartz when the narrow quartz bands grow upon a piece of substrate, such as a breccia fragment, that is found in the middle of a quartz vein. Figure 32 shows this cockade texture in the Black Jack-Trade Dollar vein with a layer of comb quartz growing outwards from a granite cobble found in the vein.

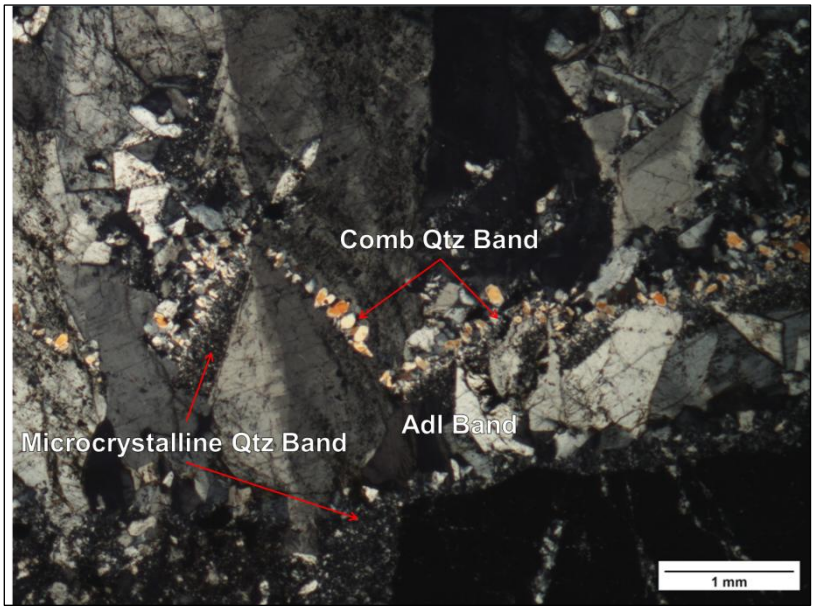

Figure 31: Photomicrograph (transmitted light with crossed polarizer) showing crustiform banding of multiple generations of quartz and adularia upon a vein wall substrate.

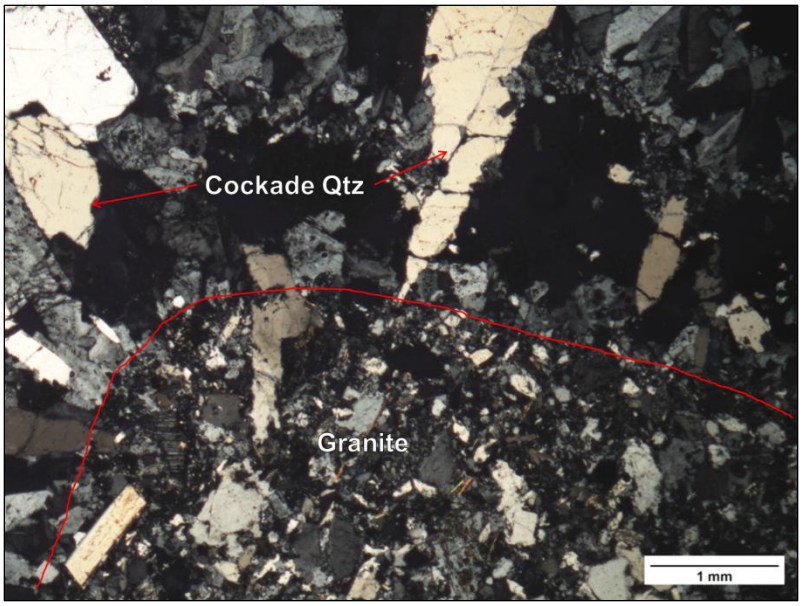

Figure 32: Photomicrograph (transmitted light with crossed polarizer) showing cockade texture with a layer of comb quartz growing outward on a granite substrate in the middle of a quartz vein.

Plumose Quartz

Plumose quartz is a texture that is typically developed within individual, large euhedral quartz grains. This texture is recognized by the small, radially-oriented, domains within a quartz crystal that develop a pseudo-undulose extinction pattern (Fig. Figure **33**). Each quartz domain goes extinct at one distinct time, but the neighboring quartz domains are usually very near entinction at the same position. Unlike true undulose extinction in quartz, this pseudo-undulose extinction developed without the quartz crystal being deformed. Plumose quartz is usually formed as a result of the recrystallization of chalcedony, or fibrous quartz (Sander and Black, 1988; Dong et al., 1995).

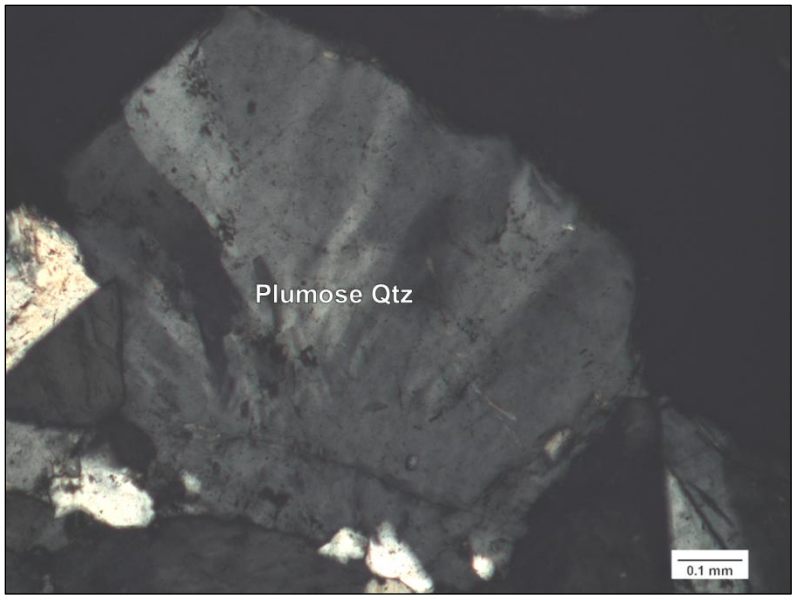

Figure 33: Photomicrograph (transmitted light with crossed polarizer) of plumose quartz crystal showing radially-oriented, distinct domains that go extinct in an undulose pattern.

Quartz Pseudomorph After Calcite

In epithermal systems, it is common to see bladed quartz crystals present in the veins. This texture occurs when early-formed calcite crystals are later replaced by silica-rich fluids. Rarely, the original calcite blades are preserved, such as at the Midas mine (Chitwood, 2012). There are several textural varieties of quartz replacing calcite (Dong et al., 1995). The first is called ghost bladed quartz and is recognized by the thin, parallel arrangements of rectangular quartz domains that make up the relict bladed texture of the calcite crystal (Fig. Figure **34**). It is common in epithermal systems for there to be many blades of quartz crystals stacked on top of each other, but these ore samples only exhibit a few small clusters of ghost bladed quartz. The second calcite replacement texture

observed in the ores is called lattice bladed quartz. This texture is recognized as a group of bladed crystals made up of quartz growing into the center of the blade, giving the blades a fuzzy appearance. These lattice bladed crystals typically occur in clusters, contain polyhedral cavities between the blades, and have quartz crystals growing on the blades themselves (Dong et al., 1995). In these ore samples, this lattice bladed quartz texture was only observed locally as lone bladed crystals with later overgrowths of other quartz textures (Fig. Figure **35**).

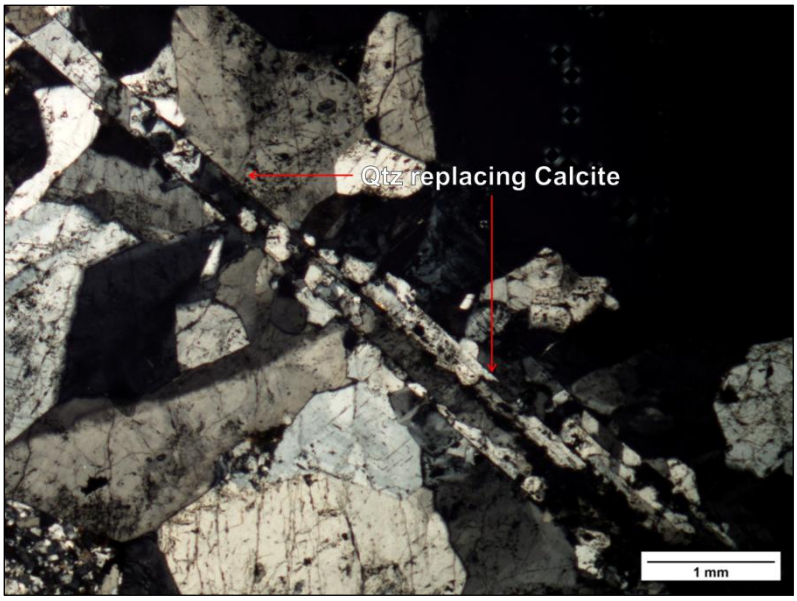

Figure 34: Photomicrograph (transmitted light with crossed polarizer) showing ghost bladed quartz replacement of several prominent bladed calcite crystals.

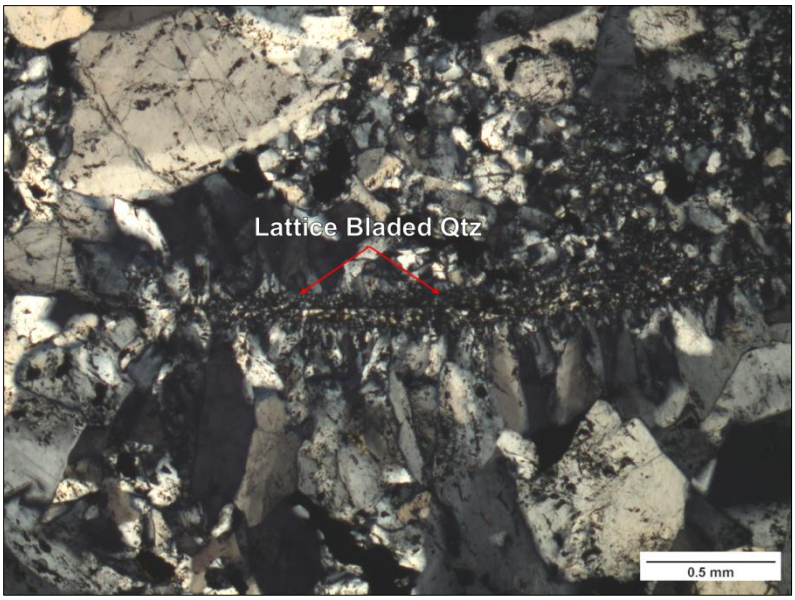

Figure 35: Photomicrograph (transmitted light with crossed polarizer) showing a single lattice bladed quartz crystal with later overgrowth of comb quartz and microcrystalline quartz.

Chalcedony

Chalcedony, or banded quartz, forms as a radially-oriented, fibrous variety of quartz. Chalcedony often forms a colloform habit, which means that the upper surface of the crystal is rounded (Dong et al., 1995). Due to this colloform habit, it is common for chalcedony to form distinct parallel layers in a crustiform vein. The fibers that make up chalcedony radiate outward from their point of nucleation. Dong et al. (1995) assert that chalcedony can be formed as both an original growth texture of quartz and as a recrystallization phase of opal. As chalcedony recrystallizes, the individual fibers merge together, eventually becoming a single quartz crystal, often with a plumose extinction. Chalcedony is often recognized for impurities that occur across the growth direction of the quartz fibers (Fig. Figure **36**).

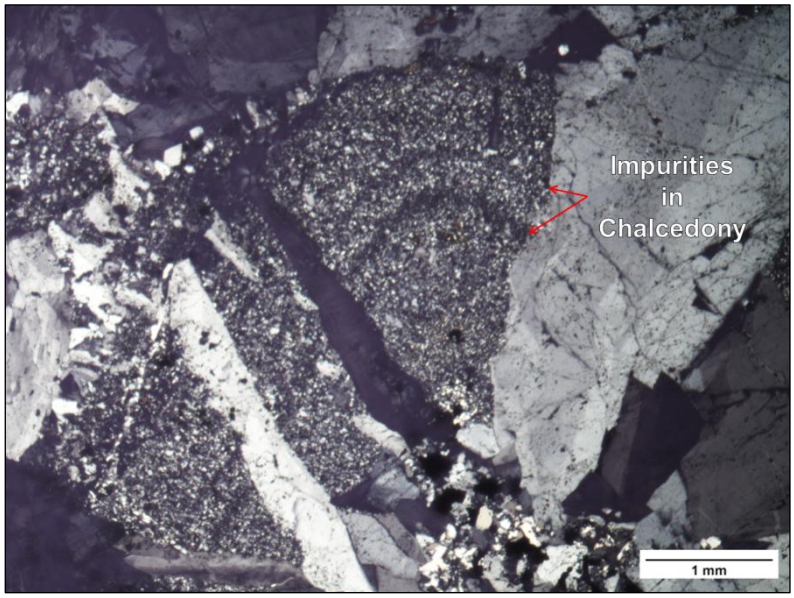

Figure 36: Photomicrograph (transmitted light with crossed polarizer) of a crystal showing chalcedony recrystallizing into coarser forms of quartz. There are several bands of impurities that occur within the chalcedony.

Mosaic/Jigsaw/Microcrystalline Quartz

Microcrystalline quartz, as its name implies, is quartz that is made of very small, equant crystals. This texture is usually recognized as a fine-grained mass that has no preferred extinction pattern and often contains Au-Ag bearing minerals (Moncada et al., 2012). It is likely the first step in the recrystallization process of opal into quartz (Fig.Figure **37**). As microcrystalline quartz grains grow larger during the recrystallization process, it forms mosaic quartz. Mosaic (or jigsaw) quartz is recognized by the small, equant quartz crystals that have irregular seriate boundaries which meet at near perfect triple junctions (Fig. Figure **38**). Occasionally, it is possible to see a growth continuum of microcrystalline quartz into mosaic quartz (Fig. Figure **39**).

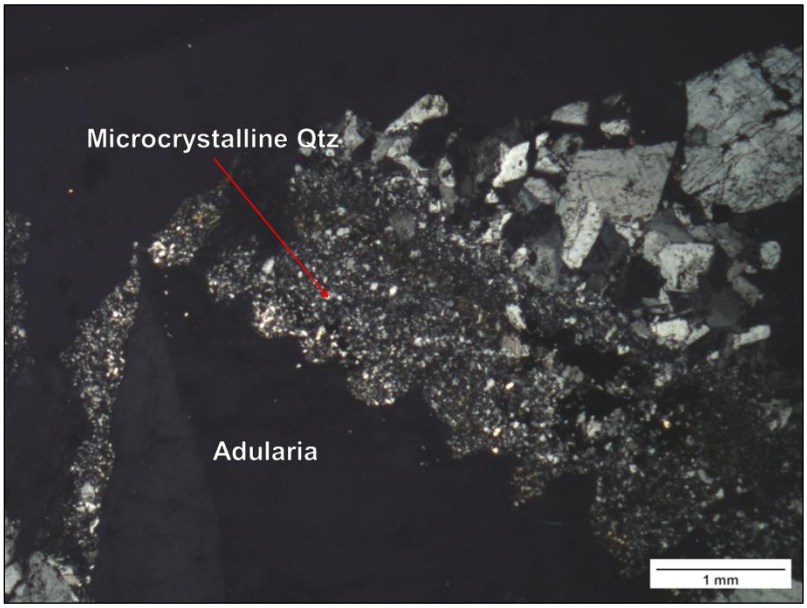

Figure 37: Photomicrograph (transmitted light with crossed polarizer) of microcrystalline quartz on an adularia crystal.

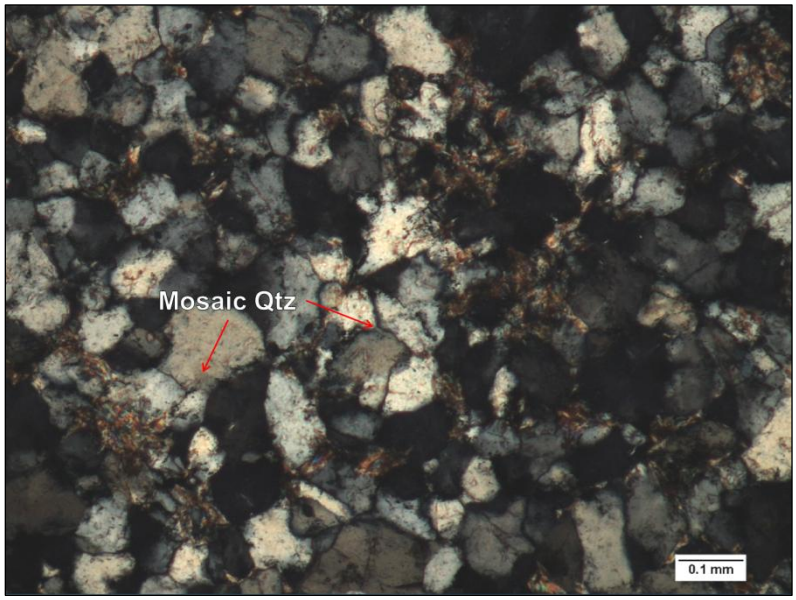

Figure 38: Photomicrograph (transmitted light with crossed polarizer) of mosaic (or jigsaw) quartz showing its characteristic regular geometric crystal shape.

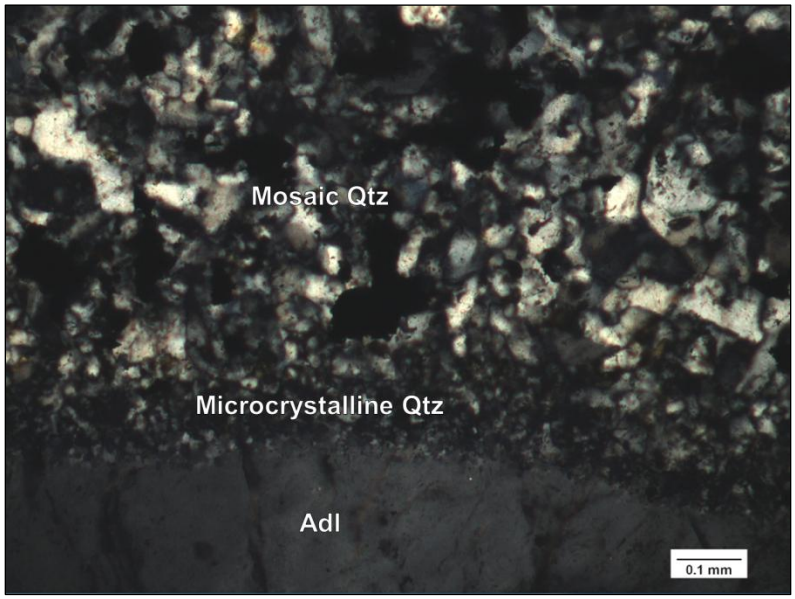

Figure 39: Photomicrograph (transmitted light with crossed polarizer) showing microcrystalline quartz on an adularia crystal. Further from the substrate, the microcrystalline quartz has recrystallized into a mosaic quartz texture.

Electron Microprobe Analysis

In order to help characterize the ore mineralogy in the Black Jack-Trade Dollar vein, it was necessary to use the electron microprobe in order to determine the composition of the electrum and differentiate the silver phases present in the ores.

In order to collect data on the composition of electrum in the ores, electrum grains were identified in reflected light and marked for further study. The microprobe performed 38 spot analyses on 11 of these marked electrum grains from four ore samples. These data are presented in Appendix 3. Using the microprobe's backscatter imaging mode, it was observed that several of the electrum grains in the ores are compositionally complex (Fig. Figure **40**) and include islands of silver minerals within the electrum. As a result, there were several analyses that contained almost no Au even though they were present

within an optically identified electrum grain. For those analyses with significant gold present, there was a range of composition from 25 to 58 atomic percent (at. %) Au, with the average electrum grain having a composition of 36.4 at. % Au.

In addition to this range of gold content in electrum, the microprobe data show that there is Se- and S-rich electrum present in the ores. Data for six of the 38 analyses are complicated by 15-20 wt. % Se+S. Because gold and silver are typically the only constituents of electrum, this means that there may be an unknown Au-Ag-Se-S phase in the highest grade ores from the Black Jack-Trade Dollar vein. Based upon the approximate atomic percentages (15% Au, 55% Ag, 15% Se, and 15% S) of this unknown phase, a chemical formula of Ag_3AuSeS can be estimated. This composition represents an unknown mineral, but it resembles the formulas of both fischesserite (Ag_3AuSe_2) and uytenbogaardtite (Ag_3AuS_2). It is possible that this unknown phase present in the electrum grains represents some compositional midpoint between the two phases.

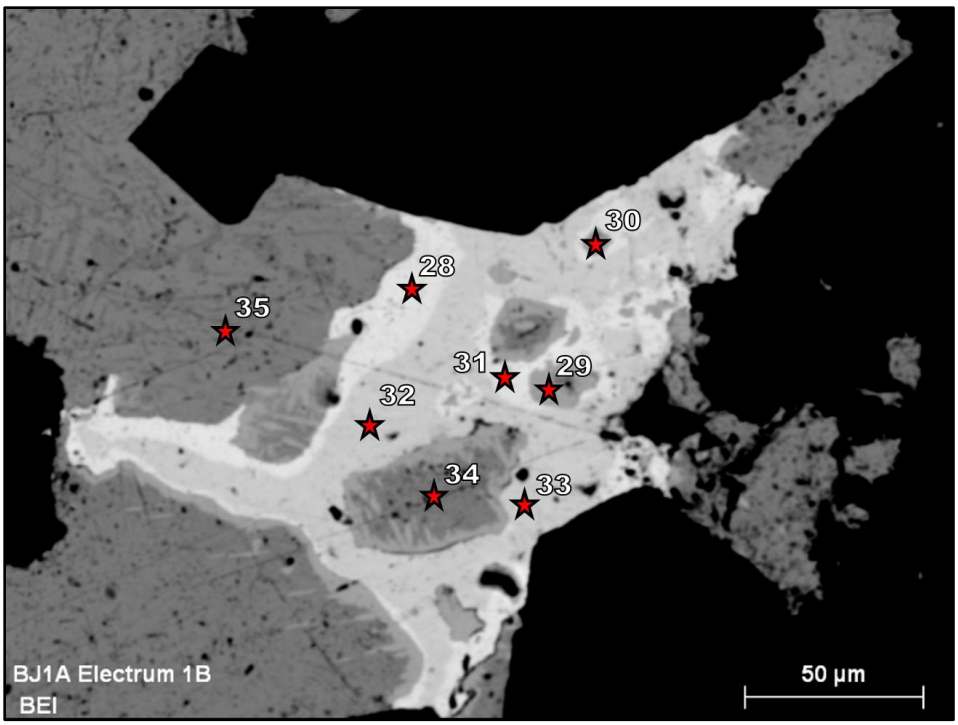

Figure 40: Backscatter electron image showing the complexity within a single grain of electrum. Spot analysis locations are marked with the line number and match the analysis numbers found in Appendix 3. Analyses 28, 31, 32, and 33 represent two distinct compositions of electrum, and analyses 29, 30, 34, and 35 show compositions that are more like Ag minerals in this sample.

In order to describe the specific composition of the silver minerals in the Black Jack-Trade Dollar vein, portions of polished ore sections with a high density of naumannite grains were identified in reflected light and marked for further study. Of particular interest were the highest grade ores (e.g., dendritic textures) and areas that appeared to have multiple silver phases. Microprobe analyses were performed on 117 spots across 10 different ore samples. These data are presented in Appendix 4. Each spot was analyzed for Ag, Se, S, As, and Sb. This group of elements comprises the compositions of the silver phases previously described on Florida Mountain, so it was assumed that these elements would completely describe any silver phase present.

Reconnaissance EDS spectra showed that several spot analyses contained measurable amounts of copper. Therefore, later analyses also included Cu data and attempted to collect a second analysis on some of the same locations as the earlier analyses.

Most of the spot analyses (Fig. Figure **41**) fall into a range along the acanthite-aguilarite-naumannite compositional continuum (Petruk et al., 1974). These data range in composition from Ag_2S (pure acanthite) to $Ag_2Se_{0.77}S_{0.23}$ (S-bearing naumannite). The highest ore grades showed the most variation in silver minerals, with several locations having as many as three distinct silver minerals in specific textural contexts (Fig. Figure **42**). The microprobe data show that Ag Phase 1, which forms exsolution lamellae within masses of Ag Phase 2, is S-bearing naumannite ($Ag_2Se_{0.75}S_{0.25}$), Ag Phase 2 is Se-bearing acanthite ($Ag_2Se_{0.23}S_{0.77}$), and Ag phase 3 is a Se-bearing acanthite of slightly different composition ($Ag_2Se_{0.25}S_{0.75}$).

Perhaps the most interesting aspect of the varying silver phases is the large amount of compositional variability over such small distances within these ores. As shown in Figure 42, all three phases occur within a single optically-identified "naumannite" grain over a total distance of less than 1 mm.

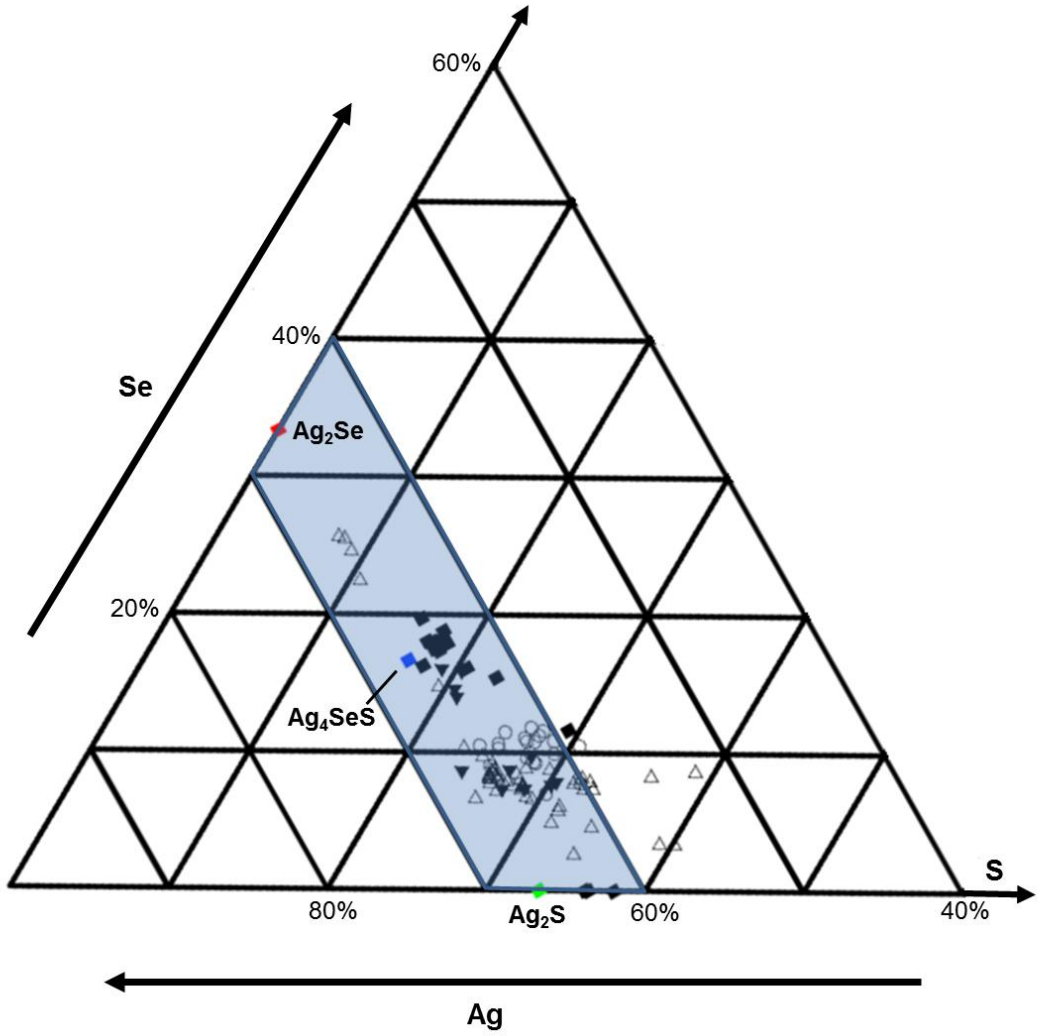

Figure 41: Ternary diagram showing the silver mineral compositions from mine dump samples at the Trade Dollar (hollow triangles), Dewey (hollow circles), Idaho Tunnel (filled triangles), and Black Jack (filled squares) mines using the microprobe data. Most analyses lie near the naumannite-aguilarite-acanthite (nm-ag-ac) compositional continuum (shown by the blue band).

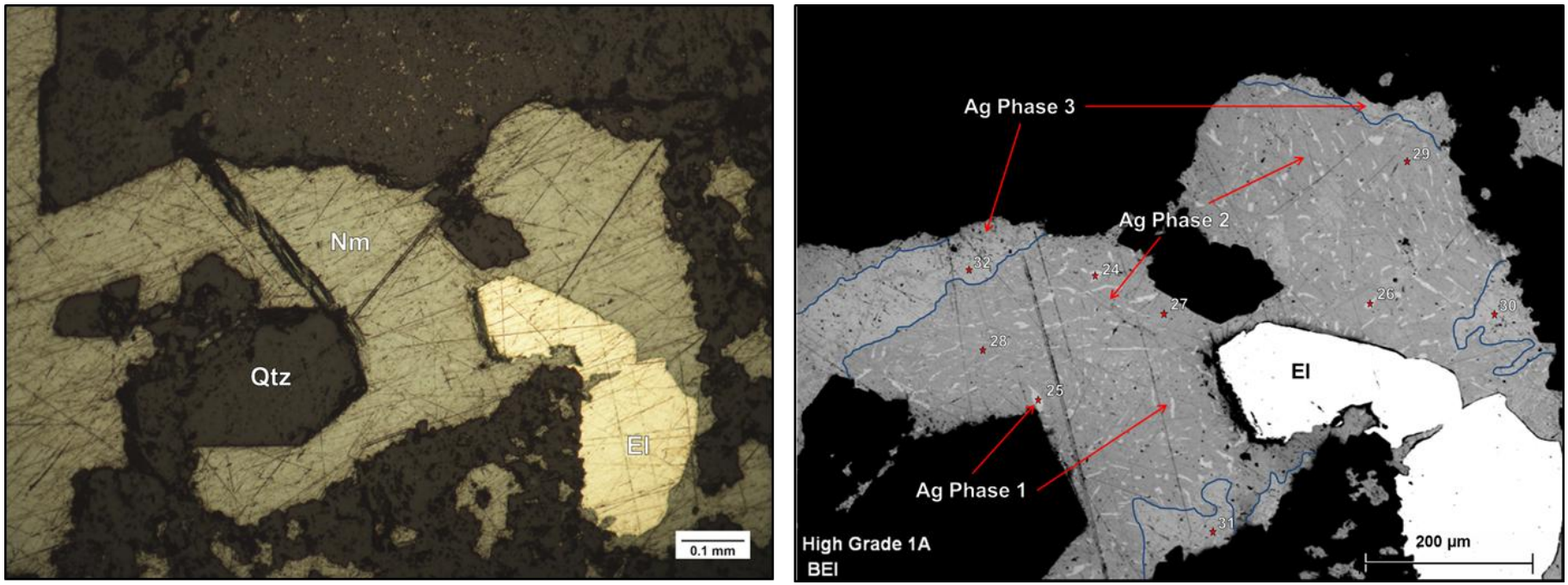

Figure 42: Reflected light photomicrograph (left) and backscatter electron image (BEI) (right) of the same grains in the TD High Grade sample showing the complexity of the silver mineralization. There are 3 distinct phases of silver present in the BEI. Ag phase 1 forms an exsolution texture within the matrix of Ag phase 2, and Ag phase 3 forms its own distinct grains on the edges of the silver grain. The spot analysis locations are marked on the BEI and labeled with the number of the analysis present in Appendix 4.

The microprobe data show several other unusual compositions. There are microprobe analyses of silver minerals that show significant amounts of copper, which would appear to imply that there are three different varieties of Ag-Se-S-Cu phase with copper contents of approximately 1-2, 5-7, and 15-18% Cu (Fig. Figure **43**). Unlike the fairly common copper-bearing phases, the ore samples contained very few arsenic- or antimony-bearing minerals. Only one grain in sample DEW4 showed any significant As or Sb (Fig. Figure **44**). This lack of arsenic- and antimony-bearing phases is unexpected because most previous workers in the area describe several sulfosalts as being present in the mineralization.

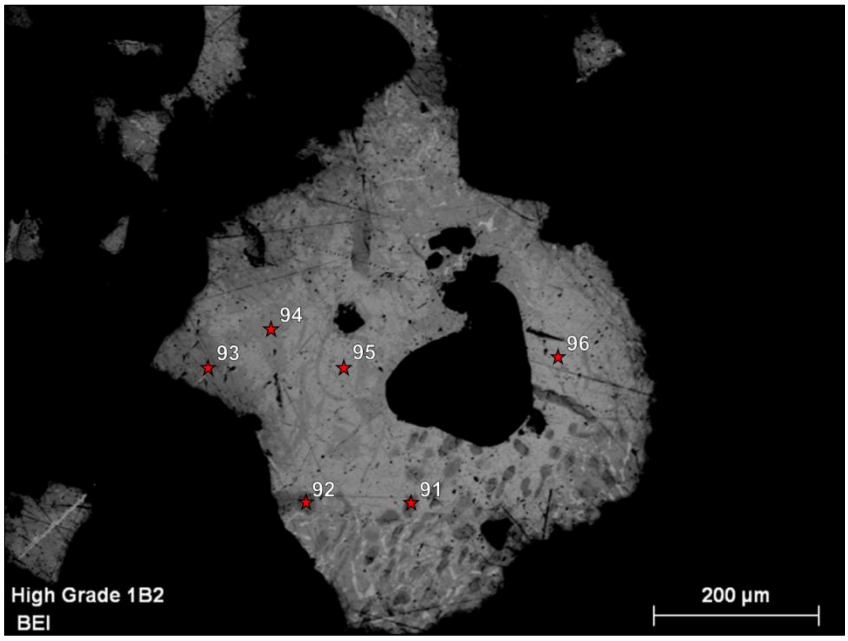

Figure 43: Backscatter electron image of a grain of silver phases that contain significant amounts of copper. The lightest gray phase (analyses 95 and 96) contains 1-2% Cu, the middle gray phase (analyses 93 and 94) contains 5-6% Cu, and the darkest gray phase (analyses 91 and 92) contains 18% Cu. The black phase in the middle of the silver is chalcopyrite. The spot analysis locations labeled correlate to the number of the analysis present in Appendix 4.

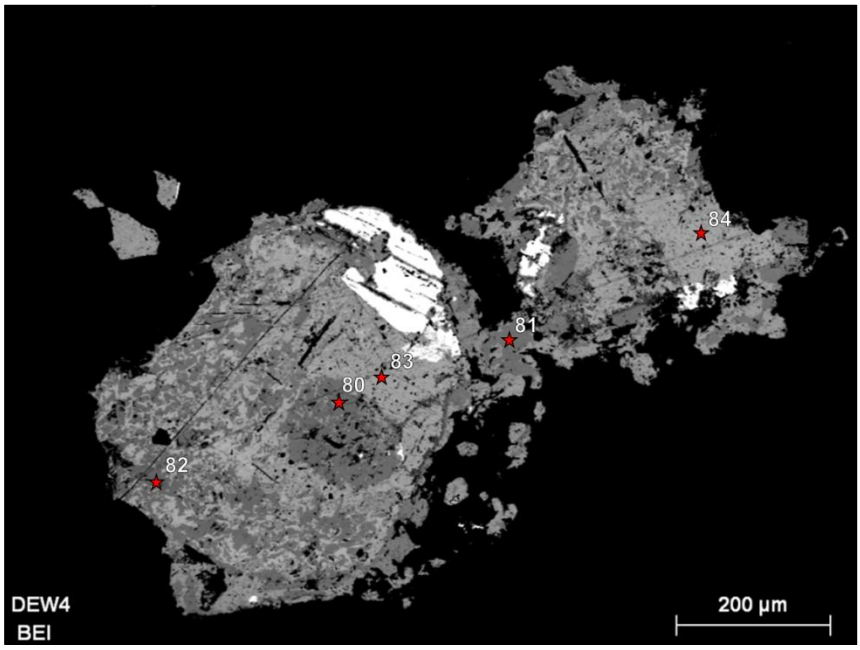

Figure 44: Backscatter electron image of a grain of silver phases that contain significant amounts of arsenic. This grain of silver phases is the same grain as shown in Figure 19. Spot analyses 80-82 contained an average of 44.4% Ag, 6.6% As, 36.9% S, and 11.8% Cu. These analyses represent the only evidence in these ore samples for sulfosalt minerals. The spot analysis locations marked on the image are labeled with the analysis number present in Appendix 4.

Isotopic Analysis

Stable isotope ratios were measured on Cu, S, and Pb isotopes taken from ore stage sulfide and selenide mineral grains. These elements are intimately associated with the ore mineralization present in the Silver City District, so by determining their isotopic signature, some constraints on the origin of these ores can be identified.

In order to ensure that isotope measurements came from ore-stage mineralization, ore samples were trimmed to reduce the amount of gangue minerals present. Samples

were then dissolved in hydrofluoric acid to leave only the metallic minerals. After this dissolution, individual mineral grains were picked out and separated using a binocular microscope. When possible, mineral separates of electrum, naumannite, and chalcopyrite were created for each ore sample. These mineral separates were then used to measure the Cu, S, and Pb isotope values for the ore sample.

Cu Isotopes

The copper isotope measurements in this study were reported using δ^{65}Cu notation, which is defined by the following equation:

$$\delta^{65}Cu = 1000 * \left[\frac{\left(^{65}Cu/^{63}Cu\right)_{sample} - \left(^{65}Cu/^{63}Cu\right)_{NIST976}}{\left(^{65}Cu/^{63}Cu\right)_{NIST976}}\right]$$

Nine ore samples from the Silver City district had their δ^{65}Cu ratio measured by Dr. Ryan Mathur. Five of these samples contained chalcopyrite as the analyzed mineral species, and the other four samples had naumannite grains analyzed for their δ^{65}Cu ratio. The distribution of these samples is shown in Figure 45 and primarily shows a cluster of values near 0±1‰.

These data from the Silver City district were part of a larger study conducted by Dr. James Saunders to determine the stable isotope character of the epithermal ore deposits of the Northern Great Basin. Much like the Silver City district data, the Northern Great Basin ores had copper isotope measurements taken from a combination of

naumannite and chalcopyrite grains (Saunders, pers. commun., 2015). The distribution of this entire data set is shown in Figure 45. Like the Silver City district, most of the Northern Great Basin ore deposits show $\delta^{65}Cu$ values over a narrow range from -2‰ to +2‰.

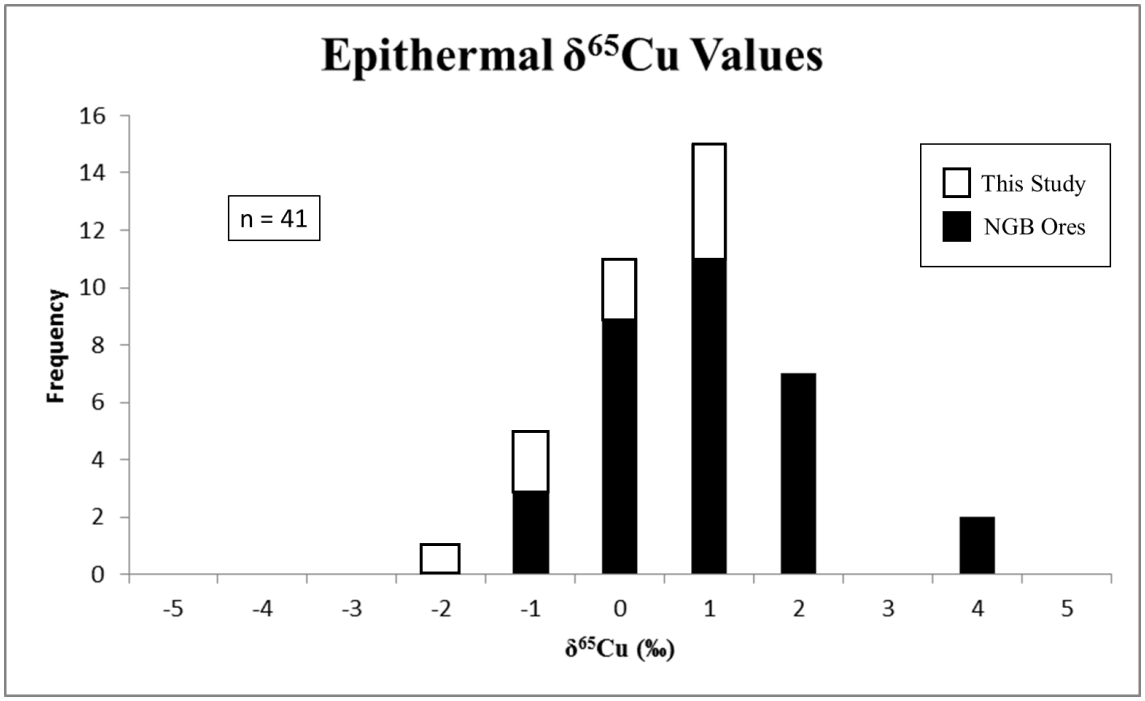

Figure 45: Histogram showing the distribution of Cu isotope values for the Silver City district and the Northern Great Basin epithermal deposits (Saunders, pers. commun., 2015). Isotope values were measured on samples of ore-stage electrum, naumannite, and chalcopyrite from the Buckskin National, Delamar, Ivanhoe, Jumbo, Midas, National, Sleeper, Seven Troughs, Trade Dollar, and War Eagle Mountain mines.

S Isotopes

The sulfur isotopes measurements in this study were reported using $\delta^{34}S$ notation, which is defined by the following equation:

$$\delta^{34}S = 1000 * \left[\frac{\left(^{34}S/^{32}S\right)_{sample} - \left(^{34}S/^{32}S\right)_{VCDT}}{\left(^{34}S/^{32}S\right)_{VCDT}}\right]$$

Sulfur isotopes from the Silver City district were measured from ore stage chalcopyrite. Relative to their standards, the measurements had an error of ±0.03 σ. A distribution of the measured $\delta^{34}S_{VCDT}$ values is shown in Figure 46. Much like for copper isotopes, the distribution is primarily centered on 0±1‰.

Like the copper isotopes study, sulfur isotopes from additional epithermal deposits in the Northern Great Basin were analyzed. The sulfur isotope values, which were all measured on chalcopyrite grains, had values in several modes from -5‰ to +4‰, with the main mode near 0‰ (Fig. Figure **46**). The samples with values of -5‰ are from Buckskin National, and the sample with values of +4‰ are from Midas. Ore samples were taken from several Silver City district mines, including the Dewey, Idaho Tunnel, and Trade Dollar mines on Florida Mountain and the Pauper mine on War Eagle Mountain.

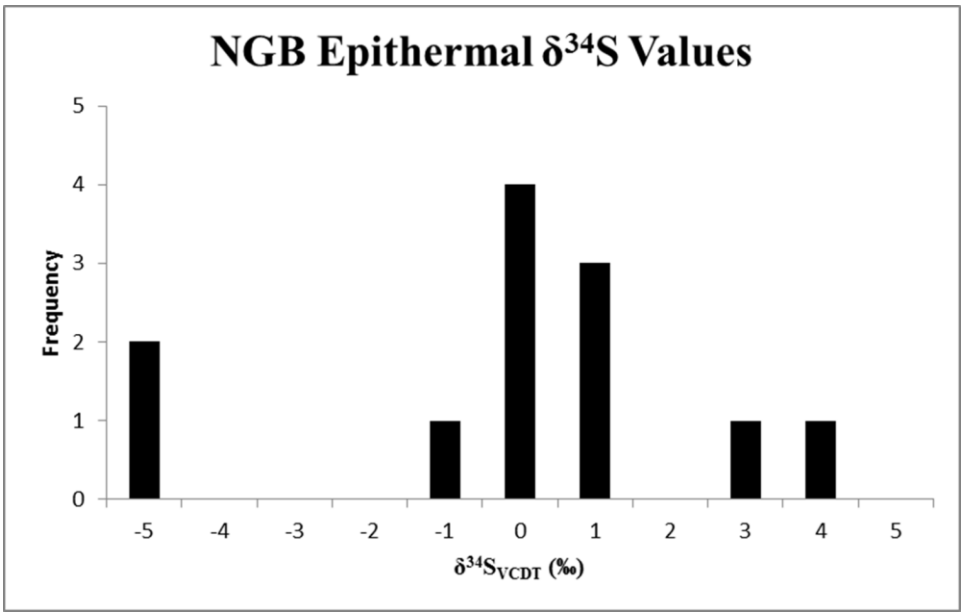

Figure 46: Histogram showing the distribution of S isotope values for the Northern Great Basin epithermal deposits (Saunders, pers. commun., 2015). Measurements were made on ore-stage chalcopyrite grains taken from the Buckskin National and Midas mines in addition to the Silver City district data.

Pb Isotopes

Thirteen lead isotope analyses were conducted on samples from the Black Jack-Trade Dollar vein. The primary goals were to determine the source of lead in the ore mineralization and the source of lead present in the adularia in the vein. Lead isotopes were measured from ore-stage naumannite, ore-stage chalcopyrite, adularia, and the silicate fraction from the Dewey, Idaho Tunnel, and Trade Dollar mines. The silicate fraction represents the portion of the ore sample that was dissolved by hydrofluoric acid. $^{206/204}$Pb values ranged from 18.974 to 19.086, $^{207/204}$Pb values ranged from 15.661 to 15.669, and $^{208/204}$Pb values ranged from 38.843 to 38.972. The distribution of these isotopes is shown in Figure 47 and Figure 48. Generally, the isotope values from the ore minerals and the adularia grains define an approximately linear array. However, the value

for the adularia sample from the Idaho Tunnel mine is different from all of the other ore and gangue mineral isotope measurements.

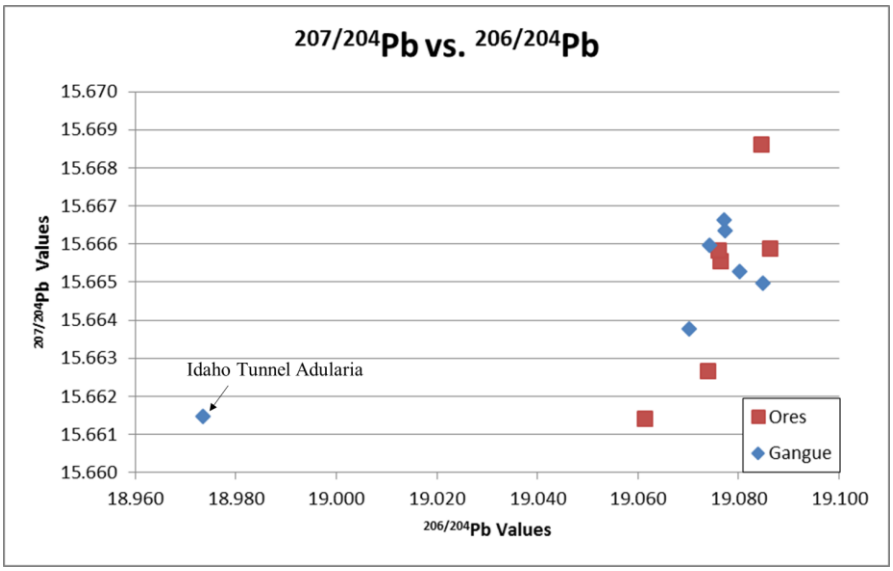

Figure 47: Plot showing lead isotope values for $^{207/204}$Pb vs. $^{206/204}$Pb. Values measured from ore minerals (chalcopyrite and naumannite) are shown as red squares, and values from gangue minerals (quartz and adularia) are shown as blue diamonds.

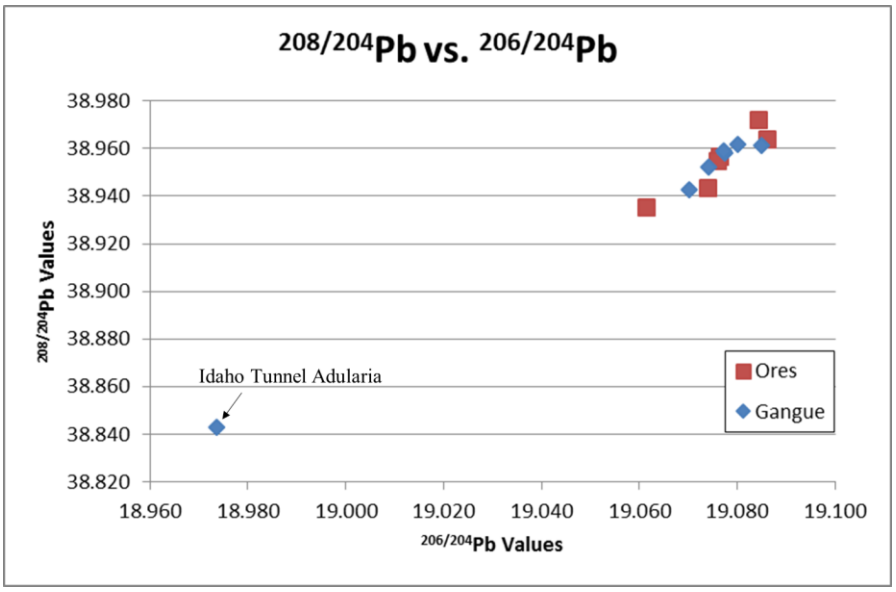

Figure 48: Plot showing lead isotope values for $^{208/204}$Pb vs. $^{206/204}$Pb. Values measured from ore minerals (chalcopyrite and naumannite) are shown as red squares, and values from gangue minerals (quartz and adularia) are shown as blue diamonds.

5. DISCUSSION

Ore Textures

Several characteristics of the ore textures in the Black Jack-Trade Dollar vein suggest possible mechanisms to explain how the mineral deposit formed. Perhaps the most curious of these is the presence of silver minerals at the base of high-grade dendrites. Because these dendrites are inferred to grow outward from the vein wall, how do silver minerals that occupy a later place in the paragenetic sequence form the dendrite root? One possibility is that a single silver phase was deposited early in the vein history with other silver minerals being deposited later, but this is unlikely due to the complexity of mineral intergrowths present in the dendrite roots (Fig. Figure **42**). The second possible reason for this texture is that some early phase has been replaced by the silver sulfo-selenides. This mechanism is also unlikely due to the lack of islands or rims of the relict earlier phase in the sulfo-selenide grains that form the base of the dendrites. The most likely reason for the apparent inversion of the paragenetic order is that deposition of ore minerals occurred so rapidly that the paragenetic order does not represent the evolution of the ore fluid, and instead is indicative of all the metals coming out of solution at once. Boiling of the ore fluid is probably necessary in order to have all of the metals leave the solution at once.

In addition to the apparent inversion of the paragenetic sequence, there are several other textures within the ores that suggest that boiling conditions were important to ore

genesis. The variety of silica and gangue mineral textures present in the ore samples suggests that conditions in the vein varied widely as ore was deposited. Comb quartz has been interpreted as forming during mostly quiescent conditions (Dong et al., 1995). Microcrystalline quartz, chalcedony, and plumose quartz, however, have all been interpreted as recrystallization of earlier-formed silica gels (Sander and Black, 1988). Fournier (1985) found that in order to form silica gels, it was necessary for a silica-supersaturated ore fluid to boil. Therefore, the presence of recrystallized silica gels together with comb quartz layers suggests that the fluid environment was changing fairly rapidly, with episodes of boiling mixed with longer quiescent periods of fluid flow through the vein. Interestingly, most of the metallic ore phases are found within the finest-grained silica phases. This seems to link ore deposition directly to the inferred boiling episodes.

Geochemistry

Minerals in the silver sulfo-selenide system (Ag_2S-Ag_2Se) constitute a large portion of the mineralization present in the Black Jack-Trade Dollar vein, but their exact composition has not been well characterized in the past. The approximately 100 spot analyses performed for this study (Fig. Figure **41**) show that the silver minerals' compositions lie along a continuum between acanthite, aguilarite, and naumannite. The majority of these analyses are clustered around the aguilarite composition and between aguilarite and acanthite. There does not appear to be a complete solid solution between the three minerals because no end-member naumannite analyses are present. The results of this study are remarkably similar to those of Aseto (2012). His silver mineral analyses

(Fig. Figure **49**) exhibited an apparent total solid solution between aguilarite and acanthite with no analyses containing pure naumannite.

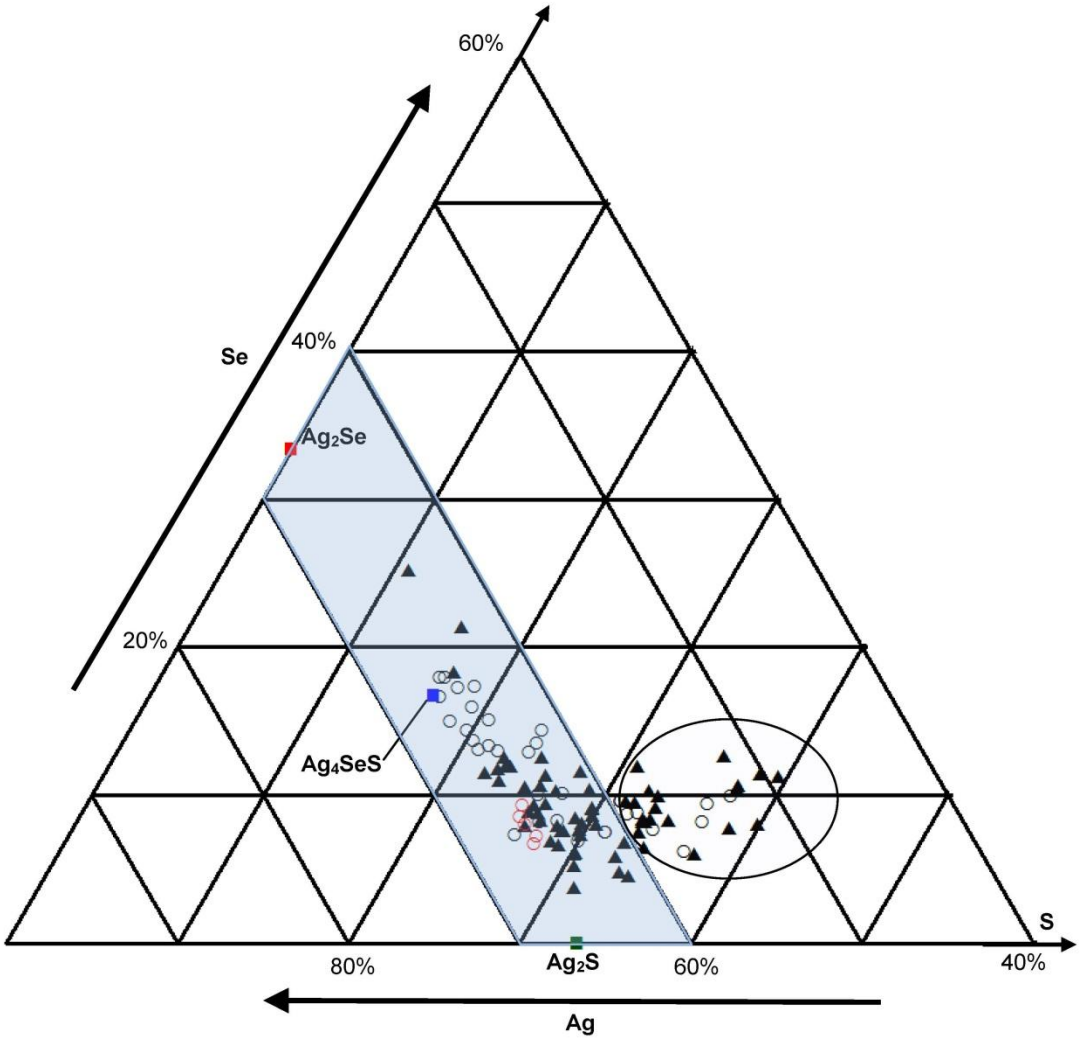

Figure 49: Ternary diagram from Aseto (2012) showing the composition of silver sulfo-selenides from War Eagle Mountain in the Silver City District. Most of the data fall within a solid solution from aguilarite (Ag_4SeS) to acanthite (Ag_2S). Analyses within the black ellipse were interpreted as possible unknown Ag-Se-S phases.

Even after seeing all of the analyses of various silver sulfo-selenides from the Silver City District, it seems obvious that the sulfur anion (S^{2-}) and the selenium anion (Se^{2-}) should be able to substitute for each other and form a complete solid solution with the general formula $Ag_2S_{1-x}Se_x$ ($0 < x < 1$). However, is there a true solid solution between naumannite and acanthite?

Many earlier workers have tried to definitively answer this question using a mix of natural and synthetic samples. Petruk et al. (1974) was the first study to characterize this system, and they found evidence of complete solid solution between both naumannite and aguilarite and aguilarite and acanthite at temperatures below 176 °C. Above 176 °C, the system exists as a cubic phase with total solid solution. Petruk et al. (1974) also found that naumannite exists in the orthorhombic system while acanthite and aguilarite are in the monoclinic system, which precludes the possibility of an isomorphous solid solution. Therefore, their depiction of a simple solid solution between naumannite and acanthite seems unlikely. Later studies showed a miscibility gap from $Ag_2S_{0.3}Se_{0.7} – Ag_2S_{0.4}Se_{0.6}$ that marked the boundary between the monoclinic phase and the orthorhombic phase (Palyanova et al., 2014; Pingitore et al., 1992). They also suggested that aguilarite does not represent a separate mineral phase and is instead a Se-bearing version of acanthite.

The most recent work done on the silver sulfo-selenide system argues against the presence of a miscibility gap and instead suggests that the orthorhombic naumannite structure and monoclinic acanthite structure both exist between $Ag_2S_{0.4}Se_{0.6}$ and $Ag_2S_{0.2}Se_{0.8}$ (Seryotkin et al., 2015). In their study, Seryotkin et al. (2015) created a synthetic sample with the composition $Ag_2S_{0.25}Se_{0.75}$ that contained both orthorhombic and monoclinic structures. This is significant because a similar texture is found in this

study (see Figure 42). The presence of two different crystal structures would explain how two different silver phases (Ag Phase 1 and Ag Phase 2) could have essentially the same composition. Overall, the nature of the silver sulfo-selenide system is still unresolved, but the presence in the Silver City District of a solid solution between aguilarite-acanthite and two separate phases in the proposed miscibility gap suggest that the model proposed by Seryotkin et al. (2015) is the most complete representation of the system.

In this study, several grains that were initially optically identified as electrum were found to contain significant sulfur and selenium, suggesting that the unusual minerals fischesserite (Ag_3AuSe_2) and uytenbogaardtite (Ag_3AuS_2) could be present in the Black Jack-Trade Dollar vein. In the Hauraki goldfield of New Zealand, Cocker et al. (2013) found hypogene grains of Se-bearing uytenbogaardtite (Ag_3AuS_2) in contact with both acanthite and electrum in low sulfidation epithermal veins. Relative to other electrum in the deposit, the electrum next to the uytenbogaardtite had a higher fineness. The mineral assemblage of acanthite-electrum-uytenbogaardtite exists in equilibrium at low temperatures (<113 °C) (Cocker et al., 2013). Because the fluid inclusion data show an ore fluid temperature of 200-250 °C, this low temperature assemblage suggests that it formed as a result of unmixing of a higher temperature phase (Cocker et al., 2013).

This texture found in New Zealand has direct applications to this study because the potential uytenbogaardtite-fischesserite phase was found in contact with both high fineness electrum and acanthite (Fig. Figure **40**). Like the New Zealand study, fluid inclusion data from Steiner et al. (2012) and Aseto (2012) show that the Silver City District ore fluids started at temperatures where the silver sulfo-selenide and uytenbogaardtite-electrum-acanthite systems were above their respective phase

separation temperatures. The conclusion that this mineral assemblage formed by unmixing of a high temperature phase helps to explain how many of the complex silver grains in this study, including those grains that form the base of the high-grade dendrites, formed.

Isotopes

Cu isotopes

Advances in the use of MC-ICP-MS to study transition metals have only recently allowed for the precise measurement of copper isotopes (Larson et al., 2003). Because of this recent emergence of copper isotope signatures as a viable analytical result, there is a limited body of work studying copper isotopes and its fractionation controls in various geologic environments; there has been no prior work done studying the copper isotope signatures of epithermal deposits. Several studies (Larson et al., 2003; Rouxel et al., 2004) have shown that 0±0.5‰ represents the bulk Earth isotopic value for δ^{65}Cu. This has been shown to be identical to the signature for hypogene chalcopyrite in porphyry copper deposits, leading to the interpretation that 0‰ represents an original magmatic signature for copper isotopes. Unlike most other stable isotopes (C, H, O, N, and S), copper is not highly effected by biological processes in bacteria (Mathur et al., 2005). Therefore, crossing a redox boundary is the most efficient method to fractionate copper isotopes (Markl et al., 2006; Asael et al., 2007; Asael et al., 2009).

The copper isotope values from the Silver City district (Fig. Figure 50) give a clear indication of a magmatic source. The ore samples have copper isotope values that

are clustered around 0‰; therefore, it is highly likely that this is a primary signature representative of an igneous magmatic source.

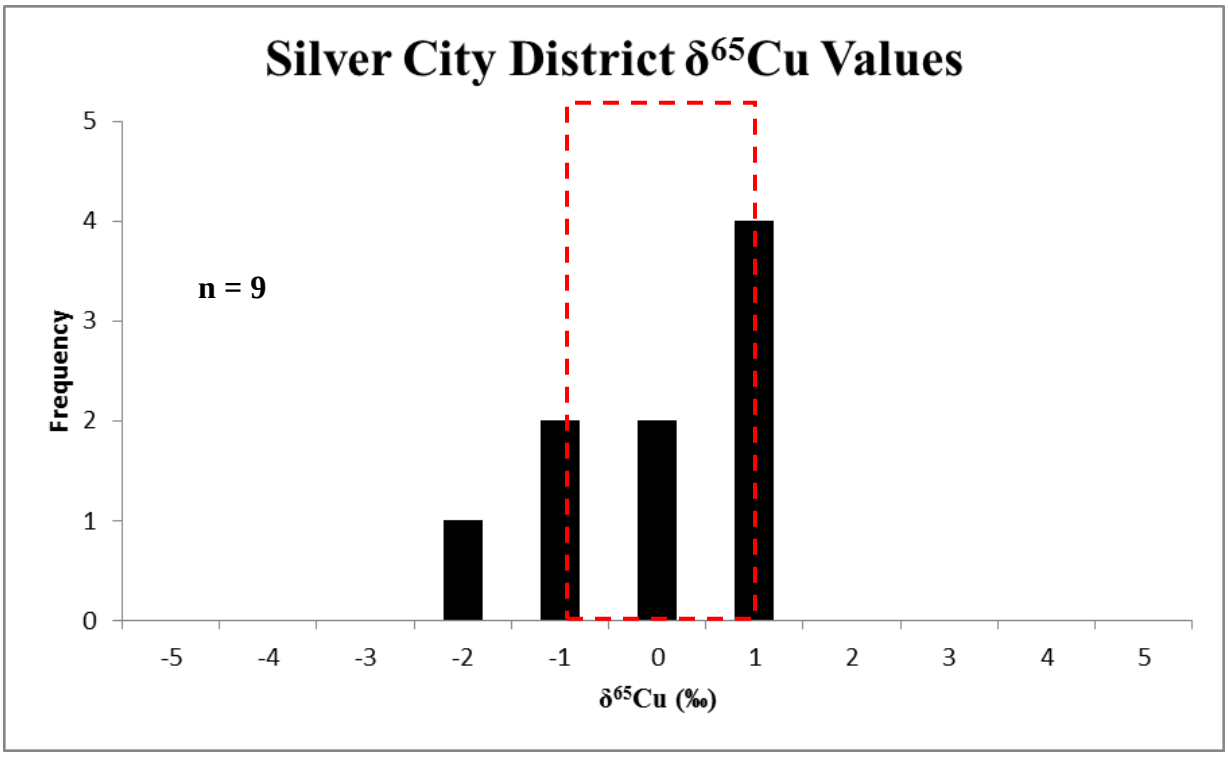

Figure 50: Histogram showing the distribution of copper isotope values in the Silver City ore samples. The red box highlights the magmatic signature of 0±0.5‰ δ^{65}Cu (Larson et al., 2003).

S isotopes

Since the early 1950s, sulfur isotopes have been used to determine the source of sulfur in many geologic settings. It is understood that there are several distinct reservoirs of sulfur in the Earth (Rye and Ohmoto, 1974). There are three main reservoirs: a positive reservoir (approximately +20‰) in evaporite rocks, a negative reservoir (from -15‰ to -5‰) in sedimentary sulfide minerals such as pyrite, and a neutral reservoir (from -3‰ to +3‰) in meteorites and igneous rocks (Seal, 2006). Like copper, the bulk Earth isotopic

value for $\delta^{34}S$ is 0‰ (Seal, 2006). This suggests that most magmatic signatures for sulfur isotopes should cluster around 0‰.

Unlike copper or lead, sulfur is a biologically useful element, and is highly affected by biological fractionation. Whenever sulfur is processed by an organism, the isotope value shifts towards the lighter isotope (^{32}S). This leads to depletion in $\delta^{34}S$, which is the measured isotope. This process can quickly become confusing if the material being fractionated was originally isotopically heavy, like a marine evaporate. Biological fractionation of sulfur can cause sulfur that was once isotopically heavy to have an isotopic signature near 0‰, giving the false impression that the sulfur came from a magmatic source. Saunders and Swann (1994) showed that this effect was present in sulfide minerals at Hazlehurst Salt Dome.

An additional factor to consider when evaluating sulfur isotope data is that when a sulfide mineral forms from a hydrothermal fluid, it has a different $\delta^{34}S$ value than the fluid (Rye and Ohmoto, 1974; Seal, 2006). The amount of sulfur isotope fractionation between the hydrothermal fluid and the sulfide mineral varies both with temperature and the specific sulfide mineral species (Rye and Ohmoto, 1974). This effect has been studied in lab experiments under equilibrium conditions. These results (Figure 51) show how different minerals fractionate the sulfur present in a hydrothermal fluid relative to pyrite derived from the same fluid. It is important to notice that relative to pyrite, chalcopyrite shows very little fractionation at any temperature. This means that any sulfur isotope values measured from ore-stage chalcopyrite grains likely reflect the original sulfur isotopic composition of the hydrothermal ore fluid. This lack of fractionation with respect

to the hydrothermal fluid is why ore-stage chalcopyrite grains were the primary target for this isotope study.

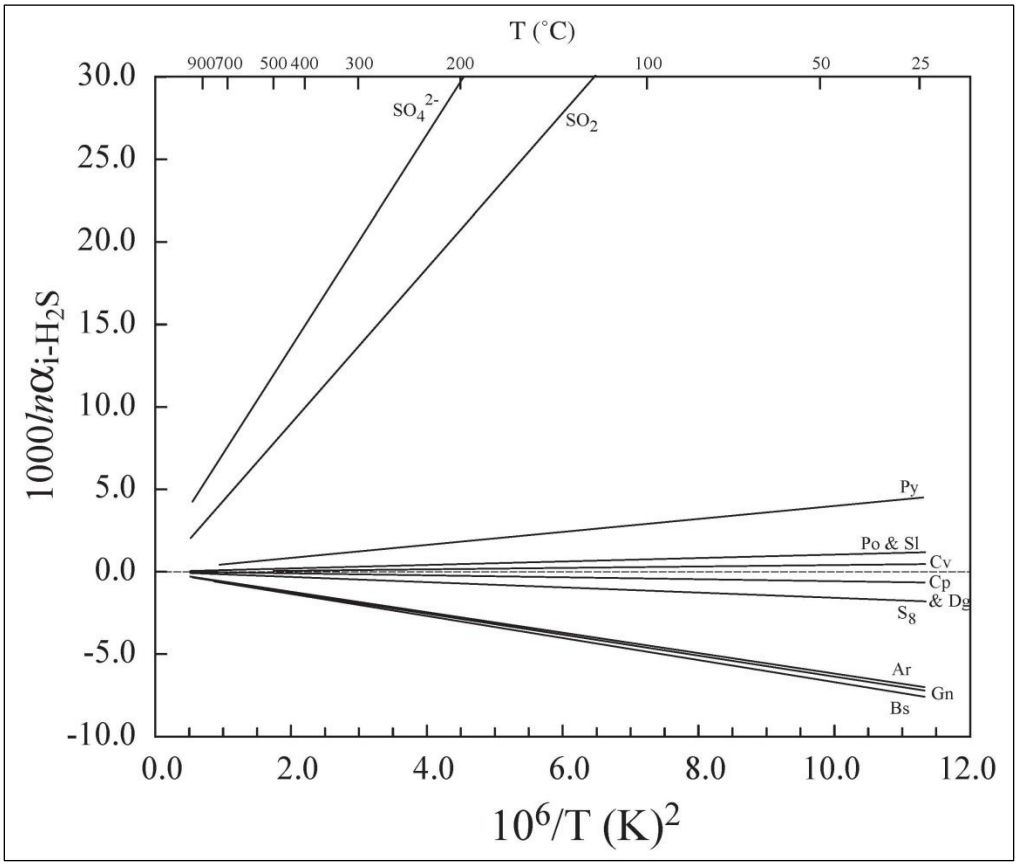

Figure 51: Graph showing the equilibrium fractionation of sulfur into various sulfide minerals relative to the original hydrothermal fluid isotopic value of 0‰. Chalcopyrite (Cp) shows very little change from the original fluid isotopic value, even at low temperature. Figure from Seal (2006).

The sulfur isotope values for the Silver City district (Fig. Figure **52**), like the copper isotope values, give a fairly clear indication as to the likely source of sulfur in the ore system. All of the isotope values fit within the magmatic sulfur source defined by Seal (2006). Other sulfide minerals in volcanic-rock-hosted epithermal deposits tend to cluster around 0‰ (Shikazono, 1999; John et al., 2003; Takahashi et al., 2012). These

other workers interpreted their sulfur isotopes to suggest a magmatic or igneous sulfur source. Since the $\delta^{34}S$ values for the Silver City ores are clustered around 0‰ and there are only igneous rocks in the district, it is likely that this signature represents a magmatic/igneous sulfur input with little to no sedimentary input.

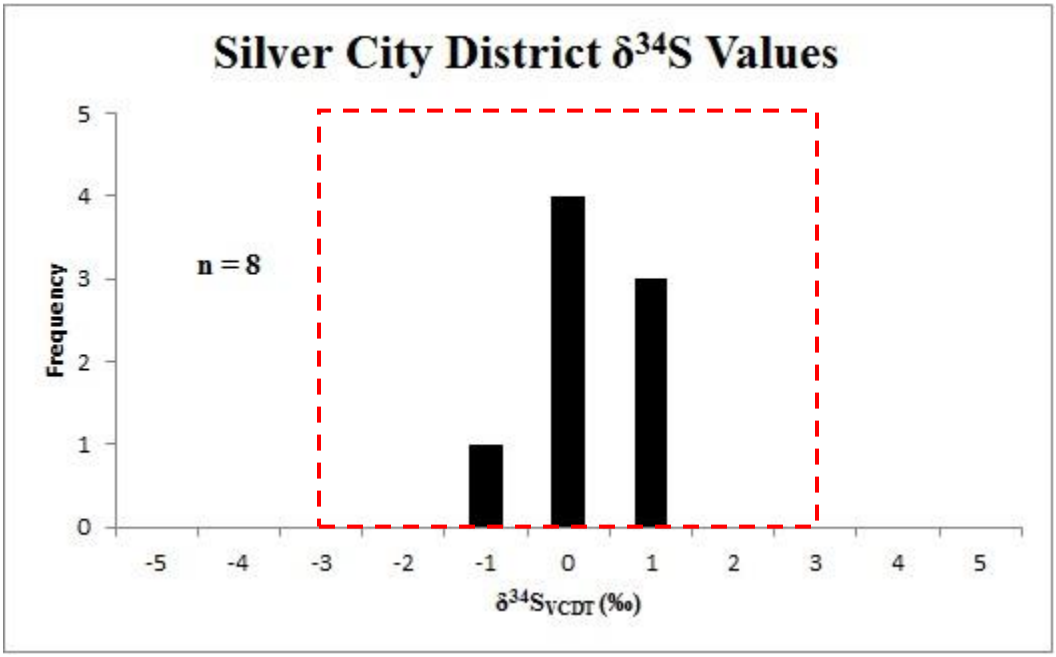

Figure 52: Histogram showing the distribution of sulfur isotope values in the Silver City ore samples. The red box highlights the magmatic sulfur source of -3‰ to +3‰ $\delta^{34}S$ (Seal, 2006).

Pb isotopes

Unlike the sulfur isotope system described earlier, the systematics of lead isotopes is complicated by the presence of radioactive effects. There are three radiogenic lead isotopes widely used in lead isotope studies: ^{206}Pb, ^{207}Pb, and ^{208}Pb, which form from radioactive decay of ^{238}U, ^{235}U, and ^{232}Th, respectively. Because the amount of lead present in a rock can vary widely, lead isotope values are always reported as ratios

relative to ^{204}Pb, which is the only stable isotope of the element. These three ratios are then plotted against each other in order to create diagrams showing different sources for the lead present in a sample.

The study of lead isotopes has been used for many years to try to establish a genetic origin for the lead present in the igneous rocks of the western United States (Zartman, 1974). In addition to grouping these igneous rocks together, lead isotopes have been used to fingerprint the source of lead present in many ore deposits across the western United States (Doe and Stacy, 1974). Later work developed models about the cycling of lead isotopes through the Earth's crust and mantle (Doe and Zartman, 1979; Zartman and Doe, 1981; Zartman and Haines, 1988). These plumbotectonic models gave estimates for the abundance of lead isotopes within different tectonic environments. This modeling is based upon the sensitivity with which uranium and lead partition differently into crustal and mantle rocks (Zartman and Haines, 1988).

More recent lead isotope work has focused on trying to determine the precise source of lead isotopes in hydrothermal systems and epithermal ore deposits. In their study of the Taupo Volcanic Zone in New Zealand, Hedenquist and Gulson (1992) found that there was a connection between the magmatic heat source and the lead present in a hydrothermal system. They noted that mineralized areas within the hydrothermal system appeared to have stronger magmatic signatures in the lead isotopes. This work was continued with ore deposits in the western United States by Kamenov et al. (2007), Hanan et al. (2008), and Saunders et al. (2011).

Kamenov et al. (2007) showed that a lead isotopic signature could be determined for ore-stage mineralization by extracting the lead alloyed with gold and silver minerals

present in Northern Great Basin epithermal deposits. Additionally, they found that the lead isotope signature for the epithermal deposits was similar to some of the primitive Columbia River Basalts (Fig. Figure **53**). Hanan et al. (2008) studied the lead isotope composition of basalts found in the Snake River Plain and noted a fairly strong linear array of the data. They explained the relatively radiogenic nature of the lead isotopes and the consistency of the values along the Snake River Plain by suggesting that the Yellowstone Hotspot provided the lead in the Snake River Plain basalts and has had a constant, homogeneous source since its initial eruption around 16 Ma. Saunders et al. (2011) expanded upon this work by showing that the lead present in ore samples from the Northern Great Basin is different from that of the surrounding country rocks and the rocks hosting the deposit. They explained the composition of lead isotopes in the epithermal ores by suggesting that the initial eruption of the Yellowstone Hotspot provided metals for the Northern Great Basin epithermal deposits.

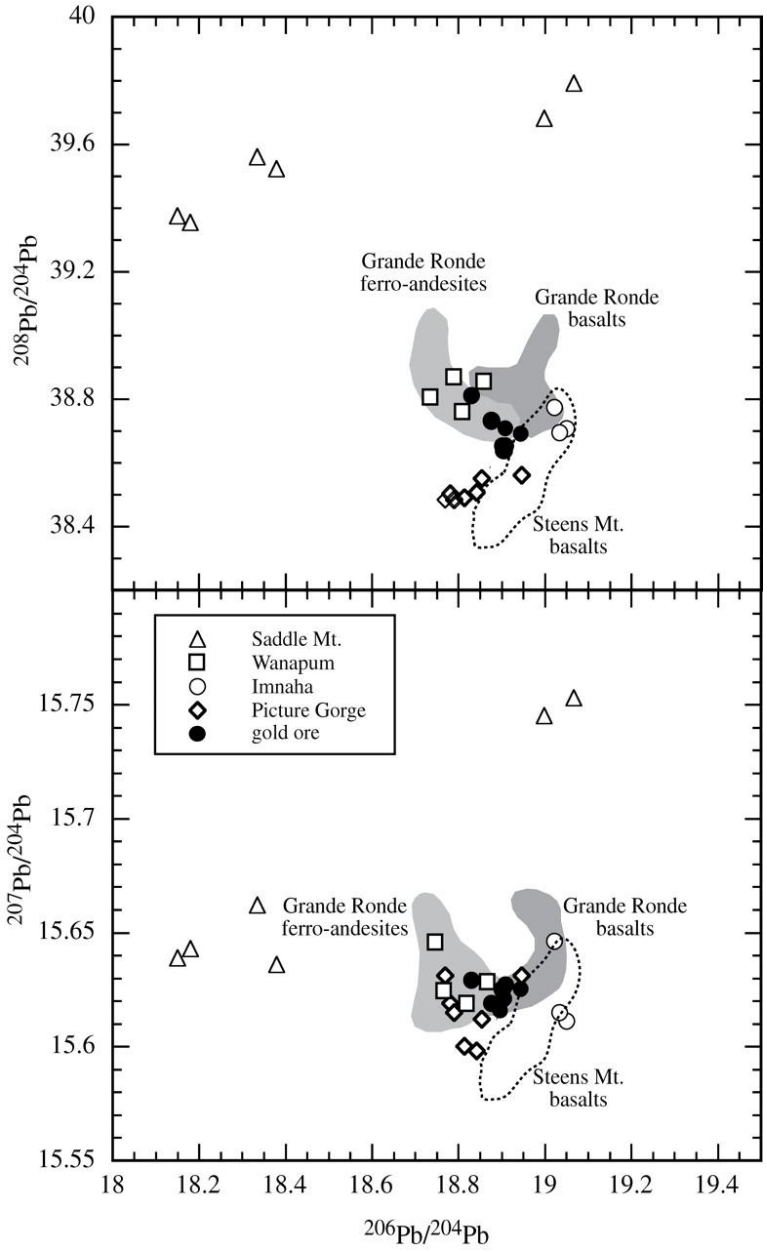

Figure 53: Plots showing lead isotope signatures for several Northern Great Basin gold ore samples compared with several Columbia River basalts (Kamenov et al., 2007).

In order to give them some context, the lead isotope data presented in this study were compared to several other sources. Several epithermal deposits from the Northern Great Basin (War Eagle Mountain, Sleeper, National, Jumbo, and Seven Troughs) with lead isotope data were included in the dataset. Country rocks from the Silver City District were included to ascertain if they could be a potential source of lead.

Once all of these comparative data sources were plotted (Fig. Figure **54**), several patterns emerged. In both the $^{208}Pb/^{206}Pb$ and $^{207}Pb/^{204}Pb$ graphs, all of the epithermal ore values plot close together. The Pb values for the granites, basalts, and rhyolites in the Silver City District all plot in close proximity to each other and happen to overlap the ore values. This similarity between the country rocks and ore samples would seem to indicate that the lead came from the same source. This is an interesting result because many of the Northern Great Basin ores show lead signatures similar to Silver City District country rocks but are located 100 miles or more from the Silver City area. The large distance between the sample locations indicates that there is some large-scale phenomenon controlling the lead isotopes in both datasets. By using the Hanan et al. (2008) field for the Yellowstone Hotspot's lead isotopic composition, it becomes apparent that the Silver City ores, Northern Great Basin ores, and Silver City country rocks all fall within or close to the hotspot field of values. The values that do not fall within the hotspot field form a roughly linear trend suggesting lead enrichment. This lead enrichment likely results from upper crustal or sediment contamination of the original magmatic lead signature that was likely sourced from magmatism associated with the Yellowstone hotspot.

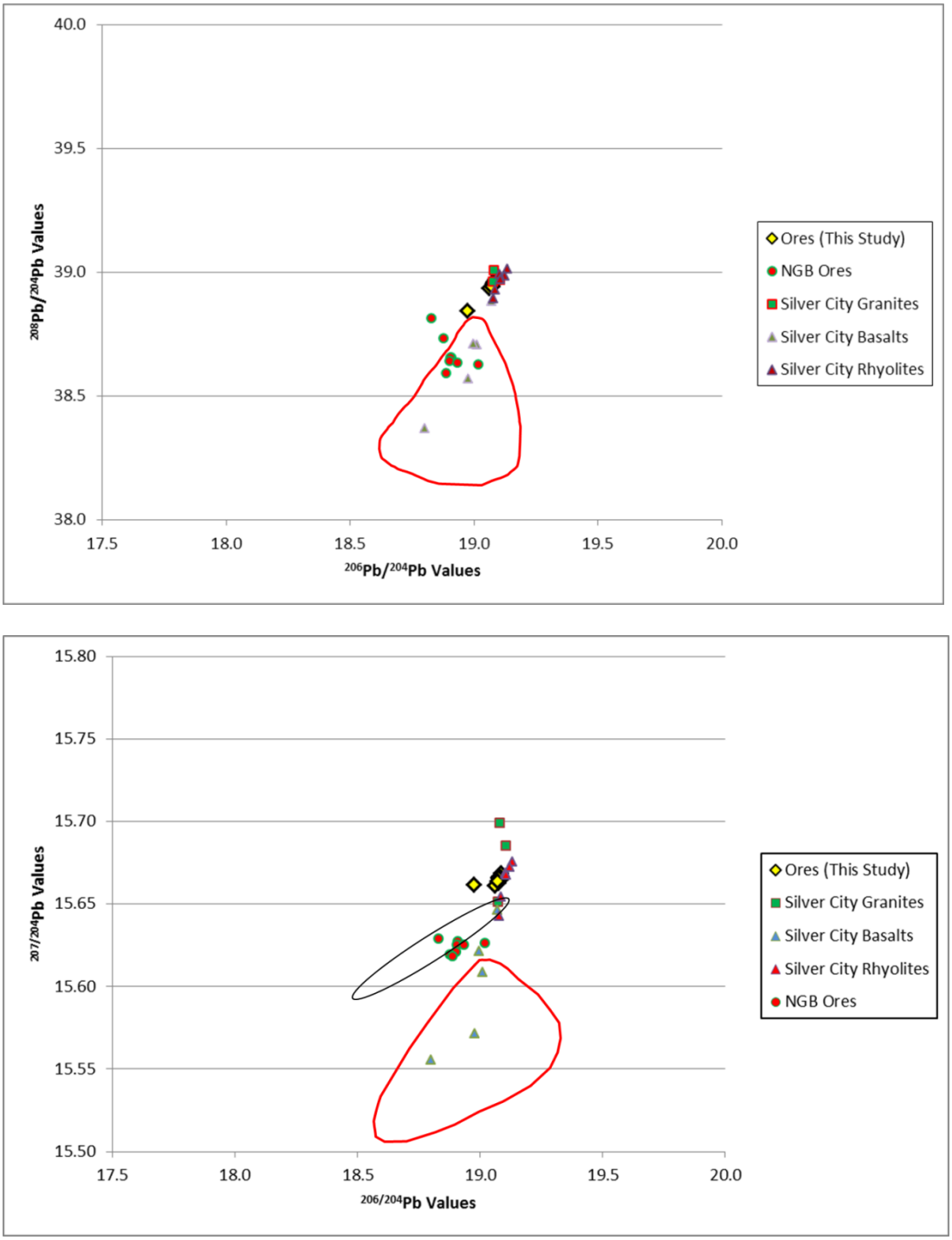

Figure 54: Plots showing $^{208}Pb/^{204}Pb$, $^{207}Pb/^{204}Pb$, and $^{206}Pb/^{204}Pb$ ratios for epithermal ores and igneous rocks found in the Silver City District. Epithermal ore data from Kamenov et al. (2007) are labeled NGB Ores, and the black ellipse shows where the Pb isotope data of Aseto (2012) fall. Igneous rock data from the Silver City District are reported in Hasten (2012). The field marked by the red shape is the Yellowstone Hotspot source described in Hanan et al. (2008).

Comparisons to Other Epithermal Au-Ag Deposits

For adularia-sericite type epithermal deposits, the mineralization is hosted by propylitically-altered volcanic rocks in banded veins with a primary mineralogy of quartz + adularia + Ag sulfides ± pyrite (Heald et al., 1987). The Black Jack-Trade Dollar vein is primarily hosted in weakly altered granite, basalt, and rhyolite and contains a mineralogy of adularia – quartz – Ag sulfo-selenides – chalcopyrite. Based upon its major characteristics, the Black Jack-Trade Dollar vein represents an adularia-sericite type epithermal Au-Ag deposit, which is also called the low sulfidation type (Hedenquist, 2000).

Many of the Black Jack-Trade Dollar vein's characteristics are similar to those of other Northern Great Basin epithermal deposits. First, the mineralization in the Silver City District formed during the mid-Miocene at approximately 16 Ma (Aseto, 2012; Halsor et al., 1988). Several other deposits in the Northern Great Basin share this mineralization age, including the Sleeper, Midas, Ivanhoe, and Mule Canyon deposits (Nash et al., 1995; Leavitt et al., 2004; Wallace, 2003; John et al., 2003). Across the Northern Great Basin, a strong silver- and selenium-rich geochemical signature, similar to that found in the Silver City District, is present (John, 2001). Additionally, the Silver City District contains evidence of a potential hot spring deposit (the Milestone deposit) that was connected to the mineralizing event (Barrett, 1985). This is similar to the environment at the Buckskin-National deposit (Vikre, 1985; Vikre, 1987).

The Black Jack-Trade Dollar vein appears to have similar characteristics expressed in Buchanan's (1981) model for epithermal deposits. Structurally, there was a main vein (Black Jack-Trade Dollar) and at least one hanging wall splay vein (Alpine)

present on Florida Mountain (Lindgren, 1900). Like the Buchanan model, the ores present on Florida Mountain appear to show an elevation control on the mineral species present, with the Trade Dollar and Dewey mines having more base metal sulfides while the Idaho Tunnel and Black Jack locations have more precious metals present (Fig. Figure **55**). Finally, the ores seem to show evidence of boiling based upon the highly mixed and chaotic nature of mineralization.

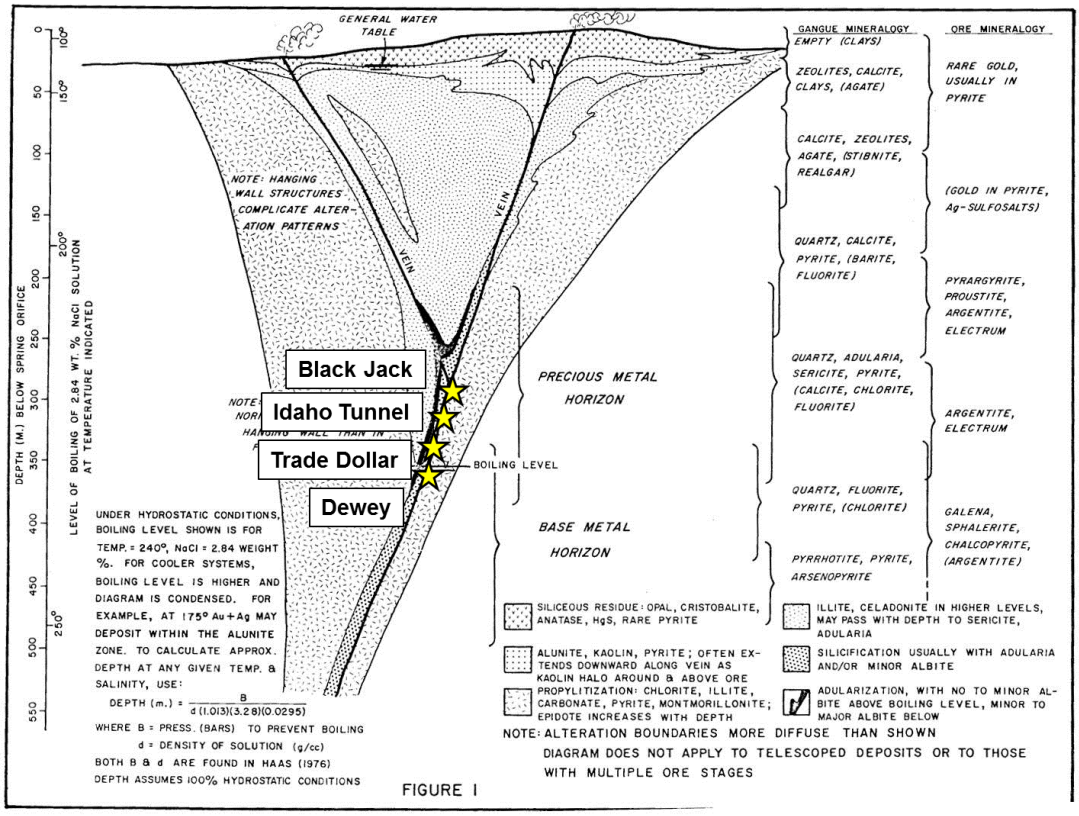

Figure 55: Schematic model [modified from Buchanan (1981)] of a typical epithermal vein with the sample locations from this study added. Sample locations were inferred based upon textural and mineralogical characteristics of the ore samples from each location.

Evidence for the Physical Transport of Metallic Colloids

The idea of physical transport of colloids playing a part in the formation of epithermal deposits has been around as long the idea of epithermal deposits themselves. Lindgren (1933) was the first person to observe that metallic colloids could potentially deposit metals in epithermal veins. His observations were largely ignored until Fournier (1985) suggested that amorphous silica was formed from silica-supersaturated fluids that had undergone boiling and likely moved upwards from deeper portions of veins into shallower regions.

Saunders (1990, 1994) was the first person to directly connect physically-transported colloids to metal deposition in an epithermal deposit, the Sleeper deposit. The Sleeper deposit contained fine-grained silica textures which hosted the electrum and were interpreted to form from recrystallization of silica gels and opal. The silica gels, opal, and the electrum dendrites found within them were interpreted to have formed from colloids that were transported to the ore deposition level from deeper within the hydrothermal system (Saunders, 1990; Saunders, 1994).

Once the idea of physically transporting colloids had been applied to one deposit, evidence of these transport textures were found in high-grade epithermal deposits from elsewhere in the world. In the Northern Great Basin, transport textures were found in the Midas, Buckskin National, and Hollister mines (Fig. Figure **56**). Transport textures were also found in ore samples from the Koryu deposit in Japan (Fig. Figure **57**) (Shimizu, 2014). The presence of these transport textures in different regions and different tectonic environments suggests that the process that formed the textures could be present in many epithermal deposits.

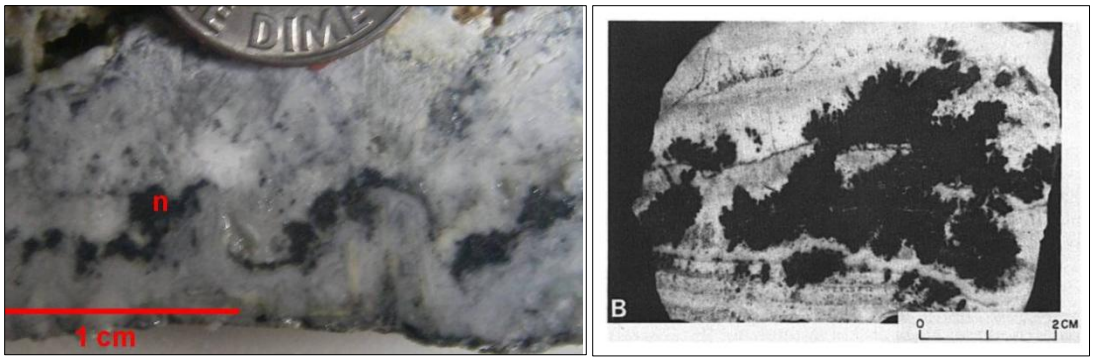

Figure 56: Photographs of ore textures showing physical transport of silver colloids in epithermal deposits of the Northern Great Basin. *Left*: "Sluice-box" texture from the Hollister deposit showing naumannite deposition on the left side of silica ridges, which leads to an inferred fluid flow direction from right to left. Figure from Saunders et al., (2012). *Right*: Naumannite dendrites from the Buckskin National deposit that are inferred to have formed due to colloidal transport of naumannite up to the deposition site. Figure from Vikre (1985).

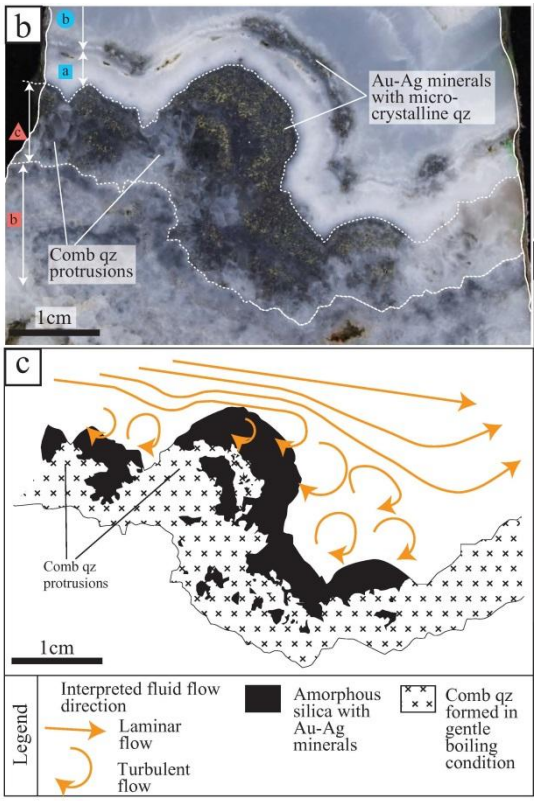

Figure 57: Photograph and interpretive diagram of ore textures from the Koryu deposit in Japan showing the deposition of chalcopyrite and naumannite with associated amorphous silica. Figure from Shimizu (2014).

The main evidence for colloidal transport of metals in the Black Jack-Trade Dollar ores comes from the doubly-terminated quartz euhedra texture (Fig. Figure **17**). The quartz euhedra are unattached to any vein wall, surrounded by metallic phases, and include small particles of these metallic inclusions. Additionally, these quartz euhedra appear very similar to a texture described by Okamoto and Tsuchiya (2009). In their study, Okamoto and Tsuchiya (2009) found symmetric, concentric-zoned quartz crystals present in quartz veins. They showed that these quartz crystals form when the fluids in the vein are moving upwards at 1-10 cm/s. If the quartz euhedra in the Black Jack-Trade Dollar ores are similar to Okamoto and Tsuchiya's (2009) zoned quartz crystals, then it suggests that the quartz euhedra formed during physical transport. Therefore, if the quartz euhedra formed during physical transport, then the ores on Florida Mountain that the quartz euhedra are found in also formed during physical transport.

There are problems with the idea of the physical transport of colloids in the Florida Mountain ores. The main problem is that there are no obvious colloidal transport textures like those at Sleeper, Ivanhoe, and Koryu. While there are some high-grade dendrites present, they do not share the same geometries as the pure electrum dendrites of other Northern Great Basin deposits, including Delamar, which have been inferred as forming from the physical transport of gold colloids in a silica-supersaturated fluid (Saunders, 1994). This possible lack of preservation of physical transport textures in the sulfo-selenide dendrites could be due to annealing and recrystallization of the sulfo-selenide minerals as the temperature in the Black Jack-Trade Dollar vein dropped.

Genetic Model for the Black Jack-Trade Dollar Vein

The epithermal Au-Ag deposit present in the Black Jack-Trade Dollar vein is the end result of a series of processes that occurred at continental, regional, and local scales. The first step in the genesis of the Black Jack-Trade Dollar vein was the flat-slab subduction of the Farallon tectonic plate during the Late Cretaceous. Richards (2009) and Saunders and Brueseke (2012) have both proposed that subduction enriches the sub-continental lithospheric mantle (SCLM) with metals and metalloids useful for creating ore deposits. Richards (2009) argues that remelting subduction-modified SCLM produces magmas commonly associated with porphyry Cu-Au deposits and epithermal Au deposits. Saunders and Brueseke (2012) expanded upon this idea by suggesting that the volatility of metals and metalloids coming off of the subducted slab leads directly to the enrichment of the SCLM and imbues the SCLM with a Se-Te zonation (Fig. Figure **2**).

After the volatile metals and metalloids were emplaced in the SCLM, a heat source was needed in order to liberate the metals and form ore deposits. John (2001) suggests that for the bimodal basalt-rhyolite assemblage in the Northern Great Basin, this heat source was provided by a stacked basalt-rhyolite magma chamber that could be explained by a mantle plume source. Saunders et al. (2008) suggested that this mantle plume heat source was explained by the initial eruption of the Yellowstone hotspot at 16.5 Ma near McDermitt, Nevada. This eruption of the Yellowstone hotspot caused partial melting of the metal- and metalloid-enriched SCLM, which produced a series of bimodal basalt-rhyolite magmas (Saunders et al., 2008).

After the eruption of the Yellowstone hotspot through the hypothesized metal-enriched SCLM, metal- and volatile-rich magmas were emplaced in the crust. As these

magmas began to cool, they degassed and evolved a low-density, volatile-rich supercritical fluid that preferentially carried the metals up to the shallow crust (Heinrich et al., 1999; Heinrich et al., 2004). Once they reached the near-surface environment, boiling was induced in the ore fluids (Buchanan, 1981). As a result of this boiling, the pH rose (Drummond and Ohmoto, 1985), which caused metallic complexes to become unstable and deposit the metals in quartz-vein-hosted, bonanza-grade epithermal ore deposits.

6. CONCLUSIONS

In general, the Trade Dollar-Black Jack vein is similar in many respects to other Se-rich bonanza epithermal deposits such as Midas, National, Buckskin National, Hishikari, Koryu, Hollister, and Mule Canyon. Specific conclusions from this study are enumerated below.

1. Geochemical data from this study show that the Black Jack-Trade Dollar vein is highly enriched in Ag and Se, which is similar to other NGB epithermal deposits.

2. Ores in the Black Jack-Trade Dollar vein exhibit a zonation similar to Buchanan's (1981) model, with higher amounts of base metal sulfides occurring at lower elevations (Dewey and Trade Dollar) and more precious metals being found at higher elevations (Black Jack and Idaho Tunnel).

3. The highest grade ores show an abundance of different mineral phases, including electrum, chalcopyrite, sphalerite, galena, opal, quartz, and numerous silver phases, all interconnected in dendritic masses.

4. Ore mineral paragenesis is generally shown to be pyrite → electrum → chalcopyrite + sphalerite + galena → silver selenide-sulfide phases.

5. Gangue mineral textures show an alternation between high-energy (microcrystalline quartz) and low-energy (comb quartz) depositional environments.

6. Silver mineral compositions are complex, with most minerals forming a limited compositional continuum between naumannite, aguilarite, and acanthite that has been reported elsewhere in the Silver City District. No silver-bearing sulfosalts were observed, but there is an unknown Ag-Au-Se-S phase present.

7. Copper isotope values in the Silver City District range from -2 to 1‰ and indicate a magmatic source for the Cu in the ores.

8. Sulfur isotope values in the Silver City District range from -1 to 1‰ and indicate a magmatic source for the S in the ores.

9. Lead isotope ratios for the Black Jack-Trade Dollar ores indicate a primarily mantle-derived source that represents the Yellowstone hotspot with some mixing of what appears to be upper crustal lead-rich sources.

10. No definitive evidence of colloidal-nanoparticle textures exists in the Black Jack-Trade Dollar ores, but ores from nearby DeLamar Mountain show these textures. Because the two locations are close together, it is likely that colloids/nanoparticles played some part in district-wide ore genesis and could help explain both the particularly high-grade nature and the magmatic isotope signatures of the ores on Florida Mountain.

11. Ores in the Black Jack-Trade Dollar vein probably formed during the boiling of hydrothermal ore fluids containing elevated levels of metals that were sourced from the subcontinental lithospheric mantle during Laramide flat-slab subduction and were mobilized by the eruption of the Yellowstone hotspot approximately 16.5 Ma.

REFERENCES

Armstrong, J.T., 1988, Quantitative analysis of silicate and oxide materials: comparison of Monte Carlo, ZAF, and phi-rho-z procedures, in Newbury, D.E., ed., Microbeam Analysis, p. 239-246.

Asael, D., Matthews, A., Bar-Matthews, M., and Halicz, L., 2007, Copper isotope fractionation in sedimentary copper mineralization (Timna Valley, Israel): Chemical Geology, v. 243, p. 238-254.

Asael, D., Matthews, A., Oszczepalski, S., Bar-Matthews, M., and Halicz, L., 2009, Fluid speciation controls of low temperature copper isotope fractionation applied to the Kupferschiefer and Timna ore deposits: Chemical Geology, v. 262, p. 147-158.

Aseto, C.O., 2012, Geology, geochemistry, and geochronology of the mid-Miocene, low-sulfidation epithermal gold-silver ores on War Eagle Mountain, Silver City District, Idaho: Unpublished M.Sc. thesis, Auburn, Alabama, Auburn University, 170 p.

Asher, R.R., 1968, Geology and mineral resources of a portion of the Silver City region, Owyhee County, Idaho: Idaho Bureau of Mines and Geology, Pamphlet 138, 106 p.

Barrett, R.A., 1985, The geology, mineralization, and geochemistry of the Milestone hot-spring silver-gold deposit near the Delamar silver mine, Owyhee County, Idaho: Unpublished M.Sc. thesis, Moscow, Idaho, University of Idaho, 474 p.

Bonnichsen, B., 1983, Epithermal gold and silver deposits, Silver City-De Lamar District, Idaho: Idaho Geological Survey Technical Report 83-4, 29 p.

Buchanan, L.J., 1981, Precious metal deposits associated with volcanic environments in the southwest: Arizona Geological Society Digest, v. 14, p. 237-262.

Bussey, S.D., 1996, Gold mineralization and associated rhyolitic volcanism at the Hog Ranch District, northwest Nevada, in Coyner, A.R., and Fahey, P.L., eds., Geological Society of Nevada Symposium 1995: Geology and Ore Deposits of the American Cordillera, Reno, Nevada, May 1995, p. 181-207.

Chitwood, R.A., 2012, Geochemistry and mineralogy of eastern Ag-rich epithermal veins in the Midas district, Nevada, USA: Unpublished M.Sc. thesis, Auburn, Alabama, Auburn University, 111 p.

Cocker, H.A., Mauk, J.L., and Rabone, S.D.C., 2013, The origin of Ag-Au-S-Se minerals in adularia-sericite epithermal deposits: constraints from the Broken Hills deposit, Hauraki Goldfield, New Zealand: Mineralium Deposita, v. 48, p. 249-266.

Doe, B.R., and Stacey, J.S., 1974, The application of lead isotopes to the problems of ore genesis and ore prospect evaluation: a review: Economic Geology, v. 69, p. 757-776.

Doe, B.R., and Zartman, R.E., 1979, Chapter 2. Plumbotectonics I, the Phanerozoic, in Barnes, H.L., ed., Geochemistry of Hydrothermal Ore Deposits, 2nd ed., Wiley-Interscience, New York, p. 22-70.

Dong, G., Morrison, G., and Jaireth, S., 1995, Quartz textures in epithermal veins, Queensland – classification, origin, and implication: Economic Geology, v. 90, p. 1841-1856.

Drummond, S.E., and Ohmoto, H., 1985, Chemical evolution and mineral deposition in boiling hydrothermal systems: Economic Geology, v. 80, p. 126-147.

Fournier, R.O., 1985, Silica minerals as indicators of conditions during gold deposition: U.S. Geological Survey Bulletin 1646, p. 15-26.

Guilbert, J.M., and Park, C.F., 1986, The geology of ore deposits: New York, W.H. Freeman and Company, 985 p.

Hanan, B.B., Shervais, J.W., and Vetter, S.K., 2008, Yellowstone plume – continental lithosphere interaction beneath the Snake River Plain: Geology, v. 36, no. 1, p. 51-54.

Halsor, S.P., Bornhorst, T.J., Beebe, M., Richardson, K., and Strowd, W., 1988, Geology of the DeLamar silver mine, Idaho - a volcanic dome complex and genetically associated hydrothermal system: Economic Geology, v. 83, p. 1159-1169.

Hasten, Z.E.L., 2012, Mid-Miocene magmatism in the Owyhee Mountains, ID: origin and petrogenesis of volcanic rocks in the Silver City District: Unpublished M. Sc. thesis, Manhattan, Kansas, Kansas State University, 211 p.

Heald, P., Foley, N.K., and Hayba, D.O., 1987, Comparative anatomy of volcanic-hosted epithermal deposits; acid-sulfate and adularia-sericite types: Economic Geology, v. 82, p. 1-26.

Hedenquist, J. W., 1992, Recognition of magmatic contributions to active and extinct hydrothermal systems, in Hedenquist, J.W., ed., Magmatic contributions to hydrothermal systems: Geological Survey of Japan, Report 279, p. 68-79.

Hedenquist, J.W., and Houghton, B.F., 1987, Epithermal gold mineralization and its volcanic environments: Earth Resources Foundation, The University of Sydney, 422 p.

Hedenquist, J., and Gulson, B.L., 1992, Intrusive and basement sources of lead in hydrothermal systems of the Taupo Volcanic Zone, New Zealand: Geochimica et Cosmochimica Acta, v. 56, p. 2821-2829.

Hedenquist, J.W., and Lowenstern, J.B., 1994, The role of magmas in the formation of hydrothermal ore deposits: Nature, v. 370, p. 519-527.

Hedenquist, J.W., Arribas, A.R., and Gonzalez-Urien, E., 2000, Exploration for epithermal gold deposits: Reviews in Economic Geology, v. 13, p. 245-277.

Heinrich, C.A., 2005, The physical and chemical evolution of low-salinity magmatic fluids at the porphyry to epithermal transition: a thermodynamic study: Mineralium Deposita, v. 39, p. 864-889.

Heinrich, C.A., Günther, D., Audétat, A., Ulrich, T., and Frischknecht, R., 1999, Metal fractionation between magmatic brine and vapor, determined by microanalysis of fluid inclusions: Geology, v. 27, p. 755-758.

Heinrich, C.A., Driesner, T., Stefánsson, A., and Seward, T.M., 2004, Magmatic vapor contraction and the transport of gold from the porphyry environment to epithermal ore deposits: Geology, v. 32, no. 9, p. 761-764.

Henley, R.W., and Ellis, A.J., 1983, Geothermal systems ancient and modern; a geochemical review: Earth Science Reviews, v. 19, p. 1-50.

John, D.A., 2001, Miocene and early Pliocene epithermal gold-silver deposits in the Northern Great Basin, western United States: Characteristics, distribution, and relationship to magmatism: Economic Geology, v. 96, p. 1827-1853.

John, D.A., Hofstra, A.H., Fleck, R.J., Brummer, J.E., and Saderholm, E.C., 2003, Geologic setting and genesis of the Mule Canyon low-sulfidation epithermal gold-silver deposit, north-central Nevada: Economic Geology, v. 98, p. 425-463.

Kamenov, G.D., Mueller, P.A., and Perfit, M.R., 2004, Optimization of mixed Pb-Tl solutions for high precision isotopic analyses by MC-ICP-MS: Journal of Analytical Atomic Spectrometry, v. 19, no. 9, p. 1262-1267.

Kamenov, G.D., Saunders, J.A., Hames, W.E., and Unger, D.L., 2007, Mafic magmas as sources for gold in middle-Miocene epithermal deposits of northern Great Basin, USA: evidence from Pb isotopic compositions of native gold: Economic Geology, v. 102, p. 1191-1195.

Kouzmanov, K., Pettke, T., and Heinrich, C.A., 2010, Direct analysis of ore-precipitating fluids: combined IR microscopy and LA-ICP-MS study of fluid inclusions in opaque ore minerals: Economic Geology, v. 105, p. 351-373.

Larson, P.B., Maher, K., Ramos, F.C., Chang, Z., Gaspar, M., and Meinert, L.D., 2003, Copper isotope ratios in magmatic and hydrothermal ore-forming environments: Chemical Geology, v. 201, p. 337-350.

Leavitt, E.D., Spell, T.L., Goldstrand, P.M., and Arehart, G.B., 2004, Geochronology of the Midas low-sulfidation epithermal gold-silver deposit, Elko County, Nevada: Economic Geology, v. 99, p. 1665-1686.

Leavitt, E.D., and Arehart, G.B., 2005, Alteration, geochemistry, and paragenesis of the Midas epithermal gold-silver deposit, Elko County, Nevada, in Rhoden, H.N., Steininger, R.C., and Vikre, P.G., eds., Geological Society of Nevada Symposium 2005: Window to the World, Reno, Nevada, May 2005, p. 563-627.

Lindgren, W., 1898, Orthoclase as gangue mineral in a fissure vein: American Journal of Science, Fourth Series, v. 30, p. 418-420.

Lindgren, W., 1900, The gold and silver veins of the Silver City, DeLamar, and other mining districts in Idaho: US Geological Survey 20th Annual Report, Part 3, p. 65-256.

Lindgren, W., 1933, Mineral deposits: New York, McGraw-Hill, 4th Ed., 930 p.

Lowenstern, J.B., and Hurwitz, S., 2008, Monitoring a supervolcano in repose: heat and volatile flux at the Yellowstone caldera: Elements, v. 4, no. 1, p. 35-40.

Markl, G., Lahaye, Y., and Schwinn, G., 2006, Copper isotopes as monitors of redox processes in hydrothermal mineralization: Geochimica et Cosmochimica Acta, v. 70, p. 4215-4228.

Mathur, R., Ruiz, J., Titley, S., Liermann, L., Buss, H., and Brantley, S., 2005, Cu isotopic fractionation in the supergene environment with and without bacteria: Geochimica et Cosmochimica Acta, v. 69, p. 5233-5246.

Mathur, R., Titley, S., Barra, F., Brantley, S., Wilson, M., Phillips, A., and Hart, G., 2009, Exploration potential of Cu isotope fractionation in porphyry copper deposits: Journal of Geochemical Exploration, v. 102, no. 1, p. 1-6.

Mitchell, V.E., 2010, History of the Florida Mountain mines, Owyhee County, Idaho: Idaho Geological Survey Staff Report 10-7, 60 p.

Moncada, D., Mutchler, S., Nieto, A., Reynolds, T.J., Rimstidt, J.D., Bodnar, R.J., 2012, Mineral textures and fluid inclusion petrography of the epithermal Ag-Au deposits at Guanajuato, Mexico: application to exploration: Journal of Geochemical Exploration, v. 114, p. 20-35.

Morrison, G., Dong, G., and Jaireth, S., 1995, Textural zoning in epithermal quartz veins: Klondike Exploration Services, Townsville, Queensland, Australia, 35 p.

Nash, J.T., Utterback, W.C., and Trudel, W.S., 1995, Geology and geochemistry of Tertiary volcanic host rocks, Sleeper gold-silver deposit, Humboldt County, Nevada: U.S. Geological Survey Bulletin 2090, 63 p.

Okamoto, A., and Tsuchiya, N., 2009, Velocity of vertical fluid ascent within vein-forming fractures: Geology, v. 37, no. 6, p. 563-566.

O'Neil, J.R., and Silberman, M.L., 1974, Stable isotope relations in epithermal Au-Ag deposits: Economic Geology, v. 69, p. 902-909.

Palyanova, G.A., Chudnenko, K.V., and Zhuravkova, T.V., 2014, Thermodynamic properties of solid solutions in the system Ag_2S-Ag_2Se: Thermochimica Acta, v. 575, p. 90-96.

Pansze, A.J., 1975, Geology and ore deposits of the Silver City – De Lamar – Flint region, Owyhee County, Idaho: Idaho Bureau of Mines and Geology Pamphlet no. 161, 79 p.

Petruk, W., Owens, D.R., Stewart, J.M., and Murray, E.J., 1974, Observations on acanthite, aguilarite, and naumannite: Canadian Mineralogist, v. 12, p. 365-369.

Pingitore, N.E., Ponce, B.F., Eastman, M.P., Moreno, F., and Podpora, C., 1992, Solid solutions in the system Ag_2S-Ag_2Se: Journal of Materials Research, v. 7, no. 8, p. 2219-2224.

Piper, A.M., and Laney, F.B., 1926, Geology and metalliferous resources of the region about Silver City, Idaho: Idaho Bureau of Mines and Geology, Bulletin 11, 165 p.

Reyment, R.A., and Jöreskog, K.G., 1993, Applied Factor Analysis in the Natural Sciences: New York, Cambridge University Press, 371 p.

Richards, J.P., 2009, Postsubduction porphyry Cu-Au and epithermal Au deposits: products of remelting of subduction-modified lithosphere: Geology, v. 27, no. 3, p. 247-250.

Rouxel, O., Fouquet, Y., and Ludden, J.N., 2004, Copper isotope systematics of the Lucky Strike, Rainbow, and Logatchev sea-floor hydrothermal fields on the Mid-Atlantic Ridge: Economic Geology, v. 99, p. 585-600.

Rye, R.O., and Ohmoto, H., 1974, Sulfur and carbon isotopes and ore genesis: a review: Economic Geology, v. 69, p. 826-842.

Sander, M.V., and Black, J.E., 1988, Crystallization and recrystallization of growth-zoned vein quartz crystals from epithermal systems – implications for fluid inclusion studies: Economic Geology, v. 83, p. 1052-1060.

Saunders, J.A., 1990, Colloidal transport of gold and silica in epithermal precious-metal systems: evidence from the Sleeper deposit, Nevada: Geology, v. 18, p. 757-760.

Saunders, J.A., 1994, Silica and gold textures in bonanza ores of the Sleeper deposit, Humboldt County, Nevada: evidence for colloids and implications for epithermal ore-forming processes: Economic Geology, v. 89, p. 628-638.

Saunders, J.A., 2012, Textural evidence of episodic introduction of metallic nanoparticles into bonanza epithermal ores: Minerals, v. 2, no. 3, p. 228-243.

Saunders, J.A., and Swann, C.T., 1994, Mineralogy and geochemistry of a cap-rock Zn-Pb-Sr-Ba occurrence at the Hazlehurst Salt Dome, Mississippi: Economic Geology, v. 89, p. 381-390.

Saunders, J.A., Cook, R.B., and Schoenly, P.A., 1996, Electrum disequilibrium crystallization textures in volcanic-hosted bonanza epithermal gold deposits in northern Nevada, in Coyner, A.R., and Fahey, P.L., eds., Geological Society of Nevada Symposium 1995: Geology and Ore Deposits of the American Cordillera, Reno, Nevada, May 1995, p. 173-179.

Saunders, J.A., Unger, D.L., Kamenov, G.D., Fayek, M., Hames, W.E., and Utterback, W.C., 2008, Genesis of middle Miocene Yellowstone hotspot-related bonanza epithermal Au-Ag deposits, Northern Great Basin, USA: Mineralium Deposita, v. 43, p. 715-734.

Saunders, J.A., Kamenov, G.D., Hofstra, A.H., Unger, D.L., Creaser, R.A., and Barra, F., 2011, "Forensic" geochemical approaches to constrain the source of Au-Ag in low-sulfidation epithermal ores, in Steininger, R., and Pennell, B., eds., Great Basin evolution and metallogeny: Geological Society of Nevada Symposium Proceedings, p. 693-700.

Saunders, J.A., and Brueseke, M.E., 2012, Volatility of Se and Te during subduction-related distillation and the geochemistry of epithermal ores of the western United States: Economic Geology, v. 107, p. 165-172.

Seal, R.R., 2006, Sulfur isotope geochemistry of sulfide minerals: Reviews in Mineralogy & Geochemistry, v. 61, p. 633-677.

Seryotkin, Y.V., Palyanova, G.A., Kokh, K.A., 2015, Sulfur-selenium isomorphous substitution and polymorphism in the $Ag_2(S,Se)$ series: Journal of Alloys and Compounds, v. 639, p. 89-93.

Shikazono, N., 1999, Sulfur isotopic composition and origin of sulfide sulfur in epithermal Au-Ag vein-type deposits in Japan: Resource Geology Special Issue, no. 20, p. 39-45.

Shimizu, T., 2014, Reinterpretation of quartz textures in terms of hydrothermal fluid evolution at the Koryu Au-Ag deposit, Japan: Economic Geology, v. 109, p. 2051-2065.

Simmons, S.F., White, N.C., and John, D.A., 2005, Geological characteristics of epithermal precious and base metal deposits: Economic Geology 100th Anniversary Volume, p. 485-522.

Skinner, B.J., 1979, The many origins of hydrothermal mineral deposits, in: Barnes, H.L. (ed.), Geochemistry of Hydrothermal Ore Deposits (2nd ed.): New York, Wiley-Interscience, p. 1-21.

Smith, J.M., Muntean, J.L., and Vikre, P.G., 2014, Controls on high grades within the Clementine vein system at the Hollister low-sulfidation epithermal Au-Ag deposit, NV [poster]: Society of Economic Geology Annual Meeting 2014.

Stanton, R.L., 1972, Ore Petrology: New York, McGraw-Hill, 713 p.

Steiner, R., Brake, S., Brinkmann, S., Saunders, J.A., Hames, W.E., and Aseto, C., 2012, Evaluation of ore mineralogy associated with precious metals mineralization at Florida Mountain, Silver City District, ID [abs.]: GSA North-Central Section – 46th Annual Meeting (23-24 April 2012).

Takahashi, R., Matsueda, H., Okrugin, V.M., Shikazono, N., Ono, S., Imai, A., Andreeva, E.D., and Watanabe, K., 2012, Ore-forming ages and sulfur isotope study of hydrothermal deposits in Kamchatka, Russia: Resource Geology, v. 63, no. 2, p. 210-223.

Taylor, H.P., Jr., 1973, O^{18}/O^{16} evidence for meteoric-hydrothermal alteration and ore deposition in the Tonopah, Comstock Lode, and Goldfields mining districts, Nevada: Economic Geology, v. 68, p. 747-764.

Taylor, H.P., Jr., 1974, The application of hydrogen and oxygen isotope studies to problems of hydrothermal alteration and ore deposition: Economic Geology, v. 68, p. 843-883.

Unger, D.L., 2008, Geochronology and geochemistry of mid-Miocene bonanza low-sulfidation epithermal ores of the northern Great Basin,USA: Unpublished M.Sc. thesis, Auburn, Alabama, Auburn University, 151 p.

Vikre, P.G., 1985, Precious metal vein systems in the National District, Humboldt County, Nevada: Economic Geology, v. 80, p. 360-393.

Vikre, P.G., 1987, Paleohydrology of Buckskin Mountain, National district, Humboldt County, Nevada: Economic Geology, v. 82, p. 934-950.

Vikre, P.G., 2007, Sinter-vein correlations at Buckskin Mountain, National District, Humboldt County, Nevada: Economic Geology, v. 102, p. 193-224.

Wallace, A.R., 2003, Geology of the Ivanhoe Hg-Au district, Northern Nevada: influence of Miocene volcanism, lakes, and active faulting on epithermal mineralization: Economic Geology, v. 98, p. 409-424.

White, D.E., 1969, Thermal and mineral waters of the United States – Brief review of possible origins, in International Geologic Congress, 23rd, Prague 1968, v. 19 Proc. Symposium 2, Mineral and thermal waters of the world – [pt.] B, Oversea countries: Prague, Academia, p. 269-286.

White, D.E., 1974, Diverse origins of hydrothermal ore fluids: Economic Geology, v. 69, p. 954-973.

Williams-Jones, A.E., and Heinrich, C.A., 2005, Vapor transport of metals and the formation of magmatic-hydrothermal ore deposits: Economic Geology, v. 100, p. 1287-1312.

Zartman, R.E., 1974, Lead isotopic provinces in the Cordillera of the Western United States and their geologic significance: Economic Geology, v. 69, p. 792-805.

Zartman, R.E., and Doe, B.R., 1981, Plumbotectonics – the model: Tectonophysics, v. 75, p. 135-162.

Zartman, R.E., and Haines, S.M., 1988, The plumbotectonic model for Pb isotopic systematics among major terrestrial reservoirs – a case for bi-directional transport: Geochimica et Cosmochimica Acta, v. 52, p. 1327-1339.

Appendix 1: Sample Locations and Names for this Study

		Location	
	Sample Name	**Latitude**	**Longitude**
AUMSM01	Sinter - Milestone	43.027897	-116.861539
AUMSM02	Vertical Sinter - Milestone	43.024775	-116.864336
AUMSM03	Mineralized Rhyolite	43.009836	-116.744375
AUMSM04	Unmineralized Rhyolite	43.003607	-116.749317
AUMSM05	Mineralized Basalt	43.009836	-116.744375
AUMSM06	Unmineralized Basalt	43.012635	-116.739123
AUMSM07	Altered Granite	43.009836	-116.744375
AUMSM08	Fresh Granite	43.016062	-116.73345
AUMSM09	TD Petrie-made slide	43.009836	-116.744375
AUMSM10	TD Adit sample	43.009836	-116.744375
AUMSM11	TD03 - same as altered granite	43.009836	-116.744375
AUMSM12	TD04 - high grade in basalt	43.009836	-116.744375
AUMSM13	TD05 - high grade vein	43.009836	-116.744375
AUMSM14	TD06 - qtz-adularia vein	43.009836	-116.744375
AUMSM15	IT01 - basalt country rock + vein wall	43.023169	-116.761728
AUMSM16	IT02 - breccia	43.023169	-116.761728
AUMSM17	IT03 - same rock as IT1	43.023169	-116.761728
AUMSM18	IT04	43.023169	-116.761728
AUMSM19	IT05	43.023169	-116.761728
AUMSM20	DEW1 - high grade puck	43.038253	-116.762144
AUMSM21	DEW2 - same as DEW2 slide	43.038253	-116.762144
AUMSM22	DEW3 - high grade	43.038253	-116.762144
AUMSM23	DEW4 - run of the mill high grade	43.038253	-116.762144
AUMSM24	DEW5 - high grade puck	43.038253	-116.762144
AUMSM25	Midas - Colorado Grande Vein	41.231128	-116.775717
AUMSM26	Buckskin	41.792558	-117.540447
AUMSM27	DeLamar	43.020853	-116.830306
AUMSM28	Republic	48.648439	-118.738419
AUMSM29	Pauper	42.997339	-116.710892
AUMSM30	Pauper	42.997339	-116.710892
AUMSM31	Blackjack 1 - really high grade	43.022297	-116.757753
AUMSM32	Blackjack 2	43.022297	-116.757753
AUMSM33	Henrietta 1 - mineralized breccia	43.013233	-116.852222
AUMSM34	Henrietta 2 - low grade	43.013233	-116.852222
AUMSM35	Milestone 1 - The Castle	43.027897	-116.861539
AUMSM36	Milestone 2 - Vertical Sinter	43.024775	-116.864336

Appendix 2: Geochemical Data for Silver City and NGB Epithermal Ore Samples

	Location	Au ppm	Ag ppm	Cu ppm	Pb ppm	Zn ppm	Sb ppm	As ppm	Se ppm	Te ppm	S ppm	Tl ppm
	Lower Detection Limit	**0.1**	**0.1**	**0.1**	**0.1**	**1**	**0.1**	**1**	**1**	**0.5**	**1000**	**0.5**
AUMSM01	Sinter - Milestone?	1.3	75.1	18.6	1.8	6	11.2	43	47	0.5	1000	1.6
AUMSM02	Vertical Sinter - Milestone?	0.2	22.3	39.9	1.9	59	7.6	5	16	0.5	1000	0.5
AUMSM03	Mineralized Rhyolite	0.1	4.2	41.2	12.6	105	6.7	42	1	0.5	2000	0.9
AUMSM04	Unmineralized Rhyolite	0.1	1.3	8.5	21.6	47	0.6	3	1	0.5	1000	0.9
AUMSM05	Mineralized Basalt	0.1	43.1	1059	13.3	168	5.3	8	4	0.5	1000	2
AUMSM06	Unmineralized Basalt	0.1	0.3	48.2	2	90	0.9	2	1	0.7	1000	0.5
AUMSM07	Altered Granite	0.1	2.7	25.3	17.8	58	1.1	3	1	0.5	1000	2
AUMSM08	Fresh Granite	0.1	0.1	4	16.2	53	0.3	2	1	0.5	1000	0.5
AUMSM09	TD Petrie-made slide	58.3	10202	2497.3	730.5	224	9.1	1	919	0.5	12000	2.9
AUMSM10	TD Adit sample	102.8	200	5961.4	88.5	13	3.8	1	1000	9.5	7000	2
AUMSM11	TD03 - same as altered granite	57.6	11231	614.9	1299.5	610	2.4	1	1000	4.1	2000	3.8
AUMSM12	TD04 - high grade in basalt	87.4	20464	10000	4289.7	1480	4.2	1	1000	3	30000	3.2
AUMSM13	TD05 - high grade vein	36.6	8413	1362.4	475.5	163	46.4	1	589	3	2000	4
AUMSM14	TD06 - qtz-adularia vein	25.8	4833	951.6	218.3	59	2.5	1	551	0.6	1000	4.1
AUMSM15	IT01 - basalt country rock + vein wall	13.8	3853	588.2	374.8	343	3.3	1	363	1.9	2000	2.5
AUMSM16	IT02 - breccia	6	200	37.4	136.7	11	2.8	1	275	0.5	4000	5.1
AUMSM17	IT03 - same rock as IT1	200	200	1018.8	142.3	210	11.2	1	411	0.5	2000	2.4
AUMSM18	IT04	109.5	200	1581.9	10000	9124	7.7	1	1000	289.3	9000	4
AUMSM19	IT05	200	200	3156	629.4	567	13.6	1	1000	0.9	5000	3.1
AUMSM20	DEW1 - high grade puck	200	200	10000	10000	10000	22.4	1	1000	12.2	100000	1.8
AUMSM21	DEW2 - same as DEW2 slide	40.9	200	3582.5	3136.2	823	5	1	1000	21.8	5000	5.2
AUMSM22	DEW3 - high grade	86.8	200	588	1628.1	1423	3	1	1000	16.4	7000	3.4
AUMSM23	DEW4 - run of the mill high grade	26.8	3050	1043	650.3	358	2.2	1	242	4.7	1000	3.7
AUMSM24	DEW5 - high grade puck	96.3	200	10000	1630.3	1764	1.3	1	1000	5.4	9000	4.2
AUMSM25	Midas - Colorado Grande Vein	155.6	3482	1082.1	173.7	137	11.3	1	969	0.5	2000	0.9
AUMSM26	Buckskin	158.1	4060	54.3	84.7	33	145.3	1	955	0.5	1000	0.6
AUMSM27	DeLamar	9.6	30809	21.2	104.7	200	24.3	1	1000	0.5	2000	0.5
AUMSM28	Republic	200	200	10000	385.7	298	1983.8	1	1000	2.3	39000	0.8
AUMSM29	Pauper	21.2	200	548	320	353	742.5	826	306	0.5	4000	0.6
AUMSM30	Pauper	86.8	3370	1752.8	621.5	252	572.2	404	255	0.6	3000	0.5
AUMSM31	Blackjack 1 - really high grade	66.6	30227	22.8	236.9	133	5.1	1	1000	0.5	2000	1
AUMSM32	Blackjack 2		200	5.4	6.1	6	7.5	1	57	0.5	1000	2.5
AUMSM33	Henrietta 1 - mineralized breccia		200	2.2	19.5	12	75.3	196	130	0.5	10000	2.6
AUMSM34	Henrietta 2 - low grade		200	5.1	1.8	2	13.4	3	619	0.5	1000	0.5
AUMSM35	Milestone 1 - The Castle		141.6	4.4	18.7	5	37.3	27	64	0.5	1000	1.6
AUMSM36	Milestone 2 - Vertical Sinter		58.3	8.4	6.5	4	15.8	37	28	0.5	1000	1.5

*Ag analyses with a value of 200 ppm represent an analytical upper detection limit. Ore samples contained significant Ag.

	Location	Mo	Co	Ni	Cd	Bi	Sn	W	Cr	Fe	Mn	Mg
		ppm	ppm	ppm	ppm	ppm	ppm	ppm	ppm	ppm	ppm	ppm
	Lower Detection Limit	**0.1**	**0.2**	**0.1**	**0.1**	**0.1**	**0.1**	**0.1**	**1**	**100**	**1**	**100**
AUMSM01	Sinter - Milestone?	1.7	1.4	2.3	0.1	0.1	0.6	0.9	12	7500	101	100
AUMSM02	Vertical Sinter - Milestone?	3.2	1.4	6.2	0.2	0.1	0.7	0.6	365	9900	94	100
AUMSM03	Mineralized Rhyolite	1.9	20.6	18	0.1	0.1	2.9	5.5	69	67900	647	4900
AUMSM04	Unmineralized Rhyolite	2.4	3.8	1.5	0.1	0.1	2.6	0.7	15	14700	232	2000
AUMSM05	Mineralized Basalt	0.8	39.8	61.7	0.3	0.1	1.5	2	127	74400	2019	18600
AUMSM06	Unmineralized Basalt	0.5	46.7	149.9	0.1	0.1	1	0.7	55	72800	1399	26000
AUMSM07	Altered Granite	0.8	1.9	3.4	0.1	0.1	0.8	0.6	80	10900	176	1700
AUMSM08	Fresh Granite	0.6	1.7	2.2	0.1	0.1	0.8	0.2	10	12000	320	2000
AUMSM09	TD Petrie-made slide	1.4	19	65.9	1.3	0.1	0.6	4.1	72	38300	604	5200
AUMSM10	TD Adit sample	0.9	4.5	10.3	0.2	0.6	0.4	0.5	12	11900	168	1500
AUMSM11	TD03 - same as altered granite	5.4	1.5	2.6	1.6	1.3	0.4	0.4	62	7100	125	2200
AUMSM12	TD04 - high grade in basalt	1.7	13.4	14.3	9.1	2	1	5.7	36	52200	306	2600
AUMSM13	TD05 - high grade vein	2.8	2.8	2	1.4	0.3	0.4	0.6	43	4200	81	700
AUMSM14	TD06 - qtz-adularia vein	0.4	1.9	0.9	0.2	0.1	0.3	0.2	6	4700	68	1500
AUMSM15	IT01 - basalt country rock + vein wall	1.2	1.2	2.4	1	0.1	0.7	0.9	58	7300	76	500
AUMSM16	IT02 - breccia	2.3	1.3	1.6	0.1	0.2	0.7	1.9	10	6700	41	200
AUMSM17	IT03 - same rock as IT1	2.1	1.3	3.7	0.7	0.1	0.5	0.5	115	6100	49	100
AUMSM18	IT04	1.9	1.9	2.5	38.8	10.9	0.4	0.1	12	10000	142	2600
AUMSM19	IT05	3.4	1.4	5.6	2.3	0.2	0.7	0.8	177	10800	72	100
AUMSM20	DEW1 - high grade puck	11.1	29.3	3.1	695.2	118.7	0.4	0.2	20	53000	50	200
AUMSM21	DEW2 - same as DEW2 slide	14.6	2.2	3.3	3.8	1.1	0.3	0.2	71	8300	55	800
AUMSM22	DEW3 - high grade	3.1	2.5	4	6.3	2	0.7	0.3	13	14200	118	1000
AUMSM23	DEW4 - run of the mill high grade	1.5	1.8	2.9	2	1.4	0.3	0.3	38	4200	30	100
AUMSM24	DEW5 - high grade puck	6.1	2.5	1.8	6	2.1	0.5	3.6	14	21700	223	2500
AUMSM25	Midas - Colorado Grande Vein	0.7	1.9	2.6	1.4	0.6	0.6	0.4	62	6700	76	800
AUMSM26	Buckskin	0.5	0.9	1.1	0.2	0.5	0.3	0.1	9	4600	120	300
AUMSM27	DeLamar	1.3	0.6	1.9	4.9	0.1	2	0.2	91	3400	36	1900
AUMSM28	Republic	1.6	1.8	2	9.4	0.1	0.4	0.1	12	39500	80	600
AUMSM29	Pauper	4.8	2.3	3.2	1.8	1.7	0.6	1.9	109	9500	77	1100
AUMSM30	Pauper	30.8	2.4	1	2.2	4.6	0.4	0.2	11	6500	57	200
AUMSM31	Blackjack 1 - really high grade	37.1	0.7	2.1	2.2	0.2	0.2	0.2	8	11800	159	900
AUMSM32	Blackjack 2	1.3	0.5	2.8	5.8	0.1	1.5	4.2	11	19100	202	100
AUMSM33	Henrietta 1 - mineralized breccia	9	0.6	1.7	0.1	0.1	3.9	4.2	10	15800	73	600
AUMSM34	Henrietta 2 - low grade	0.3	0.2	1.9	5.3	0.1	1.2	0.1	7	9500	111	200
AUMSM35	Milestone 1 - The Castle	0.6	0.3	1.1	0.1	0.1	2.1	6.5	6	11800	59	200
AUMSM36	Milestone 2 - Vertical Sinter	0.4	0.5	1.9	0.1	0.1	0.8	4.8	5	7600	79	200

	Location	Ti	Ca	K	Na	Al	P	U	Th	Sr	V	La
		ppm	ppm	ppm	ppm	ppm	ppm	ppm	ppm	ppm	ppm	ppm
	Lower Detection Limit	**10**	**100**	**100**	**10**	**100**	**10**	**0.1**	**0.1**	**1**	**1**	**0.1**
AUMSM01	Sinter - Milestone?	150	700	19200	400	16800	20	0.2	0.8	112	3	1.5
AUMSM02	Vertical Sinter - Milestone?	60	1000	5200	2500	5700	230	0.1	0.3	36	2	0.9
AUMSM03	Mineralized Rhyolite	12150	3400	17900	800	56800	1340	0.7	2.9	34	185	17.8
AUMSM04	Unmineralized Rhyolite	1790	4100	33600	17470	58800	60	2.6	16.9	99	20	37.4
AUMSM05	Mineralized Basalt	12530	57800	32500	980	80100	1580	0.5	1.7	353	259	15.4
AUMSM06	Unmineralized Basalt	9680	80200	1400	14170	85800	900	0.2	0.6	559	267	10.1
AUMSM07	Altered Granite	970	4900	33800	14020	54200	110	0.5	5	178	11	15.1
AUMSM08	Fresh Granite	1040	14100	17300	28780	61500	200	0.6	7	457	7	22.8
AUMSM09	TD Petrie-made slide	4040	28800	31000	8100	71900	370	0.1	0.2	287	127	3
AUMSM10	TD Adit sample	910	5700	39100	1350	33200	90	0.1	0.2	113	32	1.4
AUMSM11	TD03 - same as altered granite	330	2100	44100	6910	58300	50	0.2	1.6	168	4	4.5
AUMSM12	TD04 - high grade in basalt	5560	4900	46400	1340	53500	190	0.2	0.5	114	66	7.5
AUMSM13	TD05 - high grade vein	30	1900	44600	2170	60400	20	0.1	0.1	125	1	3.2
AUMSM14	TD06 - qtz-adularia vein	170	1200	53600	3760	67100	20	0.1	0.9	112	3	2.4
AUMSM15	IT01 - basalt country rock + vein wall	360	1500	43300	5090	51800	70	0.3	2.3	107	4	6.2
AUMSM16	IT02 - breccia	1880	300	73900	2510	78200	60	0.3	0.6	190	13	2.8
AUMSM17	IT03 - same rock as IT1	70	300	56100	1170	40600	10	0.1	0.4	58	2	1
AUMSM18	IT04	100	400	69300	1730	52400	30	0.1	0.1	93	3	0.2
AUMSM19	IT05	130	400	57500	1580	45200	20	0.1	0.7	72	2	1.4
AUMSM20	DEW1 - high grade puck	30	200	40900	890	30700	20	0.1	0.1	49	1	0.1
AUMSM21	DEW2 - same as DEW2 slide	10	200	73600	2440	74600	10	0.1	0.1	146	1	0.1
AUMSM22	DEW3 - high grade	270	1400	71400	4380	50300	60	0.2	2.1	143	4	6.5
AUMSM23	DEW4 - run of the mill high grade	10	300	74200	1730	51500	10	0.1	0.1	127	1	0.3
AUMSM24	DEW5 - high grade puck	80	1900	64800	3980	64300	30	0.1	0.8	206	4	1.5
AUMSM25	Midas - Colorado Grande Vein	250	1300	20700	490	17700	60	0.1	0.1	23	4	0.8
AUMSM26	Buckskin	10	500	4800	110	11900	10	0.1	0.1	20	1	0.2
AUMSM27	DeLamar	20	300	4800	140	12700	60	0.1	0.2	41	1	3.6
AUMSM28	Republic	20	1000	13500	260	13800	20	0.1	0.1	92	1	0.1
AUMSM29	Pauper	280	1100	15800	200	39800	80	0.2	1.8	26	3	6
AUMSM30	Pauper	40	700	8100	130	23100	20	0.1	0.2	31	1	0.6
AUMSM31	Blackjack 1 - really high grade	80	300	27700	620	44200	10	0.1	0.1	102	18	2.9
AUMSM32	Blackjack 2	610	300	55300	1310	44000	30	0.7	4.2	56	2	10.2
AUMSM33	Henrietta 1 - mineralized breccia	410	800	20200	810	19000	40	1.8	7.2	38	99	15.8
AUMSM34	Henrietta 2 - low grade	10	300	10300	190	12600	10	0.1	0.1	45	1	0.3
AUMSM35	Milestone 1 - The Castle	1040	500	42300	3110	32200	100	2.3	10.7	111	8	22.7
AUMSM36	Milestone 2 - Vertical Sinter	530	700	19500	360	16400	190	0.7	2.8	125	6	5.7

	Location	Ba	Zr	Ce	Y	Nb	Li	Rb
		ppm	ppm	ppm	ppm	ppm	ppm	ppm
	Lower Detection Limit	**1**	**0.1**	**1**	**0.1**	**0.1**	**0.1**	**0.1**
AUMSM01	Sinter - Milestone?	407	12.5	4	1.6	1.4	57.7	119
AUMSM02	Vertical Sinter - Milestone?	163	3.5	1	0.9	1.3	22	33.6
AUMSM03	Mineralized Rhyolite	325	76.6	42	21.4	15.2	33.7	124.9
AUMSM04	Unmineralized Rhyolite	1782	59.2	67	16.8	9.6	14.7	139.4
AUMSM05	Mineralized Basalt	324	91.1	36	24	11.9	37.8	112.6
AUMSM06	Unmineralized Basalt	103	70.8	24	19.2	6.2	53.6	4.1
AUMSM07	Altered Granite	639	2.1	32	4.2	3.3	16.2	202.5
AUMSM08	Fresh Granite	1117	2.7	42	3.5	6.8	12.6	54.2
AUMSM09	TD Petrie-made slide	243	28.4	8	7.1	2.9	15.8	211.8
AUMSM10	TD Adit sample	311	6.7	3	2.1	1	52.7	243.1
AUMSM11	TD03 - same as altered granite	532	0.6	10	1.9	1.4	20.7	279.9
AUMSM12	TD04 - high grade in basalt	163	28.5	17	6.9	5.2	31.1	257.3
AUMSM13	TD05 - high grade vein	115	0.3	12	5.8	0.2	17.8	310
AUMSM14	TD06 - qtz-adularia vein	272	0.5	5	0.6	0.6	12.5	330.6
AUMSM15	IT01 - basalt country rock + vein wall	502	1.1	13	1.9	1.7	24.8	247.7
AUMSM16	IT02 - breccia	403	12.8	6	1.8	2.8	10.2	432.8
AUMSM17	IT03 - same rock as IT1	214	0.2	2	0.5	0.6	52.9	267.7
AUMSM18	IT04	33	0.8	1	0.2	0.3	45.9	406.2
AUMSM19	IT05	253	0.4	3	0.8	1.3	36	329.2
AUMSM20	DEW1 - high grade puck	14	0.2	1	0.1	0.5	3.8	202.3
AUMSM21	DEW2 - same as DEW2 slide	143	0.1	1	0.4	0.6	9.8	457.7
AUMSM22	DEW3 - high grade	563	0.7	13	2.2	1.4	15.7	360.3
AUMSM23	DEW4 - run of the mill high grade	215	0.2	1	1.6	0.3	51.4	386.2
AUMSM24	DEW5 - high grade puck	429	0.5	3	1	1.1	13.6	371.4
AUMSM25	Midas - Colorado Grande Vein	65	3	2	1.6	0.8	44.4	100.3
AUMSM26	Buckskin	48	1	1	0.3	0.1	88.1	42.8
AUMSM27	DeLamar	210	0.3	7	1.9	0.5	63.4	42.9
AUMSM28	Republic	78	0.7	1	0.3	0.2	119.3	40
AUMSM29	Pauper	454	0.7	12	1.2	2	59.8	88.8
AUMSM30	Pauper	175	0.2	2	0.2	0.3	114.8	37
AUMSM31	Blackjack 1 - really high grade	353	1.2	7	7.2	0.3	94.2	149.2
AUMSM32	Blackjack 2	884	74.4	23	13.2	8.9	53.2	304.5
AUMSM33	Henrietta 1 - mineralized breccia	261	38.9	34	22.8	12.6	93.3	95.9
AUMSM34	Henrietta 2 - low grade	169	0.7	1	0.3	0.1	99.7	46.8
AUMSM35	Milestone 1 - The Castle	794	93.5	41	15.5	12.4	49.7	231
AUMSM36	Milestone 2 - Vertical Sinter	570	39.5	9	4.2	3.8	54.7	118.1

Appendix 3: Electron Microprobe Data Analyses for Electrum Grains

			Atomic Percent				Weight Percent					
Sample Number	**Grain Type**	**Line**	**Au At. %**	**Ag At. %**	**Se At. %**	**S At. %**	**Au Wt. %**	**Ag Wt. %**	**Se Wt. %**	**S Wt. %**	**Total Wt. %**	**Notes:**
TD High Grade 1	Electrum 1	19	38.4007	62.2208	0.055241	-0.06471	54.3354	48.2139	0.031334	-0.01491	102.059	38 Analyses
TD High Grade 1	Electrum 1	20	38.4337	61.7131	-0.00667	0.234549	52.5365	46.1976	-0.00365	0.052192	98.4646	4 Samples
TD High Grade 1	Electrum 1	21	34.0209	66.4721	-0.27101	0.138627	50.0327	53.5353	-0.15977	0.033187	103.114	11 Grains
TD High Grade 1	Electrum 1	22	37.3454	63.0834	-0.28692	0.254211	53.2466	49.2564	-0.16399	0.059002	102.059	Bold analyses indicate
TD High Grade 1	Electrum 1	23	25.7412	74.8055	-0.05617	0.2533	39.6856	63.1584	-0.03471	0.063571	102.228	significant amounts of
TD High Grade 1	Electrum 2	36	27.7317	72.4692	-0.04851	0.37865	41.5569	59.472	-0.02914	0.092368	100.651	sulfur or selenium
TD High Grade 1	Electrum 2	37	26.6187	73.5747	0.128595	0.332959	40.7804	61.7285	0.078976	0.083037	102.141	
TD High Grade 1	Electrum 2	38	33.7677	66.2008	0.09556	0.286624	50.1826	53.8775	0.056929	0.06934	103.865	
TD High Grade 1	Electrum 3	39	31.4308	68.3705	-0.05877	0.578477	46.6045	55.5181	-0.03493	0.139629	101.889	
TD High Grade 1	Electrum 3	40	34.6873	65.2427	-0.1036	0.519964	51.0434	52.5767	-0.06112	0.124555	103.336	
TD High Grade 1	Electrum 3	41	35.2869	64.6912	-0.04887	0.281182	51.7971	52.0031	-0.02876	0.067189	103.618	
TD High Grade 1	Electrum 3	42	27.3145	73.2183	-0.08761	0.161848	41.9803	61.6261	-0.05398	0.040493	103.06	
TD High Grade 1	Electrum 3	43	25.356	74.3547	-0.0004	0.690654	37.9767	60.9869	-0.00024	0.168389	98.7298	
TD High Grade 2	Electrum 1	57	31.9437	68.2521	0.062756	0.336133	47.0274	55.0267	0.037036	0.080555	101.66	
TD High Grade 2	Electrum 1	58	30.2833	69.9397	-0.05968	0.290087	43.538	55.0658	-0.0344	0.067891	98.2638	
TD High Grade 2	Electrum 2	64	29.379	70.8207	-0.23815	0.527079	44.5151	58.7656	-0.14465	0.130006	102.841	
TD High Grade 2	Electrum 2	65	28.9957	71.3727	-0.08818	0.357669	44.0354	59.3599	-0.05368	0.088423	102.825	
TD High Grade 2	**Electrum 2**	**66**	**-0.07723**	**62.0447**	**8.73858**	**29.7235**	**-0.18606**	**81.8562**	**8.43923**	**11.6566**	**101.136**	
TD High Grade 2	Electrum 3	69	32.8582	67.5276	-0.24498	0.293404	48.1919	54.2381	-0.14404	0.070051	101.97	
TD High Grade 2	Electrum 3	70	29.5609	70.9579	-0.20363	0.221153	43.5278	57.2193	-0.1202	0.05301	100.211	
IT 1	Electrum 1	79	32.1484	68.0567	-0.12988	0.106845	44.7343	51.8615	-0.07245	0.024202	96.3602	
IT 1	Electrum 1	80	41.6785	58.9301	-0.28687	0.161786	55.8772	43.2666	-0.15418	0.035309	98.6576	
IT 1	Electrum 1	81	34.103	65.9395	-0.03644	0.242199	47.804	50.6186	-0.02048	0.055267	98.1765	
IT 1	Electrum 2	82	35.6052	64.4003	-0.00164	0.212068	51.1927	50.7077	-0.00094	0.049635	101.765	
IT 1	Electrum 2	83	41.606	58.8991	-0.03952	0.11385	57.7428	44.7655	-0.02198	0.025721	102.072	
IT 1	Electrum 3	85	47.9617	52.3907	-0.06861	0.271831	65.0523	38.9148	-0.03731	0.060018	103.566	
IT 1	Electrum 3	86	48.5277	51.771	-0.15298	0.1373	65.4439	38.2348	-0.0827	0.030142	103.382	

			Atomic Percent				Weight Percent				
Sample Number	**Grain Type**	**Line**	**Au At. %**	**Ag At. %**	**Se At. %**	**S At. %**	**Au Wt. %**	**Ag Wt. %**	**Se Wt. %**	**S Wt. %**	**Total Wt. %**
BJ1A	Electrum 1	28	56.7899	44.8969	0.047886	0.016815	70.9409	30.7138	0.023979	0.003419	100.825
BJ1A	**Electrum 1**	**29**	**13.9786**	**58.4214**	**12.8837**	**15.5162**	**26.875**	**61.5106**	**9.92962**	**4.85612**	**102.404**
BJ1A	**Electrum 1**	**30**	**13.4161**	**56.7689**	**15.5777**	**15.3777**	**26.0756**	**60.4241**	**12.1371**	**4.86538**	**102.535**
BJ1A	Electrum 1	31	56.8671	44.2869	0.292235	0.866561	72.3743	30.8667	0.149095	0.179531	102.428
BJ1A	Electrum 1	32	36.8245	64.8714	-0.04668	0.327438	51.4522	49.6379	-0.02614	0.074476	100.024
BJ1A	Electrum 1	33	37.195	64.232	-0.00078	0.156183	54.6548	51.6877	-0.00046	0.037359	105.45
BJ1A	**Electrum 1**	**34**	**0.076358**	**66.5153**	**17.8217**	**16.296**	**0.170979**	**81.5646**	**15.9972**	**5.93998**	**102.86**
BJ1A	**Electrum 1**	**35**	**0.061389**	**66.9241**	**21.7044**	**11.928**	**0.1349**	**80.5366**	**19.1194**	**4.26682**	**103.328**
BJ1A	Electrum 2	47	36.7206	64.0036	0.041894	0.334936	54.1706	51.7073	0.024775	0.080433	105.303
BJ1A	Electrum 2	48	58.7894	43.2544	-0.03019	0.584057	72.3657	29.1579	-0.0149	0.117033	100.436
BJ1A	**Electrum 2**	**49**	**15.4801**	**50.8328**	**16.7784**	**17.8827**	**30.2858**	**54.4631**	**13.159**	**5.69529**	**102.779**

Appendix 4: Electron Microprobe Data Analyses for Silver Phases

			Atomic Percent						Weight Percent							
Sample Number	**Grain Type**	**Line**	**Ag At. %**	**Se At. %**	**As At. %**	**Sb At. %**	**S At. %**	**Cu At. %**	**Ag Wt. %**	**Se Wt. %**	**As Wt. %**	**Sb Wt. %**	**S Wt. %**	**Cu Wt. %**	**Total Wt. %**	**Notes:**
TD High Grade 1	Ag Phase 1	24	67.049	25.7649	0.037284	-0.58597	7.77316		76.9942	21.6575	0.029737	-0.75948	2.65331		100.495	116 Analyses
TD High Grade 1	Ag Phase 1	25	66.8027	24.7373	-0.13987	-0.49717	9.10646		77.795	21.0875	-0.11314	-0.65349	3.15233		101.248	10 Samples
TD High Grade 1	Ag Phase 1	26	66.6841	25.5296	-0.04489	-0.51472	8.1654		77.6252	21.754	-0.03629	-0.67628	2.82542		101.876	Bold analyses
TD High Grade 1	Ag Phase 2	27	64.5876	7.37082	-0.13202	-0.49557	28.6372		78.998	6.59929	-0.11216	-0.68415	10.4117		95.2841	contain significant
TD High Grade 1	Ag Phase 2	28	64.3199	7.5382	-0.0796	-0.47813	28.6368		80.8407	6.93532	-0.06949	-0.67827	10.6988		97.8711	Cu or As
TD High Grade 1	Ag Phase 2	29	64.3398	7.67397	-0.15399	-0.40716	28.5553		80.149	6.99766	-0.13324	-0.57248	10.5738		96.9967	
TD High Grade 1	Ag Phase 3	30	65.936	8.40685	0.025666	-0.38212	26.0453		83.131	7.75868	0.022476	-0.54377	9.76101		100.056	
TD High Grade 1	Ag Phase 3	31	66.1206	8.17482	-0.06876	-0.43584	26.1688		81.9628	7.41776	-0.0592	-0.6098	9.6425		98.4453	
TD High Grade 1	Ag Phase 3	32	65.5334	8.63622	-0.02322	-0.37229	26.3142		82.1413	7.92387	-0.02021	-0.52669	9.80425		99.1203	
TD High Grade 1	Ag Stringer	33	65.9549	14.785	-0.11671	-0.28907	19.5806		80.0197	13.1306	-0.09835	-0.39585	7.06155		99.9066	
TD High Grade 1	Ag Stringer	34	61.4519	4.61918	-0.09912	-0.42065	34.4651		74.4582	4.09691	-0.08342	-0.57528	12.4132		90.2732	
TD High Grade 1	Ag Stringer	35	66.6786	10.3998	-0.02864	-0.49234	23.4925		81.1864	9.26904	-0.02422	-0.67661	8.50257		98.1463	
TD High Grade 1	Ag Unknown	44	66.0262	8.09302	-0.09091	-0.39518	26.3344		82.2407	7.37896	-0.07865	-0.55557	9.75033		98.8094	
TD High Grade 1	Ag Unknown	45	65.6978	8.64733	-0.12041	-0.39899	26.1342		82.7682	7.9746	-0.10537	-0.56735	9.78693		99.9492	
TD High Grade 1	Ag Unknown	46	65.4649	11.0687	-0.07592	-0.52224	23.8949		67.0839	8.30275	-0.05403	-0.60403	7.27848		82.3244	
TD High Grade 1	Ag Unknown	47	65.7719	9.73276	-0.14202	-0.40268	25.016		83.6294	9.05877	-0.12542	-0.57791	9.455		101.496	
TD High Grade 1	Ag Unknown	48	66.2042	7.76098	-0.01918	-0.35174	26.3653		82.6654	7.09364	-0.01663	-0.49572	9.78578		99.1247	
TD High Grade 1	Ag Unknown	49	65.635	8.38785	-0.12386	-0.44486	26.5541		81.2681	7.60238	-0.10652	-0.62171	9.77329		97.897	
TD High Grade 1	Ag Unknown	50	67.7376	6.67819	-0.04731	-0.43608	26.0594		83.2754	6.0098	-0.04039	-0.60511	9.52305		98.1812	
TD High Grade 1	Ag Unknown	51	66.0543	7.24168	-0.08423	-0.39677	27.0914		85.7183	6.87902	-0.07592	-0.58115	10.4503		102.612	
TD High Grade 1	Ag Unknown	52	65.3269	8.39589	-0.05455	-0.37346	26.6972		82.6667	7.77714	-0.04795	-0.53341	10.0422		99.9233	
TD High Grade 1	Ag Unknown	53	66.1227	8.11462	0.00335	-0.47645	26.2766		82.7611	7.43461	0.002912	-0.67308	9.7762		99.2085	
TD High Grade 1	Ag Unknown	54	59.5613	2.27916	-0.00056	-0.44441	38.5042		69.8582	1.95678	-0.00045	-0.58832	13.4242		84.8652	
TD High Grade 1	Ag Unknown	55	64.1874	6.51027	-0.03375	-0.49264	29.905		66.6753	4.95027	-0.02435	-0.57759	9.23388		80.1127	
TD High Grade 1	Ag Unknown	56	65.3833	9.2023	0.041277	-0.46756	25.8068		77.8966	8.02531	0.034157	-0.62874	9.13926		94.5402	
TD High Grade 1	**Ag Chaos**	**85**	**59.2387**	**7.71833**	**-0.01476**	**-0.38497**	**26.4089**	**6.99565**	**77.7224**	**7.41273**	**-0.01345**	**-0.57008**	**10.2995**	**5.4071**	**100.349**	
TD High Grade 1	**Ag Chaos**	**86**	**51.9544**	**4.54081**	**0.069896**	**-0.30828**	**29.5302**	**14.2202**	**70.8192**	**4.53081**	**0.066175**	**-0.47429**	**11.9652**	**11.419**	**98.3081**	
TD High Grade 1	**Ag Chaos**	**87**	**52.736**	**4.29973**	**0.055999**	**-0.32074**	**29.724**	**13.505**	**72.6083**	**4.33346**	**0.053552**	**-0.49843**	**12.165**	**10.9539**	**99.6158**	
TD High Grade 1	**Ag Chaos**	**88**	**58.838**	**7.24195**	**-0.04166**	**-0.38774**	**26.92**	**7.41408**	**75.577**	**6.80929**	**-0.03717**	**-0.56214**	**10.2785**	**5.61028**	**97.7119**	
TD High Grade 1	Ag Chaos	89	64.4534	8.50389	0.044385	-0.40173	25.5205	1.87948	81.4405	7.86551	0.038953	-0.57293	9.58538	1.39903	99.7565	
TD High Grade 1	Ag Chaos	90	64.2428	8.12769	-0.04585	-0.49439	26.1684	1.98564	79.9292	7.40223	-0.03962	-0.69427	9.67795	1.45538	97.7666	
TD High Grade 1	**Ag Chaos**	**91**	**47.7456**	**1.97556**	**0.049846**	**-0.20811**	**32.2444**	**18.1859**	**69.5898**	**2.10774**	**0.050462**	**-0.34235**	**13.9698**	**15.615**	**101.008**	
TD High Grade 1	**Ag Chaos**	**92**	**48.1572**	**1.764**	**0.069986**	**-0.31247**	**32.2667**	**17.9811**	**70.6038**	**1.89313**	**0.071268**	**-0.51708**	**14.062**	**15.5302**	**101.84**	
TD High Grade 1	**Ag Chaos**	**93**	**60.4636**	**8.05444**	**-0.08187**	**-0.46861**	**25.3989**	**6.61826**	**78.2295**	**7.62827**	**-0.07357**	**-0.68432**	**9.76824**	**5.04447**	**99.9487**	
TD High Grade 1	**Ag Chaos**	**94**	**60.5028**	**7.63176**	**-0.11404**	**-0.43777**	**26.6534**	**5.80226**	**77.5647**	**7.16189**	**-0.10155**	**-0.63344**	**10.157**	**4.38209**	**98.4408**	
TD High Grade 1	Ag Chaos	95	64.0146	7.8973	-0.07311	-0.40942	26.1362	2.49644	81.0538	7.3196	-0.0643	-0.58512	9.83699	1.86213	99.2797	
TD High Grade 1	Ag Chaos	96	64.8258	8.12277	-0.00899	-0.45136	25.6144	1.89741	82.6436	7.58019	-0.00796	-0.64947	9.7067	1.42501	100.698	
TD High Grade 2	Ag Unknown	59	64.3421	6.78395	-0.01536	-0.47333	29.1973		77.8913	6.01161	-0.01291	-0.64674	10.5066		94.1153	
TD High Grade 2	Ag Unknown	60	63.5398	2.61395	-0.09854	-0.43714	34.4057		78.6832	2.36945	-0.08475	-0.61099	12.6646		92.9676	
TD High Grade 2	Ag Unknown	61	64.8147	7.57942	0.047618	-0.45866	27.9546		83.7211	7.16658	0.042722	-0.6687	10.7335		101.142	
TD High Grade 2	Ag Unknown	62	62.8115	5.75412	0.034256	-0.32973	31.7145		81.9937	5.49838	0.031059	-0.48582	12.3062		99.3801	
TD High Grade 2	Ag Unknown	63	63.5369	8.87271	-0.06709	-0.49917	28.1966		80.7624	8.2557	-0.05923	-0.71615	10.6538		98.8038	

			Atomic Percent						Weight Percent						
Sample Number	**Grain Type**	**Line**	**Ag At. %**	**Se At. %**	**As At. %**	**Sb At. %**	**S At. %**	**Cu At. %**	**Ag Wt. %**	**Se Wt. %**	**As Wt. %**	**Sb Wt. %**	**S Wt. %**	**Cu Wt. %**	**Total Wt. %**
Dewey 4	**Ag Unknown**	**80**	**46.5687**	**0.07897**	**6.73599**	**-0.3528**	**36.5359**	**10.4197**	**67.4373**	**0.083705**	**6.77523**	**-0.57664**	**15.7272**	**8.88911**	**98.3717**
Dewey 4	**Ag Unknown**	**81**	**42.2721**	**0.9997**	**6.78455**	**-0.26677**	**37.3387**	**12.9249**	**63.369**	**1.097**	**7.06416**	**-0.45138**	**16.6382**	**11.4142**	**98.9856**
Dewey 4	**Ag Unknown**	**82**	**44.4811**	**0.42298**	**6.48309**	**-0.29249**	**36.908**	**11.9973**	**67.1635**	**0.467509**	**6.79918**	**-0.49847**	**16.5655**	**10.6718**	**101.169**
Dewey 4	Ag Unknown	83	65.1415	10.4627	-0.05415	-0.36694	24.2358	0.675542	81.5588	9.58898	-0.04709	-0.51855	9.01975	0.498266	99.8842
Dewey 4	Ag Unknown	84	65.2414	8.99949	-0.01499	-0.42574	25.5958	0.572797	81.8643	8.26616	-0.01307	-0.60297	9.54695	0.423416	99.5564
IT 1	Ag Unknown	76	64.3969	8.74743	0.079119	-0.41822	27.1235		82.7392	8.227	0.070607	-0.6065	10.359		100.957
IT 1	Ag Unknown	77	64.2279	7.3938	-0.09757	-0.44394	28.8344		83.6679	7.05046	-0.08828	-0.65273	11.1653		101.346
IT 1	Ag Unknown	78	61.9104	7.89199	-0.0526	-0.39013	30.6017		81.1111	7.56864	-0.04786	-0.5769	11.9176		100.065
IT 1	Ag Unknown	84	62.542	9.78832	-0.02273	-0.36074	27.9542		77.8358	8.91724	-0.01965	-0.50674	10.3414		96.793
IT 1	Ag Unknown	87	62.4026	7.6829	-0.01932	-0.42384	30.3576		76.7235	6.91457	-0.0165	-0.58817	11.0948		94.1283
IT 1	Ag Unknown	88	65.6673	7.38258	0.00831	-0.53416	27.4171		79.8219	6.56894	0.007016	-0.73285	9.90649		95.702
IT 1	Ag Unknown	89	67.5412	8.73271	-0.00555	-0.4568	24.1971		80.6735	7.63529	-0.00461	-0.61584	8.59112		96.2607
IT 2	**Ag Unknown**	**55**	**67.2655**	**14.6813**	**0.00795**	**-0.34557**	**18.4657**	**-0.05114**	**84.1257**	**13.4405**	**0.006908**	**-0.48781**	**6.8648**	**-0.03768**	**103.858**
IT 2	**Ag Unknown**	**56**	**68.8936**	**7.56114**	**0.1308**	**0.2941**	**23.7245**	**-0.60421**	**11.2139**	**0.900904**	**0.014787**	**0.054031**	**1.14789**	**-0.05794**	**13.2735**
IT 2	Ag Unknown	57	65.4983	14.1423	-0.02314	-0.44941	21.2544	-0.40676	82.4433	13.0305	-0.02023	-0.63848	7.95243	-0.30162	102.43
IT 2	Ag Unknown	58	65.0998	14.62	-0.02816	-0.4078	20.7002	-0.07924	81.5832	13.4117	-0.02451	-0.57683	7.71117	-0.0585	102.264
IT 2	Ag Unknown	59	64.0962	15.9941	-0.0275	-0.42891	20.5145	-0.18089	79.1731	14.4618	-0.0236	-0.59798	7.53239	-0.13163	100.487
IT 2	Ag Unknown	60	65.184	16.1131	-0.1397	-0.45769	19.1849	0.156567	78.5418	14.2119	-0.11691	-0.62245	6.87137	0.111136	98.9063
BJ1A	Ag Unknown	25	63.7707	17.9181	-0.02358	-0.38729	18.5119	0.152398	77.7499	15.9914	-0.01996	-0.53296	6.70894	0.109459	100.135
BJ1A	Ag Unknown	26	64.7367	17.4331	-0.10091	-0.50065	18.3206	0.077683	78.239	15.4228	-0.08471	-0.68294	6.58169	0.055309	99.605
BJ1A	Ag Unknown	27	64.7436	18.0929	0.011986	-0.50062	17.6417	0.052993	77.8629	15.9278	0.010012	-0.67955	6.30664	0.037544	99.3721
BJ1A	Ag Unknown	36	64.1593	18.4797	-0.12453	-0.36282	18.1859	-0.30486	77.4102	16.3211	-0.10436	-0.49409	6.52228	-0.21669	99.3663
BJ1A	Ag Unknown	37	64.8044	17.5221	-0.056	-0.42552	17.9432	0.252051	79.477	15.7304	-0.0477	-0.58903	6.54128	0.182105	101.204
BJ1A	Ag Unknown	39	63.7773	18.8847	-0.04954	-0.38367	17.8482	-0.05182	75.8412	16.4385	-0.04092	-0.51496	6.30898	-0.03631	97.942
BJ1A	Ag Unknown	41	64.4377	19.7034	-0.05286	-0.44174	15.9557	0.356314	77.922	17.4412	-0.0444	-0.60292	5.73536	0.253833	100.797
BJ1A	Ag Unknown	42	62.1271	15.487	-0.07195	-0.4554	22.9704	-0.04937	78.4061	14.307	-0.06307	-0.64869	8.61713	-0.0367	100.564
BJ1A	Ag Unknown	43	66.1618	16.3223	-0.001	-0.44071	17.8281	0.12947	79.5178	14.36	-0.00083	-0.59784	6.36925	0.091669	99.74
BJ1A	Ag Unknown	44	63.3439	16.0642	0.024705	-0.34703	20.6407	0.273472	78.8841	14.644	0.021369	-0.48778	7.64073	0.200629	100.903
BJ1A	Ag Unknown	45	65.0973	18.1302	-0.06639	-0.3628	17.2778	-0.07614	79.5154	16.2109	-0.05633	-0.50019	6.2734	-0.05479	101.388
BJ1A	Ag Unknown	46	58.9408	11.6184	-0.06298	-0.33016	29.2231	0.255788	75.4238	10.8832	-0.05598	-0.47687	11.1159	0.192827	97.9124
BJ2A	Ag Unknown	50	69.6395	-0.18504	0.121556	-0.47068	30.7193	0.157916	74.387	-0.14468	0.090185	-0.56747	9.75388	0.099372	83.6523
BJ2A	Ag Unknown	51	62.5037	-0.4351	-0.06405	-0.38675	38.3783	-0.05174	83.2497	-0.42421	-0.05925	-0.58142	15.1945	-0.0406	97.4741
BJ2A	Ag Unknown	52	63.5145	-0.86426	-0.08588	-0.3836	37.5863	0.154691	68.9903	-0.68719	-0.06479	-0.4703	12.1358	0.098986	80.1579
BJ2A	Ag Unknown	53	64.3779	-0.36817	-0.07516	-0.42357	36.5201	-0.05277	82.6788	-0.34611	-0.06704	-0.61399	13.9417	-0.03992	95.6042
BJ2A	Ag Unknown	54	63.8798	-0.45078	-0.04463	-0.46563	36.6338	0.360887	82.501	-0.42616	-0.04004	-0.67875	14.0638	0.274576	95.8985

			Atomic Percent						Weight Percent						
Sample Number	**Grain Type**	**Line**	**Ag At. %**	**Se At. %**	**As At. %**	**Sb At. %**	**S At. %**	**Cu At. %**	**Ag Wt. %**	**Se Wt. %**	**As Wt. %**	**Sb Wt. %**	**S Wt. %**	**Cu Wt. %**	**Total Wt. %**
TD High Grade 2	Electrum 2	66	62.0447	8.73858	-0.01732	-0.4122	29.7235		81.8562	8.43923	-0.01587	-0.61381	11.6566		101.136
TD High Grade 2	Ag Unknown	67	65.4528	7.93739	-0.08033	-0.45068	27.2054		82.5426	7.32727	-0.07036	-0.6415	10.1983		99.2077
TD High Grade 2	Ag Unknown	68	63.8124	4.91658	-0.04435	-0.38504	31.7004		82.0576	4.62798	-0.03961	-0.55886	12.1172		98.2043
TD High Grade 2	Ag Unknown	71	57.5571	3.32862	0.07826	-0.30335	39.3087		73.818	3.12494	0.069714	-0.43912	14.9857		91.6311
TD High Grade 2	Ag Unknown	72	56.7838	3.32688	-0.16842	-0.33635	40.4091		74.618	3.20015	-0.15372	-0.49887	15.7842		92.9138
TD High Grade 2	Ag Unknown	73	64.2497	8.5191	-0.10262	-0.40313	27.7205		79.0249	7.6701	-0.08767	-0.55965	10.1349		96.2196
TD High Grade 2	Ag Unknown	74	67.1856	22.4979	-0.10551	-0.37097	10.7468		77.8733	19.0883	-0.08495	-0.48532	3.70269		100.192
TD High Grade 2	Ag Unknown	75	65.1097	7.93108	0.008393	-0.42192	27.3972		81.1451	7.23541	0.007265	-0.5935	10.1496		97.8882
TD 3	Ag Unknown	97	60.5482	5.90691	-0.03823	-0.46906	30.6097	3.44977	80.5542	5.75256	-0.03532	-0.70435	12.1052	2.70379	100.358
TD 3	Ag Unknown	98	62.9393	6.53044	0.021921	-0.40401	29.0602	1.89081	79.589	6.04489	0.019253	-0.57663	10.9233	1.40856	97.3192
TD 3	**Ag Unknown**	**99**	**50.0365**	**1.80283**	**0.00328**	**-0.31256**	**33.0493**	**15.3397**	**72.6901**	**1.91715**	**0.003306**	**-0.51251**	**14.2717**	**13.128**	**101.713**
TD 3	Ag Unknown	100	62.0095	7.767	-0.08036	-0.37972	27.2367	3.39364	80.318	7.36416	-0.07229	-0.55512	10.4866	2.58951	100.257
TD 3	Ag Unknown	101	62.5445	7.23874	-0.04081	-0.46262	27.8186	2.87117	80.763	6.84228	-0.0366	-0.67426	10.6779	2.18413	99.8282
TD 3	**Ag Unknown**	**102**	**59.7732**	**4.61705**	**-0.06291**	**-0.40975**	**30.9751**	**5.08506**	**78.6163**	**4.44514**	**-0.05747**	**-0.60828**	**12.11**	**3.94001**	**98.4992**
TD 3	Ag Unknown	103	52.1037	8.56633	-0.03924	-0.33209	38.4591	1.27016	73.2199	8.81191	-0.0383	-0.52673	16.0652	1.05152	98.5117
TD 6	Ag Unknown	104	60.4239	7.37946	-0.03846	-0.38154	32.471	0.123357	78.4326	7.01176	-0.03468	-0.559	12.5288	0.094329	97.5266
TD 6	Ag Unknown	105	59.7866	7.31016	-0.0822	-0.36361	33.0955	0.223653	77.1094	6.90152	-0.07363	-0.52931	12.6881	0.169931	96.3365
TD 6	Ag Unknown	106	60.1236	8.14414	-0.0263	-0.35936	32.0397	0.122603	78.901	7.82342	-0.02397	-0.53228	12.4983	0.094784	98.6549
TD 6	Ag Unknown	107	60.6299	8.07734	-0.08406	-0.35936	31.721	0.076718	76.585	7.46861	-0.07375	-0.51234	11.9105	0.057088	95.2933
TD 6	Ag Unknown	108	60.5521	7.73545	-0.10635	-0.38807	31.4647	0.609286	79.6932	7.45233	-0.09722	-0.57647	12.3095	0.472399	99.5731
TD 6	Ag Unknown	109	59.7747	7.8603	-0.06411	-0.4212	32.6546	0.248036	77.8117	7.48998	-0.05797	-0.61886	12.6356	0.190212	97.3263
TD 6	Ag Unknown	110	54.7398	8.18073	-0.04461	-0.3543	35.686	1.8424	74.6382	8.16515	-0.04225	-0.54526	14.4637	1.47991	98.0348
Dewey 2	Ag Unknown	61	60.7912	9.89941	0.019825	-0.37435	29.225	0.461115	80.2255	9.56303	0.018172	-0.5576	11.4644	0.358489	101.018
Dewey 2	Ag Unknown	62	62.4351	9.58721	-0.01746	-0.34929	27.5624	0.73012	82.6457	9.28962	-0.01605	-0.52186	10.8451	0.569352	102.937
Dewey 2	Ag Unknown	64	62.4	10.8495	0.007839	-0.42553	27.2163	0	76.675	9.75874	0.00669	-0.59017	9.94086	0	95.6831
Dewey 2	Ag Unknown	65	61.1441	11.248	-0.0303	-0.34232	27.7042	0.198837	77.9202	10.4926	-0.02682	-0.49238	10.4946	0.149276	98.7179
Dewey 2	Ag Unknown	66	64.1477	10.2996	-0.02303	-0.37763	25.5939	0.328725	82.1799	9.6587	-0.0205	-0.54605	9.74642	0.248092	101.339
Dewey 2	Ag Unknown	67	61.9557	10.8353	-0.11028	-0.40943	27.7663	0	81.2232	10.3981	-0.10042	-0.60583	10.8204	0	101.645
Dewey 2	Ag Unknown	68	60.4694	7.81848	-0.00499	-0.40142	32.0471	0.071411	82.4073	7.79951	-0.00472	-0.61745	12.9821	0.057331	102.624
Dewey 2	Ag Unknown	69	63.0506	7.07157	-0.05625	-0.39988	30.3375	-0.02598	81.7773	6.71389	-0.05067	-0.58539	11.6963	-0.01985	99.5848
Dewey 2	Ag Stringer	70	63.3901	11.504	0.00776	-0.50357	25.4983	0.126688	80.7865	10.732	0.006869	-0.72436	9.65949	0.095115	100.501
Dewey 2	Ag Stringer	71	60.2923	10.8292	-0.04681	-0.35313	28.7712	0.439215	78.9035	10.374	-0.04255	-0.5216	11.1922	0.338616	100.407
Dewey 2	Ag Stringer	72	61.3749	11.8277	-0.06881	-0.4496	26.8385	0.546672	79.2456	11.1789	-0.06171	-0.65522	10.3007	0.415822	100.261
Dewey 2	Ag Stringer	73	58.8503	10.5049	-0.04207	-0.40941	30.5251	0.636873	78.6873	10.2817	-0.03907	-0.61785	12.1321	0.501654	100.785
Dewey 2	Ag Stringer	74	62.3536	9.34241	-0.07703	-0.40411	28.2106	0.567068	81.171	8.90252	-0.06965	-0.59376	10.9163	0.434881	100.779
Dewey 2	Ag Stringer	75	62.4264	9.3019	-0.0262	-0.46677	28.4458	0.244285	81.4422	8.88317	-0.02375	-0.68732	11.0313	0.187747	101.011
Dewey 2	Ag Stringer	76	62.4963	10.0171	0.011877	-0.48393	27.7953	0.223952	80.7588	9.47525	0.01066	-0.70582	10.6766	0.170485	100.243
Dewey 4	Ag Unknown	77	64.1426	10.5999	0.064772	-0.37101	25.4565	0.076041	80.677	9.75932	0.056585	-0.5267	9.51757	0.056344	99.6117
Dewey 4	Ag Unknown	78	61.7363	10.9478	-0.0811	-0.34439	26.6801	1.07716	76.8366	9.97395	-0.07011	-0.48379	9.87053	0.789775	96.881
Dewey 4	Ag Unknown	79	60.7304	11.6078	-0.08573	-0.34545	27.7782	0.322432	77.9964	10.9127	-0.07647	-0.50076	10.6047	0.243951	99.1625